Fall 1-31-2009

Loss of synchrony in an inhibitory network of type-I oscillators

Myongkeun Oh
New Jersey Institute of Technology

ABSTRACT

LOSS OF SYNCHRONY IN AN INHIBITORY NETWORK OF TYPE-I OSCILLATORS

by
Myongkeun Oh

Synchronization of excitable cells coupled by reciprocal inhibition is a topic of significant interest due to the important role that inhibitory synaptic interaction plays in the generation and regulation of coherent rhythmic activity in a variety of neural systems. While recent work revealed the synchronizing influence of inhibitory coupling on the dynamics of many networks, it is known that strong coupling can destabilize phase-locked firing. Here we examine the loss of synchrony caused by an increase in inhibitory coupling in networks of type-I Morris-Lecar model oscillators, which is characterized by a period-doubling cascade and leads to mode-locked states with alternation in the firing order of the two cells, as reported recently by Maran and Canavier (2007) for a network of Wang-Buzsáki model neurons. Although alternating-order firing has been previously reported as a near-synchronous state, we show that the stable phase difference between the spikes of the two Morris-Lecar cells can constitute as much as 70% of the unperturbed oscillation period. Further, we examine the generality of this phenomenon for a class of type-I oscillators that are close to their excitation thresholds, and provide an intuitive geometric description of such "leap-frog" dynamics. In the Morris-Lecar model network, the alternation in the firing order arises under the condition of fast closing of K^+ channels at hyperpolarized potentials, which leads to slow dynamics of membrane potential upon synaptic inhibition, allowing the presynaptic cell to advance past the postsynaptic cell in each cycle of the oscillation. Further, we show that non-zero synaptic decay time is crucial for the existence of leap-frog firing in networks of phase oscillators. However, we demonstrate that leap-frog spiking can also be obtained in *pulse-coupled* inhibitory networks of one-

dimensional oscillators with a multi-branched phase domain, for instance in a network of quadratic integrate-and-fire model cells. Also, we show that the entire bifurcation structure of the network can be explained by a simple scaling of the STRC (spike-time response curve) amplitude, using a simplified quadratic STRC as an example, and derive the general conditions on the shape of the STRC function that leads to leap-frog firing. Further, for the case of a homogeneous network, we establish quantitative conditions on the phase resetting properties of each cell necessary for stable alternating-order spiking, complementing the analysis of Goel and Ermentrout (2002) of the order-preserving phase transition map. We show that the extension of STRC to negative values of phase is necessary to predict the response of a model cell to several close non-weak perturbations. This allows us for instance to accurately describe the dynamics of non-weakly coupled network of three model cells. Finally, the phase return map is also extended to the heterogenous network, and is used to analyze both the order-alternating firing and the order-preserving non-zero phase locked state in this case.

LOSS OF SYNCHRONY IN AN INHIBITORY NETWORK OF TYPE-I OSCILLATORS

by
Myongkeun Oh

A Dissertation
Submitted to the Faculty of
New Jersey Institute of Technology and
Rutgers, The State University of New Jersey – Newark
in Partial Fulfillment of the Requirements for the Degree of
Doctor of Philosophy in Mathematical Sciences

Department of Mathematical Sciences
Department of Mathematics and Computer Science, Rutgers-Newark

January 2009

APPROVAL PAGE

LOSS OF SYNCHRONY IN AN INHIBITORY NETWORK OF TYPE-I OSCILLATORS

Myongkeun Oh

Dr. Victor Matveev, Dissertation Advisor — Date
Assistant Professor, Department of Mathematical Sciences, NJIT

Dr. Amitabha Bose, Committee Member — Date
Professor, Department of Mathematical Sciences, NJIT

Dr. Farzan Nadim, Committee Member — Date
Professor, Department of Mathematical Sciences, NJIT and Federated Department of Biological Sciences, NJIT and Rutgers-Newark

---

Dr. Jorge Golowasch, Committee Member — Date
Associate Professor, Department of Mathematical Sciences, NJIT and Federated Department of Biological Sciences, NJIT and Rutgers-Newark

---

Dr. Camelia Prodan, Committee Member — Date
Assistant Professor, Department of Physics, NJIT

BIOGRAPHICAL SKETCH

Author: Myongkeun Oh

Degree: Doctor of Philosophy

Date: January 2009

Undergraduate and Graduate Education:

- Doctor of Philosophy in Mathematical Sciences,
  New Jersey Institute of Technology, Newark, NJ, 2009
- Master of Science in Applied Mathematics,
  New Jersey Institute of Technology, Newark, NJ, 2008
- Master of Science in Mathematics,
  Pusan National University, Pusan, Korea, 2000
- Bachelor of Science in Mathematics,
  Pusan National University, Pusan, Korea, 1998

Major: Mathematical Sciences

Presentations and Publications:

M. Oh and V. Matveev, "Loss of phase-locking in non-weakly coupled inhibitory networks of type-I model neurons," *J. of Computational Neuroscience,* 2008.

M. Oh and V. Matveev, "Loss of synchrony in non-weakly coupled inhibitory networks of type-I oscillators," *Mathematical Biology Seminar*, Department of Mathematical Sciences, NJIT, October 7, 2008.

M. Oh and V. Matveev, "Loss of synchrony in an inhibitory network of type-I model neurons," *Howard Hughes Medical Institute Interfaces Scholar Meeting*, Bethesda, MD, September 16-18, 2008.

M. Oh and V. Matveev, "Loss of synchrony in an inhibitory network of type-I oscillators," *Computational Neurosciences*, Portland, Oregon, July 19-24, 2008.

In memory of my father, Hae Duck Oh.

For my husband, Jung Hoon Song and all my family members

ACKNOWLEDGMENT

First of all, I would like to express my gratitude to my advisor, Dr. Victor Matveev who has been abundantly helpful and offered invaluable assistance, support and guidance. He provided a great deal of help during my Ph.D research. I would like to thank my committee members Dr. Amitabha Bose and Dr. Farzan Nadim who gave me useful suggestions for my dissertation and helped me to understand important knowledge of biology and mathematics during my PhD research. I would also like to thank my committee members Dr. Jorge Golowasch and Dr. Camelia Prodan who read my thesis and guided me. I would like to thank many faculty members in the Department of Mathematical Sciences at NJIT.

I would also like to thank Joon Ha for helping me out in understanding theory of dynamical systems and discussing many things related to my research. I would also like to thank Lakshmi Chandrasekaran and Leonardo Espin Estevez sharing and discussing many things as a graduate student with me.

Finally, this research would not have been possible without the support of my husband, Jung Hoon Song. I would like to express my thanks to my mother Sook Nyun Kim and my sisters and brother, Hyun Joo Oh, Hyun Ok Oh, Hyun Pil Oh and Dong Suck Oh, for their support throughout this process. My special thanks go to my parents-in-law, Jong Man Song and Heui Soon Park for their prayers and support.

TABLE OF CONTENTS

TABLE OF CONTENTS
(Continued)

Chapter **Page**

LIST OF FIGURES

Figure **Page**

LIST OF FIGURES
(Continued)

Figure **Page**

LIST OF FIGURES
(Continued)

Figure **Page**

Figure **Page**

LIST OF FIGURES
(Continued)

Figure **Page**

Figure **Page**

Figure **Page**

Figure **Page**

CHAPTER 1

INTRODUCTION

1.1 Synchronization of Oscillators

The most spectacular example of synchronous phenomenon in nature is a rhythmic flashing of fireflies [8, 7, 36, 79]. It was reported that thousands of male fireflies congregate in trees and flash in synchrony in certain parts of southeast Asia at night. Synchronization occurs in many other populations of biological oscillators. For instance, the pacemaker cells of the heart [66], central pattern generation [46, 68], chemical waves [50], the networks of neurons in the circadian pacemaker [14, 65, 92, 93, 94] and hippocampus [85], rhythmic activity in the brain [34, 74], crickets that chirp in unison [87], the insulin-secreting cells of the pancreas [73], and groups of women whose menstrual periods [54, 71] become mutually synchronized.

Also, many synchronized phenomena such as the transition from a periodic orbit to a chaotic attractor, the attraction to the periodic orbit, and noise-induce synchronization, can be observed in various regions of the brain. Such synchronous firing has been observed in the sensory processing of cat visual cortex [33, 23, 49] in early experiments (see below). For another example, Freeman et al. [21, 22] have shown that spatial electroencephalogram (EEG) patterns in the olfactory bulb of rabbits are transformed into equilibrium, periodic or chaotic states with conditioning to odors.

Many phenomena in biology, chemistry, and engineering can be described by a network of oscillators. Many biological rhythms, ranging from breathing to walking, are described in part by central pattern generating (CPG) networks built from neurons. Oscillations are a prevalent phenomenon in biological neural networks and manifest themselves experimentally in electroencephalogram (EEG), recordings of local field

potentials (LFP), and multi-unit recordings. Oscillations play an important role in the coding of sensory information. In the olfactory system an ongoing oscillation of the population activity provides a temporal frame of reference for neurons coding information about the odorant [51, 12]. Similarly, place cells in the hippocampus exhibit phase-dependent firing activity relative to a background oscillation [59]. Finally, rhythmic spike patterns in the inferior olive may be involved in various timing tasks and motor coordination [52, 90, 44]. Moreover, synchronized behavior in the nervous systems can be frequently illustrated as a nonlinear dynamical model of large or small numbers of coupled oscillators [28, 6, 25].

The first observation of synchronization reported by Dutch scientist Huygens in his experiments with pendulum clocks in the 17th century. This synchronized phenomenon was also discovered in neuronal systems. The experiments showing synchronized phenomena have been performed on awake behaving kittens that had multiple electrodes implanted in the visual cortex in 1986. The goal of these experiments was to follow the time course of experience dependent changes in the receptive field properties of cortical neurons following short periods of monocular deprivation [55]. During these experiments it was noted that groups of neurons which are recorded simultaneously and segregated spatially engaged in synchronous oscillatory activity when activated by visual stimuli. These oscillations suggested that the oscillations and their synchronization were due to internal neuronal interactions.

Motivated by the discovery of the synchronization phenomena more and more labs joined into the search for relations between cognitive and executive functions and the synchronization of oscillatory activity. Laboratories applying EEG- and MEG- recording methods provided rapidly growing evidence for a close relation between synchronous oscillatory activity in the beta- and gamma- frequency range and a variety of cognitive functions such as perceptual grouping focused attention,

maintenance of contents in short term memory, poly-sensory integration, formation of associative memories and sensory motor coordination (review in [75]).

This phenomenon is best seen in local field potentials (LFP) which reflect the synchronous activity of local groups of neurons in the first studies on synchronous gamma oscillations in the visual cortex. This led to a revival of studies exploiting the field potential recordings for the detection of synchronized activity in these studies. This performed by a number of laboratories, provided independent evidence from a variety of species (monkeys, cats, ferrets, rats, mice and birds). The cognitive and executive functions are often associated with the oscillatory patterning and the synchronization of the responses of neuronal groups. And it can occur over widely distributed networks.

Synchronous firing of two or more neurons is one mechanism for conveying information in a population correlation code, which means individual spikes do not encode independently of each other and correlation between spike times may carry additional information. Rhythmic oscillations of population activity provide another possible mechanism. Both synchronous firing and oscillations are common features of the activity of neuronal populations. Synchronization depends on the intrinsic mechanism of oscillation as well as on the nature of coupling.

From the evidence above, it appears that the oscillatory patterning of neuronal activity and the associated synchronization of discharges serve important functions for the computations performed by neuronal networks. The main effect of the oscillatory modulation of membrane potential is that it constrains the time interval during which cells are susceptible to excitatory input and can emit action potentials themselves. These effects of an oscillatory modulation of cell excitability can be exploited in many different ways in order to encode information and to define relations between the activity of spatially distributed neuron groups. When neuronal groups become entrained in synchronous oscillations, they will tend to emit spikes in synchrony

and this enhances the impact that these output signals will have on target cells. Synchronization can thus be used to select signals for further joint processing and to accelerate the propagation of the signals across distributed networks.

The discovery of synchronous oscillatory activity in the cerebral cortex has motivated a very large number of theoretical studies investigating the functional properties of networks consisting of coupled oscillators in neurobiology. These studies provided deep insights into both the mechanisms that sustain oscillations and their synchronization as well as the putative functions that can be accomplished by such networks with essentially non-linear dynamics. Thus, theoretical studies of such synchronization phenomena of coupled oscillators in neuronal networks is of fundamental importance for understanding highly integrated neural information processing in physiological nervous systems, such as learning, associative memory and consciousness [82, 60, 6, 37]. Synchronization phenomena also occur in a system of two reciprocally coupled oscillators. In order to better understand the dynamics of multi-neuron networks, it is important to fully examine the case of a two-cell network, particularly relevant in the study of central pattern generators which often contain sub-circuits composed of mutually inhibitory pairs of cells.

The rhythmic activity of coupled oscillators in networks results from an interplay of synaptic interactions and intrinsic membrane properties. Much of the theoretical work in this area uses the analysis of phase-coupled oscillators developed by Kuramoto [50]. The Kuramoto model was originally motivated by the phenomenon of collective synchronization, in which an enormous system of oscillators spontaneously locks to a common frequency, despite the inevitable differences in the natural frequencies of the individual oscillators. A useful approach method was pioneered by Winfree [92] on collective synchronization. He formulated the problem in terms of a huge population of interacting limit cycle oscillators and intuitively recognized that simplification would occur if the coupling were weak and the oscillators nearly identical. Using

numerical simulations and analytical approximations, Winfree discovered that such oscillator populations could exhibit the temporal analog of a phase transition. Kuramoto himself began working on collective synchronization in 1975. He used Winfree's intuition about phase models. Kuramoto [50] used the perturbation method of averaging to show that a model of weakly coupled oscillating neurons having nearly identical limit cycle can be reduced to a phase model, where each neuron is represented by a phase coordinate. The Kuramoto model is the simplest method in the phase approximation which describes the effect of a small forcing in the phase framework. [50]. The issue of stability and partially synchronized states is discussed by Strogatz [81].

When the coupling between oscillators is weak, synchronization and its stability can be analyzed using the well-known geometric phase-reduction approach and the method of averaging (reviewed in [50, 15, 16, 38, 42]). The general method to analyze synchronization is a phase resetting curve (PRC), also called a spike time response curve (STRC) in the weakly coupled neural oscillators. A phase resetting curve is measured by perturbing the oscillation with a brief stimulus at different times in its cycle and measuring the resulting phase-shift from the unperturbed period. The theory of weakly coupled neural oscillators [16] requires the infinitesimal PRC (iPRC), which is mathematically equivalent to the partial derivative of phase with respect to voltage, since generally only perturbations in voltage are considered and for weak coupling a perturbation in current can be assumed to be equivalent to a perturbation in voltage. Hansel et al. [35] identified two types of neural phase resetting curves corresponding to distinct bifurcation structures that determine the classification of excitable membranes.

The weak-coupling theory is very general in its applicability and powerful analysis, and for a homogeneous two-cell network predicts stable phased-locked firing, either

synchronous or anti-synchronous, depending on the properties of the coupling and the intrinsic dynamics of the oscillators [35, 86, 18].

For example, a variety of models shows that the weak coupling leads to stable antisynchronization in the case of excitatory synaptic coupling and stable synchronization in the case of inhibitory synaptic coupling if synaptic response is slower than the width of an action potential. Vreeswijk et al. [86] showed this using two identical integrate-and-fire (IF) neurons mutually coupled by identical excitatory or inhibitory synapses (see also Hansel et al [35]). They also show that this can be extended to any model that can be described by averaging as a phase-coupled model. Any pair of oscillators coupled with arbitrary synaptic dynamics can be reduced to a pair of phase equations if the interactions are sufficiently weak (see also [15]). In particular, the phase interaction function can be written as a convolution of the instantaneous interaction function with the synaptic response function. Using both the phase description and computer simulation, they show how inhibition and not excitation synchronizes two Hodgkin-Huxley model neurons. The results of both integrate-and-fire models and phase-coupled models apply to more accurate models provided that the synaptic rise time is not short. Sato and Shiino [72] also show anti-synchronous dynamics for excitatory coupling and synchronous dynamics for inhibitory coupling in the coupled IF model and the piecewise-linear (PL) version of FitzHugh-Nagumo (FHN) when the decaying relaxation rate of synaptic current is small and synaptic strength is not strong. They present these results by reconstructing a phase diagram in the parameter space of the strength and the decaying relaxation rate of synaptic couplings. The phase reduction method is also applied when neuron models of the PL and FHN types are mutually connected by weak couplings.

But this assumption of weak coupling may give rise to incorrect predictions if the coupling is not sufficiently small. Strongly coupled networks can exhibit a much richer variety of dynamic behaviors, but their analysis presents a much greater challenge,

as there is no general method of determining the stable modes of network activity in this case. However, in the case of pulsatile coupling which is lasting only briefly relative to the length of the unperturbed period, the dynamics of strongly coupled networks can be analyzed using Poincaré return maps for the inter-spike intervals, derived from the phase-resetting curves of the coupled cells [27, 94, 45, 48, 9, 1, 43]. The Poincaré firing map approach is also useful in the analysis of strongly coupled relaxation oscillators [80, 40, 70], and for networks of one-dimensional model cells such as integrate-and-fire units [56, 86, 4].

1.2 Background

1.2.1 Phase of Oscillation

Many physical, chemical, biological systems can produce rhythmic oscillations [94], which can be describe as a periodic orbit γ of a nonlinear dynamical system

$$x' = f(x), \qquad x \in R^m.$$

Let x_0 be an arbitrary point on γ, then any other point on the periodic orbit can be characterized by the time, θ, since the last passing of x_0. The variable θ is called phase of oscillation, and it is bounded by the period of oscillation T. The phase is often normalized by T or $T/2\pi$, so that it is bounded by 1 or 2π, respectively.

The phase of oscillation can also be defined outside γ using the notion of isochrons. Isochron is a set of points that relax to the same point on γ in the limit $t \to \infty$, i.e. a set of points with the same asymptotic phase value. The change of variables $\theta = \Theta(x(t))$ transforms the nonlinear system in a neighborhood of γ into a simpler phase model

$$\theta' = 1$$

1.2.2 Phase Model for Weakly Coupled Oscillators

Consider dynamical systems of the form

$$x' = f(x) + \epsilon S(t), \qquad x \in R^m \tag{1.1}$$

describing periodic oscillators, $x' = f(x)$, forced by a weak time-depended input $\epsilon S(t)$, e.g., from other oscillators in a network (for a Morris-Lecar neurons, $m = 2$ and $x = (V, w)^T$). The same change of variables transforms (1.1) into the phase model

$$\theta' = 1 + \epsilon \bar{\Delta}(\theta) \cdot S(t),$$

where the dot, "$\cdot$", denotes the dot product of two vectors; The vector function $\bar{\Delta}(\theta)$ is called *linear response function*, or *infinitesimal phase response curve (PRC)*. It can be found from the gradient of the phase transform, $\bar{\Delta}(\theta) = \text{grad}\ \Theta(x)$. Each component of vector function $\bar{\Delta}(\theta)$ describes the effect of perturbation in each of the components of x on the phase variable θ. In the case we consider, coupling is only through the voltage variable ($S(t)$ has only one component), and so the dot product can be replaced with the scalar product.

Let us treat $S(t)$ in (1.1) as the input from the network, and consider weakly coupled oscillators

$$x_i' = f_i(x_i) + \epsilon \sum_{j=1}^{n} S_{ij}(x_i, x_j), \quad x_i \in R^m. \tag{1.2}$$

The corresponding phase model

$$\theta_i' = 1 + \epsilon \bar{\Delta}_i(\theta_i) \cdot \sum_{j=1}^{n} S_{ij}(x_i(\theta_i), x_j(\theta_j)), \tag{1.3}$$

where each $x_i(\theta_i)$ is the point on the limit cycle having phase θ_i.

Introducing a rotating reference frame $\theta_i = t + \phi_i$ where the fast variable t is normalized to the resting period, one can transform the system above Eqs. (1.3) into

the form

$$\phi_i' = \epsilon\bar{\Delta}_i(t+\phi_i)\cdot\sum_{j=1}^{n} S_{ij}(x_i(t+\phi_i), x_j(t+\phi_j)).$$

Notice that the right hand-side is of order ϵ, reflecting the slow dynamics of phase deviations ϕ_i. Thus, it contains two time scales: fast oscillations (variable t) and slow phase modulation of phase (variable ϕ). The classical method of averaging, reviewed by Hoppensteadt and Izhikevich [38] consists in nearly identity change of variables that transforms this system into the phase model

$$\phi_i' = \epsilon\omega_i + \epsilon\sum_{j\neq i}^{n} H_{ij}(\phi_j - \phi_i), \tag{1.4}$$

where each function

$$H_{ij}(\phi_j - \phi_i) = \frac{1}{T}\int_0^T \bar{\Delta}_i(t)\cdot S_{ij}(x_i(t), x_j(t+\phi_j-\phi_i))dt$$

describes the interaction between oscillators, and each $\omega_i = H_{ii}(\phi_i - \phi_i) = H_{ii}(0)$ describes constant frequency deviation from the free-running oscillation.

1.2.3 Two Oscillators

Consider Eqs. (1.2) with n=2, describing two mutually coupled oscillators. Let us introduce "slow" time $\tau = \epsilon t$ and rewrite the corresponding phase model (1.4) in the form

$$\phi_1' = \omega_1 + H_{12}(\phi_2 - \phi_1)$$
$$\phi_2' = \omega_2 + H_{21}(\phi_1 - \phi_2)$$

where $' = d/d\tau$ is the derivative with respect to slow time. Let $\chi = \phi_2 - \phi_1$ denote the phase difference between the oscillators, then the two-dimensional system above

becomes one-dimensional

$$\chi' = \omega + H(\chi) = \omega + \frac{1}{T}\int_0^T \bar{\Delta}(t) \cdot S(t+\chi)dt \tag{1.5}$$

where $H(\chi) = H_{21}(-\chi) - H_{12}(\chi)$, $\omega = \omega_2 - \omega_1$, $\bar{\Delta}(t)$ is a linear PRC, and $S(t)$ is a synaptic variable.

If oscillators are identical, $\omega = 0$ and the $H(\chi)$ is an odd function (i.e., $H(-\chi) = -H(\chi)$), and $\chi = 0$ and $\chi = T/2$ are always equilibria, corresponding to the in-phase and anti-phase synchronized solutions. Then the stability of all equilibria of Eqs. (1.5) is determined by the sign of

$$H'(\chi) = \frac{1}{T}\int_0^T \bar{\Delta}(t) \cdot S'(t+\chi)dt \tag{1.6}$$

Equilibrium χ_{eq} is stable if $H'(\chi_{eq}) > 0$, and unstable otherwise. This integral in Eqs. (1.6) can be rewritten in terms of derivative of PRC, $\bar{\Delta}'(t)$, by integration by parts:

$$\begin{aligned} H'(\chi) &= \frac{1}{T}\left([\bar{\Delta}(t)S(t+\chi)]_0^T - \int_0^T \bar{\Delta}'(t)S(t+\chi)dt\right) \\ &= -\frac{1}{T}\int_0^T \bar{\Delta}'(t)S(t+\chi)dt \end{aligned} \tag{1.7}$$

The first term in right-hand side in first equality in Eqs. (1.7) vanishes because we consider the case of fast synaptic decay time, whereby the synaptic current $S(t+\chi)$ is shorter than intrinsic period T of each oscillator.

In other words, the stability of each equilibrium is determined by the slope of PRC. For example, synchronous firing is stable if $\bar{\Delta}'(t) < 0$ for $t \leq \tau_{syn}$ where τ_{syn} is synaptic decay time. This condition is satisfied for a weakly coupled network of Morris-Lecar (ML) model neurons. Since we are concerned with inhibitory networks of type-I oscillators, synaptic perturbation will always lead to a phase delay, so for convenience we introduce $\Delta(\phi) = -\bar{\Delta}(\phi) > 0$.

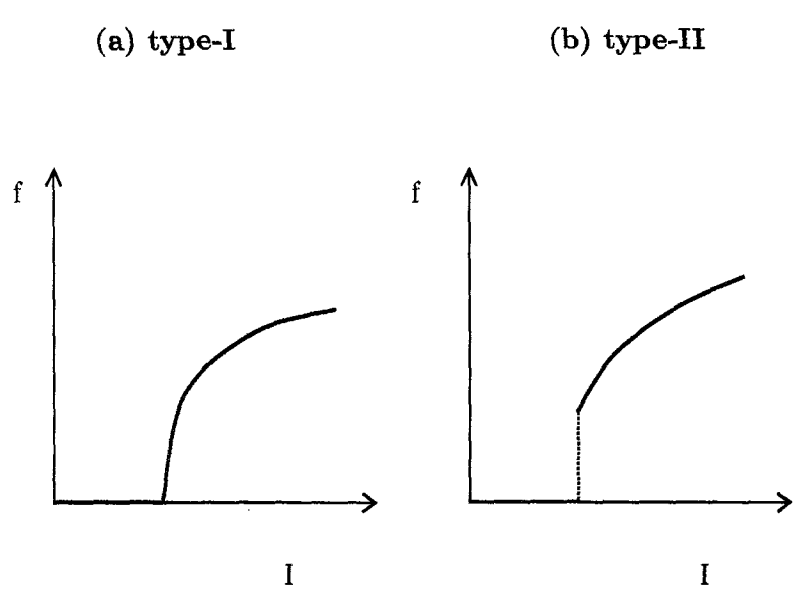

Figure 1.1 Frequency as a function of injected current for two different membrane models: (a) type-I model - the frequency f during a limit cycle oscillation is a continuous function of the applied current I (b) type-II model - the frequency f is a discontinuous function of applied current I.

1.2.4 Type-I Oscillator

Rinzel and Ermentrout [69] reviewed the classification of excitable membranes by Hodgkin (1948) in terms of their dynamics as a current is injected. There are two main types of excitable axons: type-I and type-II. Type-I membranes are characterized mainly by the appearance of oscillations with arbitrarily low frequency as current is injected whereas for type-II membranes, the onset of repetitive firing is at a nonzero frequency. The Connor model [11] and the Morris-Lecar model [57] (in a certain parameter range) are examples of type-I excitability. The Hodgkin-Huxley model is an example of type-II membranes.

The difference between these two models arises in the mechanism by which repetitive firing ensues. In "type-II" membranes, the following occurs: For low currents, there is a single equilibrium state and it is asymptotically stable. As the current increases, this state loses stability via a (subcritical) Hopf bifurcation and

repetitive firing ensues. By contrast in "type-I" membranes, there are three fixed points for currents below the critical current: a stable fixed point to the left, a saddle point in the middle, and an unstable fixed point to the right. If I (applied current) is increased, the V-nullcline moves upwards and the stable fixed point merges with the saddle and disappears. At the bifurcation point, there is homoclinic trajectory starting and ending at the fixed point which has an infinite period. It has zero frequency because it passes through the two merging fixed points (saddle-node) where the velocity of the trajectory is zero. If I is increased further, the saddle-node disappears, and the homoclinic orbit transforms into a periodic limit cycle. The velocity along the limit cycle close to the position of the fixed points is very low. Thus the onset of oscillation is continuous and occurs with zero frequency. Figure 1.1(a) and (b) show the frequency as function of injected current for the type-I membrane and for the type-II membrane, respectively.

Hansel et al. [35], have numerically shown that the phase resetting curve is strictly positive and as a consequence brief stimuli can only advance the oscillator. Ermentrout [18] showed that this is a general property of Type-I membrane models using singular perturbation methods and averaging.

CHAPTER 2

HOMOGENOUS NETWORK

2.1 Introduction

While recent work has revealed the synchronizing role of inhibitory synaptic interaction on the activity of many networks (reviewed in White et al. [91]), it is known that non-weak coupling can destabilize phase-locked dynamics [17]. For instance, many network models exhibit the transition to the "oscillator death" mode as the coupling strength is increased, whereby some of the neurons become trapped at a fixed point by the strong synaptic currents arriving from the active cell [16, 3]. Further, several recent studies explored the emergence of more complex non phase-locked states in the case of heterogeneous networks, whereby both neurons are active at different intervals of the oscillation period (see e.g. [91, 4]). In particular, recent work of Maran and Canavier [53] revealed that the assumption of preserved firing order does not hold in a network of Wang-BuzsáKB model neurons with type-I excitability [88]. They showed the emergence of 2:2 mode-locked states (see Figure 2.1(b),(c)), and examined the influence of heterogeneity and second-order phase resetting on this network activity state.

The goal of our work is to reveal the generality of such alternating-order firing (termed "leap-frog" spiking by G.B. Ermentrout, or "leader switching" by Acker et al. [1]) for inhibitory networks of type-I oscillators. In particular, we examine leap-frog dynamics observed in a network of simpler Morris-Lecar model neurons in a parameter regime corresponding to type-I excitability. This network exhibits synchronous firing for weak coupling, which is readily destabilized even by a moderate increase in coupling strength (Figures. 2.1 and 2.2). Our aim is to provide an intuitive geometric description of this activity state, by examining the features of the phase-

space trajectory of the two cells during spike-order switching. We show that leap-frog dynamics can arise in inhibitory networks of cells which are close to their excitation thresholds, under the additional condition of slow dynamics of membrane potential upon hyperpolarization. In the Morris-Lecar model we consider, such slow dynamics is caused by the fast closing of K^+ channels at hyperpolarized potentials, which leads to time-scale separation and associated trapping of the trajectory by the nullcline of the recovery variable. This allows even a moderate synaptic inhibition to retard the dynamics of the postsynaptic cell for a duration which is greater than the interval since the preceding spike of that cell, leading to the change of the spiking order.

An interesting aspect of the alternating-order spiking is that it cannot be obtained in a network of phase oscillators with instantaneous synaptic coupling, and that non-zero synaptic time constant is crucial for achieving leap-frog spiking in such networks. However, we show that order alternation can be obtained in a purely *pulse-coupled* network if the phase domain of each oscillator is augmented with an additional negative-value branch representing the strong suppression of the cell upon synaptic inhibition. For instance, we find that leap-frog spiking can also be achieved in a network of pulse-coupled quadratic integrate-and-fire model neurons. Further, such pulse-coupled augmented phase model network provides an accurate description for the dynamics of the Morris-Lecar model network. Following Maran and Canavier [53], we use the phase-resetting method to analyze leap-frog spiking on a quantitative level, and provide a simplified analysis of existence and stability conditions for leap-frog spiking for the case of identical cells. Restricting our consideration to a homogeneous network allows us to establish the most basic conditions on the phase-resetting properties necessary for leap-frog spiking.

We note that alternating-order firing was examined previously in homogeneous networks of two coupled relaxation oscillators with excitatory synapses by Bose et al. [2] and with inhibitory synapses by Sato and Shiino [72]. However, in both

works the stable phase difference between successive spikes of the two cells is much smaller than the width of an action potential. This is also true for the activity states explored by Maran and Canavier [53]. For this reason, earlier studies referred to the alternating-order spiking as a near-synchronous state. In contrast, here we show that the interval between the neighboring spikes of the two cells can constitute more than one half of the resting oscillation period. This is particularly true for the multiple-period leap-frog spiking, in which case the interval between the spikes of the two cells can reach 70% of the unperturbed period, and is an order of magnitude longer than the decay time of synaptic inhibition (see e.g. Figure 2.1(c) and Figure 2.2(a) when $\bar{g}_{syn} = 0.23$). Thus, alternating-order activity represents a distinct activity state that cannot be described as a near-synchronous state.

2.2 Model

We consider a pair of two identical model neurons with type-I excitability [69], each modeled as a Morris-Lecar oscillator [57]. Each cell possesses a periodic limit cycle trajectory corresponding to an action potential, which results from the interplay between the depolarizing calcium current I_{Ca} and the activation w of the repolarizing potassium current, I_K. The two cells are assumed to be identical, and are coupled by an inhibitory synaptic current, $I_{syn}(V, s)$:

$$\begin{aligned} C\frac{dV}{dt} &= -I_{Ca} - I_K - I_L - I_{syn}(V,s) - I_{app} \\ \frac{dw}{dt} &= (w_\infty(V) - w)/\tau_\infty(V) \\ I_{Ca} &= \bar{g}_{Ca} m_\infty(V)(V - V_{Ca}) \\ I_K &= \bar{g}_K w(V)(V - V_K) \\ I_L &= \bar{g}_L(V - V_L) \end{aligned} \tag{2.1}$$

where $C = 2\ \mu F/cm^2$ is the membrane capacitance, V is the cell membrane voltage in mV, t is time in ms, I_L is the passive leak current, and $I_{app} = -14\ \mu\text{A/cm}^2$ is

the applied current. The remaining parameters are $V_{Ca} = 120\text{mV}$, $V_K = -84\text{mV}$, $V_L = -60\text{mV}$, $g_{Ca} = 4\text{mS/cm}^2$, $g_K = 8\text{mS/cm}^2$, $g_L = 2\text{mS/cm}^2$.

The steady-state activation of calcium current is

$$m_\infty(V) = \frac{1}{2}\left[1 + \tanh\left(\frac{V+12}{18}\right)\right]$$

The potassium current activation amplitude and activation rate are

$$w_\infty(V) = \frac{1}{2}\left[1 + \tanh\left(\frac{V+8}{6}\right)\right]$$

$$\frac{1}{\tau_\infty(V)} = \frac{2}{3}\cosh\left[\frac{V+8}{12}\right] \tag{2.2}$$

Given this choice of model parameters, each of the two uncoupled oscillators exhibits periodic spiking with a period of about 45 ms. Note the fast approach of $\tau_w(V)$ to zero at hyperpolarized potentials (Eq. 2.2), whereby the trajectory overlaps the w-nullcline in the quiescent phase of the oscillation (see schematic representation of the limit cycle in Figure 2.4). The fast closing of the K^+ channels is a critical condition for achieving alternating-order spiking in the Morris-Lecar model. Such fast kinetics of the w variable can be somewhat relaxed without destroying the qualitative aspects of the dynamics, and alternating-order firing can also be achieved in the type-I parameter regime corresponding to Figure 7.7 of Rinzel and Ermentrout [69].

The two cells are coupled through the synaptic current given by

$$I_{syn} = \bar{g}_{syn} s(t)(V - V_{inh})$$

where $\bar{g}_{syn}$ is the maximum synaptic conductance and $V_{inh} = -80\ mV$ is the reversal potential. The dynamics of the synaptic gating variable $s(t)$ depends on the presynaptic cell potential, V_{pre}:

$$\frac{ds}{dt} = -\frac{s}{\tau_{syn}}\sigma(V_{th} - V_{pre}) + \frac{1-s}{\tau_\gamma}\sigma(V_{pre} - V_{th}) \tag{2.3}$$

where $V_{th} = -3$ mV is the synaptic threshold, $\sigma(\cdot)$ is a sigmoid function, $\sigma(x) = [1 + \tanh(4x)]/2$, and τ_{syn} and $\tau_\gamma = 0.2$ ms are the synaptic decay and rising time constants, respectively. We focus primarily on short synaptic decay times of about $\tau_{syn} = 1 - 5$ ms, and in Subsection 2.3.8 discuss the effect of longer τ_{syn}.

2.3 Two-Cell Network

2.3.1 Network Activity States

We start by exploring in detail the behavior of the system described by Eq. 2.1, the two identical ML model neurons with mutually inhibitory synaptic interaction. Figure 2.1 shows the diversity of behaviors exhibited by this network for different values of the maximal synaptic conductance, $\bar{g}_{syn}$, and the bifurcation diagram presented in Figure 2.2 demonstrates the transitions between the different activity states. For very small values of this coupling parameter, the two neurons fire in synchrony, as predicted by the weak coupling theory. When $\bar{g}_{syn}$ is increased, the synchronized state loses stability, and the network transitions to the alternating-order 2:2 mode-locked state shown in Figure 2.1(b), also referred to as "leap-frog" spiking by Maran and Canavier [53]. In this state, there is a stable non-zero time interval between the spikes of the two cells, with cells changing firing order in each cycle of the oscillation. For yet higher values of the coupling, the interval between consecutive spikes of the two cells alternates in each cycle between two distinct values, as shown in Figure 2.1(c). For higher still values of $\bar{g}_{syn}$, the alternating-order firing state undergoes a period-doubling cascade and gives way to chaotic firing in which the inter-spike intervals and the spiking order change irregularly. Further, for narrow ranges of $\bar{g}_{syn}$ values multi-spike $m : n$ alternating order firing states emerge, as shown in Figure 2.1(e), which represent a form of bursting. Finally, very strong coupling leads to the so-called "oscillator death" state shown in Figure 2.1(f), whereby the spiking of one

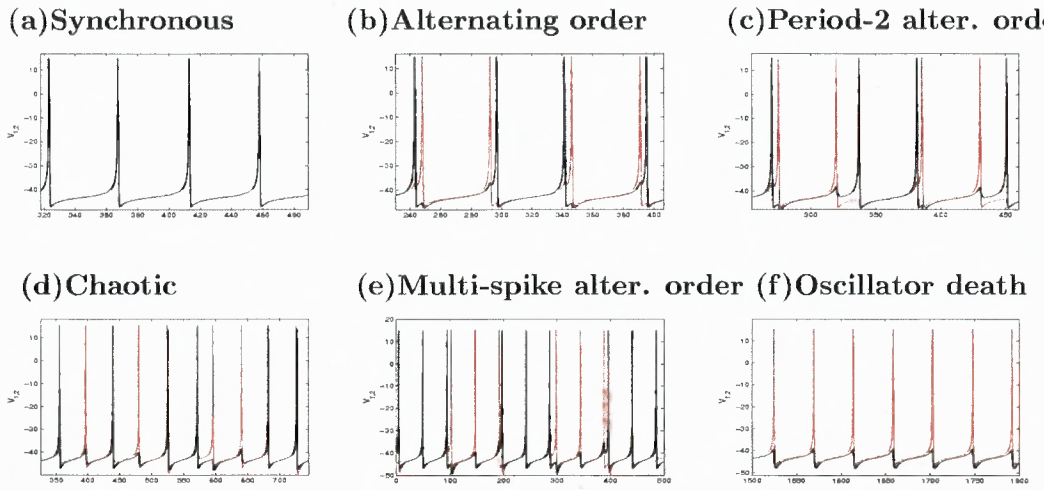

Figure 2.1 Network activity states at different values of coupling strength, $\bar{g}_{syn}$. The potentials of the two cells are shown as red and black traces, respectively. (a) Synchronous phase-locked firing ($\bar{g}_{syn} = 0.03$). The spiking period is close to the unperturbed period of 45 ms. (b) Alternating-order (leap-frog) spiking ($\bar{g}_{syn} = 0.17$) (c) Period-2 alternating-order spiking ($\bar{g}_{syn} = 0.22$) (d) Chaotic state, irregular inter-spike intervals ($\bar{g}_{syn} = 0.29$) (e) Bursting (3:3 alternating-order firing, $\bar{g}_{syn} = 0.34$) (f) Spike-suppress state ("oscillator death", $\bar{g}_{syn} = 0.5$)

neuron provides enough inhibition to completely prevent the spiking of the partner cell [16, 3].

Bifurcation diagram presented in Figure 2.2 explores the transitions between these different behaviors, showing the coupling-strength dependence of the asymptotic (equilibrium) intervals between two consecutive network spikes, which may or may not be the spikes of the same cell. These inter-spike intervals are normalized to the period of the uncoupled cell, and are denoted ISI_∞. The values of $\bar{g}_{syn}$ corresponding to each of the activity states shown in Figure 2.1 are marked by vertical dashed lines. Even though the set of ISI_∞ values does not fully characterize the network state, since it does not explicitly contain information about the spiking order of the two cells, it allows one to easily infer the dynamics at any given value of $\bar{g}_{syn}$. Note in particular that the presence of the value $ISI_\infty \approx 1$ indicates that at least one of the cell spikes twice in a row in each cycle, with negligible interference from the other cell.

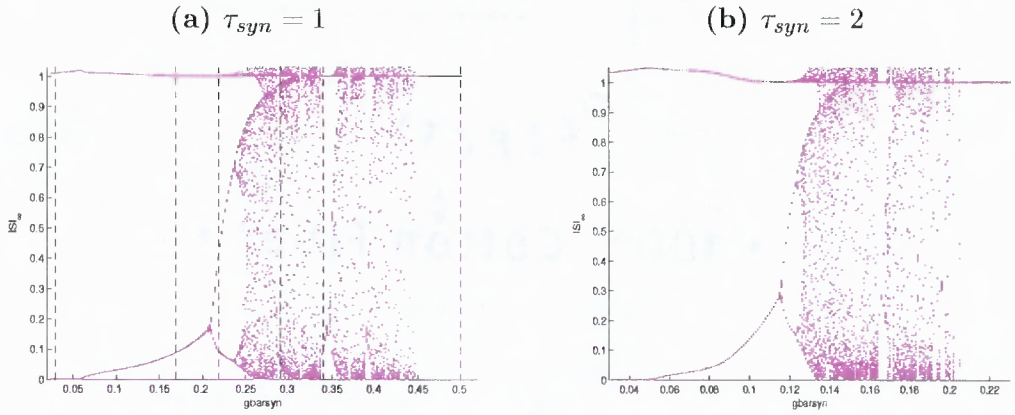

Figure 2.2 Bifurcation diagram of the Morris-Lecar model network. ISI_∞, the asymptotic values of the intervals between consecutive spikes (not necessarily spikes of the same cell) are plotted as a function of the coupling strength, $\bar{g}_{syn}$, for two values of synaptic decay time: (a) $\tau_{syn} = 1$ and (b) $\tau_{syn} = 2$. The dotted lines correspond to each of the six activity states in Figure 2.1(a)-(f). Note the difference in scale along the $\bar{g}_{syn}$ axis.

This is only possible if the cells change their firing order in each oscillation cycle. The fact that the interval between the spikes of the same cell in Figure 2.1(b)-(c) is close to the unperturbed period indicates that the second-order phase resetting is not crucial for the alternating order state, and that the first-order phase resetting dominates (cf. Maran and Canavier [53]). It is one of our main goals to provide a simple geometric explanation and quantitative analysis of the alternating-order spiking behavior seen in Figure 2.1(b)-(c), and to explain the period-doubling cascade evident in Figure 2.2.

Figure 2.2(b) presents the bifurcation diagram for a larger value of the synaptic decay time constant ($\tau_{syn} = 2$ as opposed to $\tau_{syn} = 1$ used in all the simulations in this paper), and demonstrates that the qualitative features of the network behavior are preserved for a range of τ_{syn} values. The main effect of prolonging synaptic decay is to increase the total amount of inhibition that each cell receives from its partner, thereby compressing the bifurcation diagram along the $\bar{g}_{syn}$ axis. The dynamics of the network undergoes a significant change only for values of τ_{syn} beyond about 6

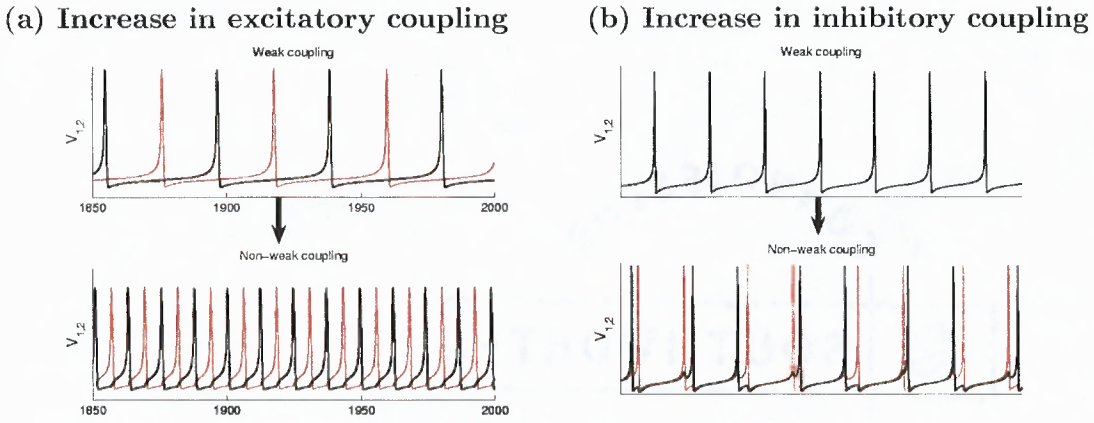

Figure 2.3 Effect of an increase in coupling strength on the stability of phase-locked firing in (a) an excitatory network, and (b) an inhibitory network. $\bar{g}_{syn}$ changes from 0.01 to 0.2 in both cases. In the case of excitation (a), anti-phase synchronous firing is stable for a wide range of coupling strength, while the phase-locked synchronous firing is readily destabilized in the case of mutual inhibition (b).

ms, or roughly 1/8 of the unperturbed period of 45 ms. The case of longer synaptic decay time is examined in Subsection 2.3.8.

2.3.2 Destabilization of Phase-Locked Firing: Comparison of Excitation and Inhibition

Given the type-I Morris-Lecar parameter regime we consider, the weak coupling theory predicts stable anti-synchronous and synchronous firing for excitatory and inhibitory synaptic coupling, respectively [86, 35, 18]. As demonstrated in Figure 2.3, this agrees with the dynamics exhibited by our model in the case of small synaptic conductance (top panels, $\bar{g}_{syn} = 0.01$). As the synaptic conductance is increased however, there is a qualitative difference between the stability of phase-locked firing in the case of excitation versus inhibition. Namely, the anti-synchronous state remains stable for non-weak excitatory coupling (see Figure 2.3(a)), but an increase in inhibitory coupling quickly destabilizes phase-locking and leads to the alternating-order state shown in Figure 2.3(b).

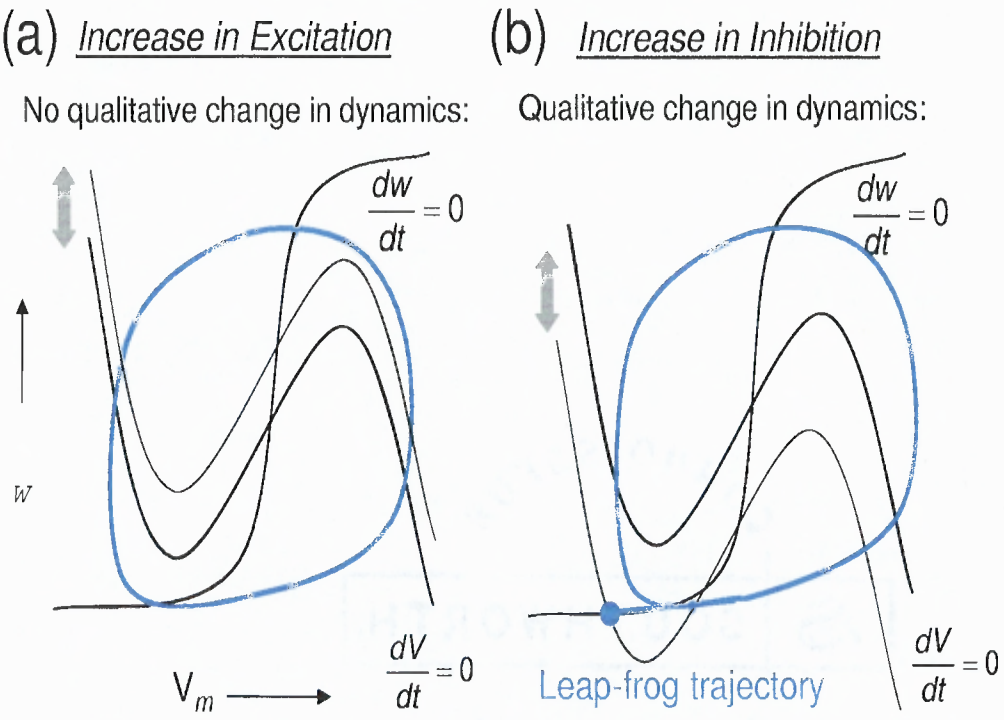

Figure 2.4 Effect of non-weak coupling on the phase-plane trajectory of the postsynaptic cell. Double arrows indicate the movement of the V-nullcline during each cycle of the network oscillation. (a) In the case of excitation, an increase in synaptic coupling causes no qualitative change in the phase-plane dynamics. (b) For sufficiently strong inhibition, the V-nullcline of the post-synaptic cell intersects the w-nullcline with each presynaptic input, pushing the cell below the excitation threshold and off the limit cycle trajectory. Thick blue curve indicates the trajectory of each cell during one cycle of the alternating-order spiking shown in Figure 2.1(b),(c). Note that the trajectory overlaps the w-nullcline during the hyperpolarized phase of the oscillation.

This difference between the effects of non-weak excitation and inhibition becomes obvious when one considers the phase plane dynamics of the system. Figure 2.4 illustrates schematically the effect of non-weak synaptic interaction on the phase-plane dynamics of the post-synaptic cell. Note that there is no qualitative change in the geometry for a wide range of excitatory conductances. However, an obvious qualitative change occurs when the inhibition strength becomes sufficiently strong to suppress the cell below its excitation through the saddle-node on the invariant cycle bifurcation [38]. If such suppression last for the entire period of the oscillation, the oscillator death occurs ("spike-suppress" state, Figure 2.1(f)). However, for intermediate strength of inhibitory coupling, the suppression occurs only for part of the oscillation period, resulting in a transient subthreshold trapping of each cell during each cycle of the oscillation. This may lead to the alternation of the firing order (Figure 2.1(b),(c)), whereby one cell is able to bypass its partner cell along the limit cycle by transiently keeping the other cell in the subthreshold "tail" branch of the trajectory, as depicted in Figure 2.5. Therefore, synchrony in networks of type-I oscillators can be destabilized even for moderate increase in inhibitory coupling.

Interestingly, we find that in the Morris-Lecar model network we consider, this leader-switch mechanism remains valid even in the limit of infinitely short synaptic current. This is the result of a fast approach of the trajectory to the w-nullcline at hyperpolarized potentials, as shown in Figures 2.4(b) and 2.5(b), which leads to the separation of time scales, with slow dynamics in the V direction, whereby the w-nullcline plays the role of the slow manifold of the system. A perturbation of sufficient strength along the slow manifold (the w-nullcine) allows to achieve a strong time delay which is longer than the time to the preceding spike. This condition is crucial for achieving leader-switching for infinitesimally short synaptic interaction. Such strong reset corresponds to an isochron that curls around the limit cycle, intersecting it at a position that is retrograde to the peak of the action potential, as shown in Figure

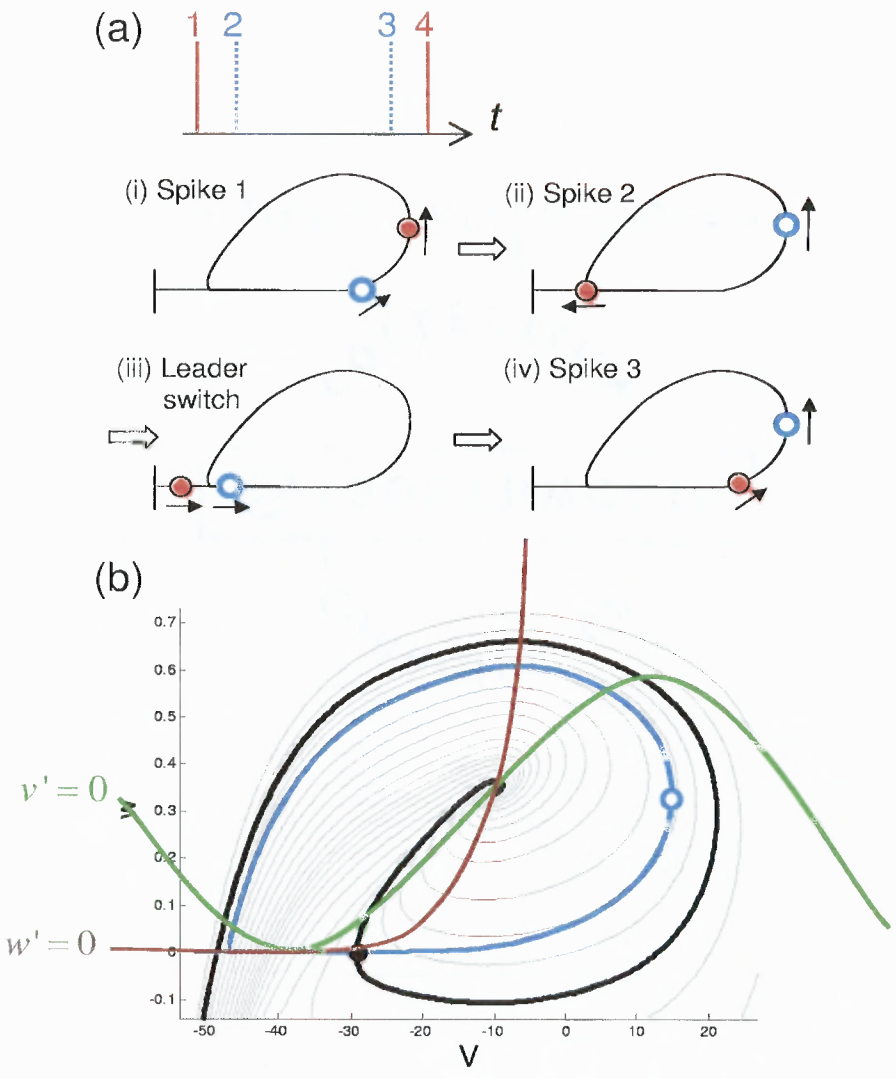

Figure 2.5 Phase-plane dynamics of the coupled Morris-Lecar model cells during periodic alternating-order spiking. (a) Tadpole-shaped curves represent the phase-plane trajectory in panel (b), schematically shown in Figure 2.4(b). The sequence of four panels describes the leap-frog spike sequence at the top, with filled red and open blue circles representing the two cells: (i) "red" cell spikes; (ii) "blue" cell spikes, pushing the "red" cell into the subthreshold branch of the trajectory (tadpole tail); (iii) "blue" cell bypasses the "red" cell along the unperturbed limit cycle trajectory; (iv) "blue" cell spikes again. The process then repeats itself, with the "red" cell emitting the next spike. (b) Isochron foliation of the limit cycle neighborhood. Thick blue curve labels the leap-frog trajectory, which partially overlaps the w-nullcline (not shown) at hyperpolarized values of potential. Note that an isochron corresponding to the hyperpolarized portion of the trajectory may intersect the limit cycle at a position (filled circle) which is retrograde to the peak of the preceding action potential (open circle).

2.5(b) (cf. discussion in Brown et al. [5]). This dynamical feature is closely linked to the cell's characteristic phase-resetting properties and the concept of negative phase, explored in the following subsections.

The mechanism described above has some generality and is not specific to the Morris-Lecar model cells that we consider. In particular, we believe that the same mechanism is at play in the network of Wang-BuzsáKB oscillators [88] studied by Maran and Canavier [53]. However, the existence and stability of this dynamical state must require certain conditions on the phase-resetting properties of the cells (implicitly described by the isochron pattern of Figure 2.5(b)), which will be established in Subsection 2.3.4.

2.3.3 Phase-Reduced Descriptions

Before we analyze the observed leap-frog spiking transition on a quantitative level in the next subsection, let us explore qualitatively the conditions required for the existence of this activity state. In particular, it is instructive to examine whether leap-frog firing can be obtained using a phase-reduced description of the coupled oscillators, with two phase variables ϕ_1 and ϕ_2 describing the position of each of the two cells along their unperturbed limit cycles. Note that this phase description is only possible in the weak-coupling limit, whereby the cells stay close to the limit cycle trajectory, and the phase value can be defined using the isochron foliation of its basin of attraction [94, 42]. Figure 2.6(a) schematically illustrates the phase plane trajectory of the 2:2 periodic alternating-order firing state in terms of the corresponding (ϕ_1, ϕ_2) variables in such a general phase-reduced description, not necessarily corresponding to the specific ML network that we examine. Here the right and top boundary values $(\phi_{1,2} = 1)$ correspond to the peak of an action potential of the respective cell. In the case of continuous synaptic interaction, the periodic trajectory is a continuous closed curve on the (ϕ_1, ϕ_2) torus, and its curvature is a measure of synaptic current that

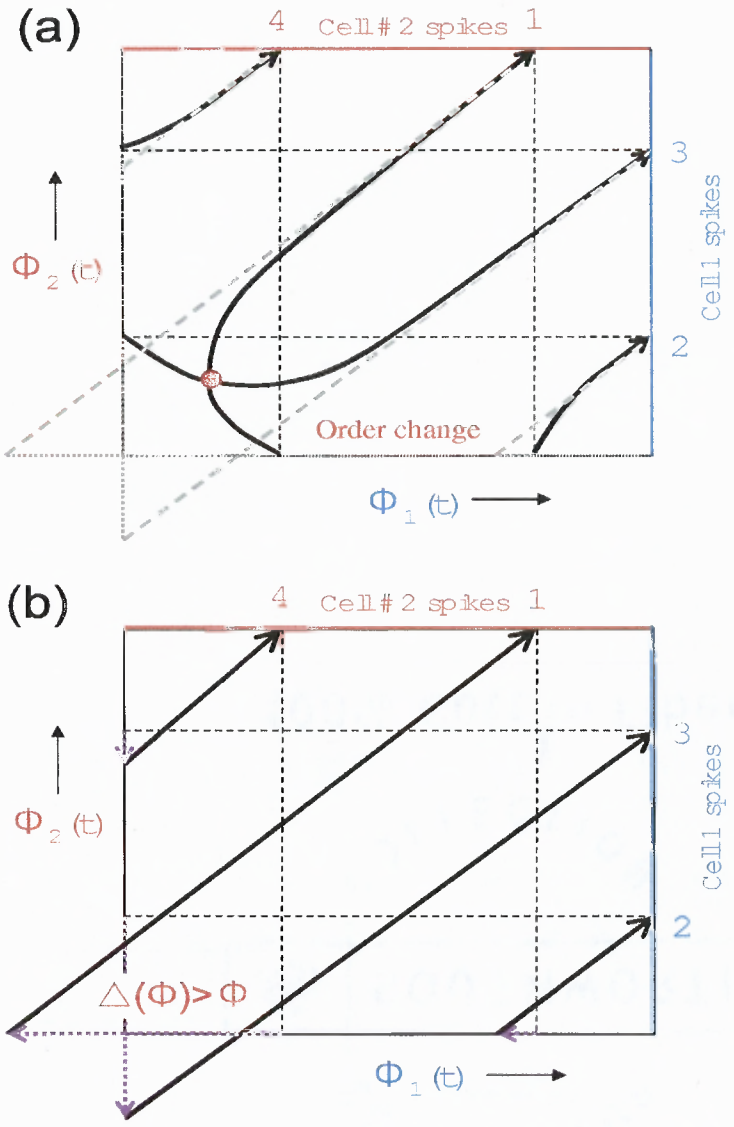

Figure 2.6 Reduced phase description of the alternating-order state. (a) In the model with continuous synaptic interaction, the alternating-order state describes a continuous trajectory on the 2-torus. The spike times of the two cells correspond to the intersections of the trajectory with the $\phi_1 = 1$ and the $\phi_2 = 1$ boundaries, respectively. The change in spiking order requires the trajectory to self-intersect. The dashed gray lines indicate the correspondence between the continuous coupling description and the pulse-coupled model description shown in (b). In (b), the spike of cell i ($\phi_i = 1$) causes a discontinuous drop (dashed arrow) in the phase of the partner cell j by amount $\Delta(\phi_j)$, where $\Delta(\phi)$ is the spike-time response characteristic of the cell, defined to be positive in case of a phase delay. The change in firing order requires the phase domain to be augmented with an additional negative value branch. In order for the spiking order to change, the spike-triggered phase delay $\Delta(\phi)$ should be greater than current phase ϕ during the first spike that a cell receives in one cycle of the oscillation.

deflects the trajectory from a straight line. Note that the trajectory would have to self-intersect on the 2-D surface of the torus in order for the cell spike order to change in each cycle of the oscillation. Therefore, the network exhibiting alternating-order firing cannot be described in terms of autonomous flow on the (ϕ_1, ϕ_2) torus. In particular, it cannot be obtained in the framework of the weak-coupling theory, which reduces network dynamics to such an autonomous flow (reviewed in [38, 69, 42]):

$$\begin{aligned} \dot{\phi}_1 &= 1 + \epsilon H_{12}(\phi_2 - \phi_1) \\ \dot{\phi}_2 &= 1 + \epsilon H_{21}(\phi_1 - \phi_2) \end{aligned} \tag{2.4}$$

Here $H(\phi)$ is the connection function that quantifies the weak synaptic interaction, averaging it out over one oscillation period. In the case of leap-frog spiking, this averaging cannot be performed since the phase perturbation in each cycle is not an infinitesimal quantity relative to the unperturbed oscillation period. The non-existence of alternating-order firing in a network of phase oscillators is a corollary of a more general theorem of Golubitsky et al. [32].

However, the phase topology of Figure 2.6(a) provides an entirely valid description of the 2:2 activity state if it is viewed as a projection of a higher-dimensional trajectory onto the (ϕ_1, ϕ_2) plane. The additional degrees of freedom could represent the two synaptic gating variables $s_{1,2}(t)$ that evolve according to Eq. 2.3 (*buffer* variables in the terminology of Golubitsky et al. [32]):

$$\begin{aligned} \frac{d\phi_1}{dt} &= 1 - \bar{g}_{syn}\Delta(\phi_1)s_2(\phi_2, t) \\ \frac{d\phi_2}{dt} &= 1 - \bar{g}_{syn}\Delta(\phi_2)s_1(\phi_1, t) \\ \frac{ds_1}{dt} &= \sigma(sin\phi_1)\frac{1 - s_1}{\tau_{rise}} - \frac{s_1}{\tau_{decay}} \\ \frac{ds_2}{dt} &= \sigma(sin\phi_2)\frac{1 - s_2}{\tau_{rise}} - \frac{s_2}{\tau_{decay}} \end{aligned} \tag{2.5}$$

where $\sigma(\phi)$ is a sigmoid spike thresholding function.

Thus, we conclude that the presence of synaptic degrees of freedom is crucial for achieving leap-frog firing in a network of phase oscillators. In particular, the non-zero synaptic decay time course is indispensable in order for such networks to exhibit the change in the firing order. In order to verify the phase description in Figure 2.6(a), we constructed its implementation involving two S^1 phase oscillators coupled by continuous synaptic gating variables, and observed leap-frog spiking for an appropriately chosen functional form of the interaction term (see Appendix B).

Although non-zero synaptic decay time is a crucial condition for leap-frog spiking in a network of phase oscillators, we find that this dynamical state can also be achieved in a purely pulse-coupled network of oscillators that are *not* phase oscillators on the S^1 phase domain. Figure 2.6(b) illustrates such a possibility, and can be viewed as the formal limit of the dynamics in Figure 2.6(a) with respect to shortening the duration of the synaptic current ("straightening out" the trajectory), while keeping fixed the total amount of phase resetting due to each spike. In this limit the synaptic interaction is no longer continuous, but becomes pulsatile (i.e., it can be described by a delta function). Although the descriptions in panels (a) and (b) are formally similar in terms of the spike sequence and the spike-time phase-resetting values, note that the latter description requires the extension of the phase domain to negative values, and therefore is not a true phase-reduced model. The negative phase value is induced when the spike-triggered phase delay is greater than the inter-spike phase difference between the two cells, i.e. $\Delta(\phi) > \phi$, where $\Delta(\phi)$ is the spike-time response curve, STRC (described below). Thus, the alternating-order firing state can be obtained in the framework of an extended phase model with instantaneous coupling, with no additional synaptic degrees of freedom, if the phase domain is supplanted with a negative value branch. In particular, in Subsection 2.3.7 we show that it can be obtained in a pulse-coupled network of quadratic integrate-and-fire cells. Alternatively, the dynamics in Figure 2.6(b) can be implemented by explicitly

prohibiting the model cell to spike again if its winding number is not increased since the preceding spike [5, 32]. Note however that in the latter case it would be impossible to independently define the magnitude of phase resetting caused by a second synaptic input that arrives while the postsynaptic cell is still in the negative-phase suppressed subthreshold state.

In the Morris-Lecar model network we consider, the synaptic decay time is short relative to the unperturbed limit cycle period, and the leap-frog spiking corresponds to the phase diagram of Figure 2.6(b) rather than Figure 2.6(a). In fact, the negative phase has a definite biophysical meaning in this case, and represents the transient suppression of a cell into the subthreshold branch of the trajectory (off the limit cycle) by the inhibitory input, as shown in Figs. 2.4(b) and 2.5, allowing the presynaptic cell to pass ahead, reversing the spiking order of the two cells.

2.3.4 Analysis of Existence and Stability of Periodic Alternating-Order Firing

Although Figures 2.5-2.6 explain qualitatively the dynamics of the alternating-order firing state, we turn to the phase return map approach to study it on a quantitative level. The return map analysis is a powerful method of describing the dynamics of a coupled network [94], but relies on several crucial assumptions. It requires that the cell's spike width and amplitude are invariant and are not affected by the afferent synaptic currents, and also assumes that the perturbation only affects the time to the next spike of the perturbed cell, and has no effect on the dynamics of the cell thereafter. However, this method can be extended to the case where perturbation affects several periods of the post-synaptic cell, under an additional assumption of linear summation of the phase resetting effects due to multiple presynaptic inputs. In fact, Maran and Canavier [53] demonstrated alternating-order firing in an inhibitory network of type-I Wang-BuzsáKB model cells in the presence of significant second

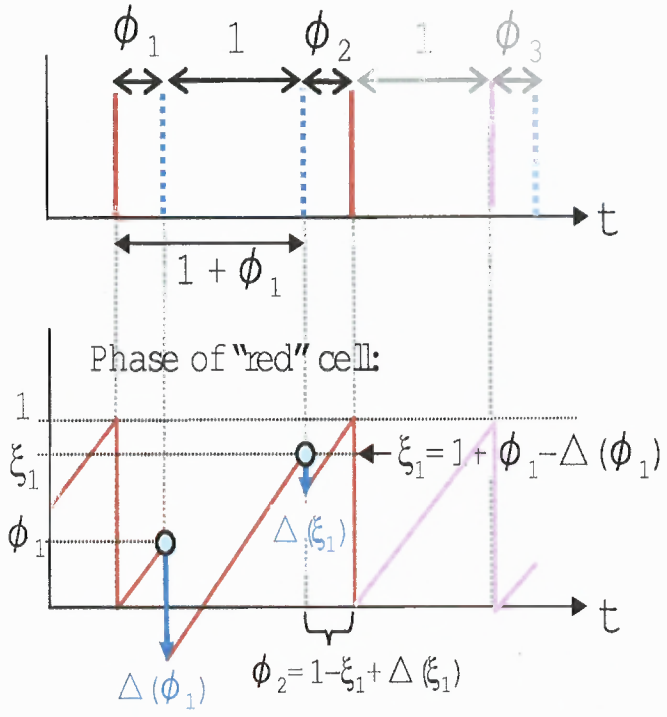

Figure 2.7 Constructing the inter-spike phase return map for the periodic alternating-order spiking, $\phi_2 = \Phi(\phi_1)$. In one cycle of the alternating-order spiking, one of the cells spikes twice between two spikes of the partner cell (dashed blue and solid red bars in top panel). The phase intervals ϕ_i are inter-spike intervals normalized by the unperturbed period of each oscillator. Bottom panel shows the phase time-course of the cell emitting the red spikes in top panel. Note that the phase difference between two dashed blue spikes equals 1 (the unperturbed period). The phase delays due to each of the two spikes (blue arrows) equal $\Delta(\phi_1)$ and $\Delta(\xi_1)$, where ξ_1 is the phase of the cell at the time of arrival of the second input, $\xi_1 = 1 + \phi_1 - \Delta(\phi_1)$. The second inter-spike interval ϕ_2 is found by the first-passage time condition $\xi_1 - \Delta(\xi_1) + \phi_2 = 1$, yielding the phase return map, Eq. 2.6

order phase resetting, although they also showed that alternation in the firing order could emerge in a pulse-coupled map without second-order resetting. We follow the approach of Maran and Canavier [53], but restrict ourselves to the special case of identical cells, with only first-order phase resetting.

The alternating-order firing is completely characterized by the inter-spike phase sequence labeled $\{\phi_1, \phi_2\}$ in Figure 2.7. Here we will construct the return map relating these alternating phase differences, using the phase-resetting curve, or the spike-time response curve (STRC) of each cell, $\Delta(\phi)$. We define $\Delta(\phi)$ to be positive if it produces a phase delay, and negative if it produces a phase advance, with $\phi = 0$ point defined as

the peak of the membrane potential, V. $\Delta(\phi)$ is computed numerically, by calculating the time between successive membrane potential maxima, while synaptic conductance pulses are applied at different positions of the model cell along the numerically reconstructed limit cycle. The applied perturbation represents a single spike of the presynaptic cell, and is defined numerically by recording the spike-triggered synaptic conductance, $s(t)$ in Eq. 2.3. Figure 2.8(a) presents the STRCs for three different values of the synaptic conductance parameter, g_{syn}, corresponding to the distinct activity states shown in panels (a)-(c) of Figure 2.1.

The phase return map derived here is a special case of a more general return map derived by Maran and Canavier [53]. Apart from simplifying the analysis, restricting ourselves to the case of a *homogeneous* network with only first-order phase resetting allows us to probe the most elementary conditions on the phase resetting properties required for the change in firing order. Our derivation can be viewed as complementary to the analysis of the order-preserving phase transition map by Goel and Ermentrout [27], since we explicitly break the map invertibility assumption adopted in that study (condition 2 on p. 199 therein), by allowing the phase variable to turn negative. The case of strong phase resetting was previously considered in the analysis of strongly coupled neurons by Acker et al. [1] (see also [43, 47, 58]), and in the study of strongly forced oscillators by Glass et al. [26].

Note that the homogeneous network case implies a permutation symmetry between the two neurons, which means that the map relating phases ϕ_2 and ϕ_1 in Figure 2.7 is identical to the map relating phases ϕ_3 and ϕ_2. Therefore, it is sufficient to analyze the phase dynamics of only one of the two cells, while it receives two spikes from its partner cell. Let ϕ_1 denote the phase of cell 1 (*red* spike and *red* trace in Figure 2.7) at the arrival time of the first synaptic current pulse due to the spike of the pre-synaptic cell (dashed blue line), where phase is defined as the time since the last spike, normalized to unperturbed oscillation period. The amount of phase delay

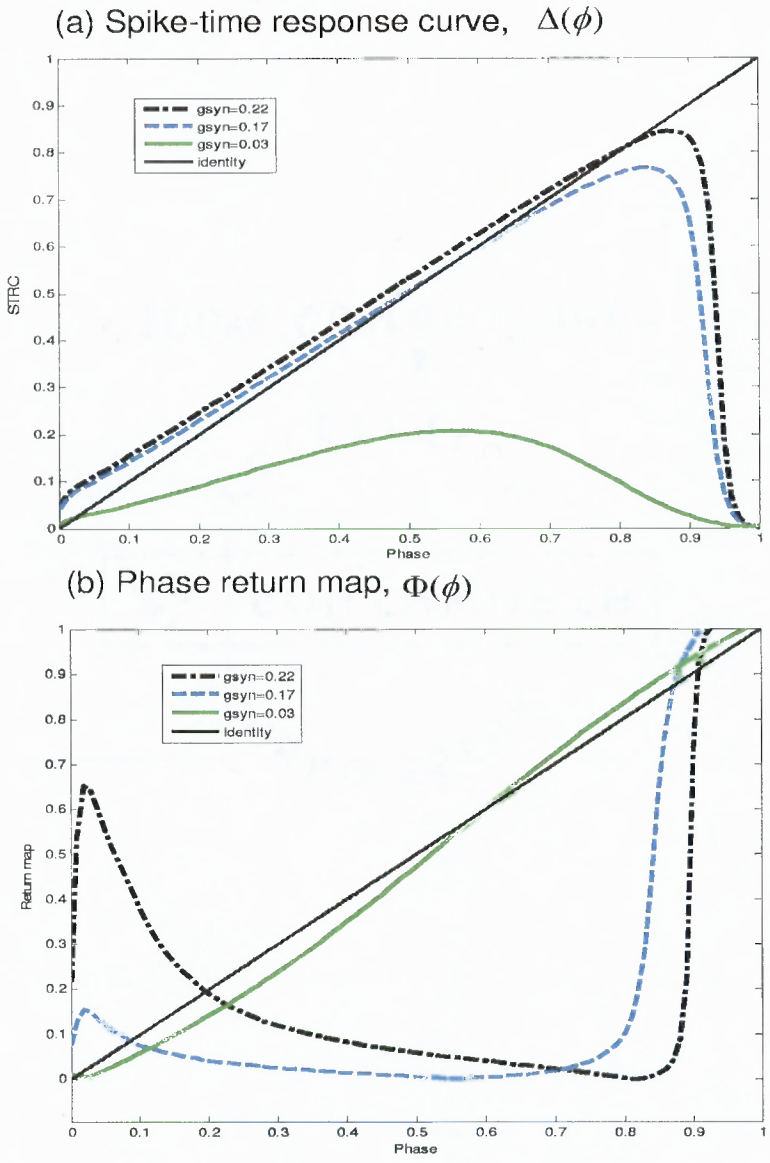

Figure 2.8 Phase resetting properties of the Morris-Lecar oscillator. (a) Numerically reconstructed STRC, $\Delta(\phi)$, for three different values of coupling strength corresponding to distinct activity patterns (a)-(c) of Figure 2.1. (b) Phase return maps for each of the three STRCs in panel (a); the intersections of each curve with the diagonal line represent fixed points of that map. For $g_{syn} = 0.03$, the order-preserving map is shown, with only one stable fixed point at $\phi = 0^+$ ($\phi = 1^-$), corresponding to synchronous firing. The two curves corresponding to $g_{syn} = 0.17$ and $g_{syn} = 0.22$ show both the order-alternating phase map (Eq. 2.6) on the phase interval where $\Delta(\phi) > \phi$, and the order-preserving map of Goel and Ermentrout (2002) on the portion of the phase domain where $\Delta(\phi) < \phi$. Note that there is one stable fixed point for $g_{syn} = 0.17$ corresponding to leap-frog spiking, while the alternating order fixed point for $g_{syn} = 0.22$ is unstable, leading to period-2 leap-frog dynamics shown in Figure 1(c). The order-preserving fixed point on the right end of the interval is unstable for both $g_{syn} = 0.17$ and $g_{syn} = 0.22$.

induced by the synaptic input at phase ϕ_1 equals $\Delta(\phi_1)$, since we define phase delay as positive phase resetting, contrary to the sign convention of Goel and Ermentrout [27]. For sufficiently strong synaptic inhibition this phase reset satisfies $\Delta(\phi_1) > \phi_1$ which delays the first passage time to next spike of the post-synaptic cell (cell 1) to a value greater than 1, the intrinsic (uncoupled) oscillation period. Note that this breaks the conditions on the STRC assumed by Goel and Ermentrout [27]. As a result, the pre-synaptic cell 2 has a chance to spike again (second dashed line), after a phase interval corresponding to the unperturbed oscillation period, $\Delta\phi = 1$, since cell 2 receives no input from cell 1 during this period. This second synaptic current from cell 2 arrives when the phase of cell 1 equals $\xi_1 \equiv 1 + \phi_1 - \Delta(\phi_1)$, which takes into account the delay due to the first spike. Therefore, the second spike induces a phase delay equal to $\Delta(1 + \phi_1 - \Delta(\phi_1))$. It is only after receiving this second input that cell 1 finally has a chance to spike, after a phase interval defined as ϕ_2. The total phase delay due to both inputs is thus equal to

$$\phi_1 + \phi_2 = \Delta(\phi_1) + \Delta(1 + \phi_1 - \Delta(\phi_1))$$

Therefore, the return map for the phase intervals ϕ_i is given by

$$\phi_2 \equiv \Phi(\phi_1) = \Delta(\phi_1) + \Delta(1 + \phi_1 - \Delta(\phi_1)) - \phi_1 \tag{2.6}$$

or, expressed in terms of the phase of the post-synaptic cell at the time of arrival of the second spike, $\xi_1 = 1 + \phi_1 - \Delta(\phi_1)$:

$$\phi_2 \equiv \Phi(\phi_1) = 1 + \Delta(\xi_1) - \xi_1 \tag{2.7}$$

Figure 2.8(b) shows this phase transition map for each of the three STRCs shown in panel (a). Note that this map is only defined on the phase domain where $\Delta(\phi) > \phi$. On the rest of the domain, Figure 2.8(b) shows also the order-preserving map of Goel and Ermentrout [27]. Fixed points of map (2.6)-(2.7) correspond to the periodic 2:2

alternating-order (leap-frog) activity:

$$\phi = 1 + \Delta(\xi) - \xi \tag{2.8}$$

Since $\xi \equiv 1 + \phi - \Delta(\phi)$, this condition can be written in a more symmetric form

$$\phi = \frac{\Delta(\phi) + \Delta(\xi)}{2} \tag{2.9}$$

Taking into account the constraint on the phase domains, $\xi \leq 1$ and $\Phi(\phi) \leq 1$, we also obtain

$$\Delta(\phi) > \phi \tag{2.10}$$

$$\Delta(\xi) < \xi \tag{2.11}$$

Conditions Eqs. 2.9-2.11 are examined geometrically in Figure 2.9. Note that the synchronous firing solution $\{\phi = 0^+, \xi = 1^-\}$ always satisfies the periodicity condition (2.9), if one assumes $\Delta(0^+) = \Delta(1^-) = 0$.

If the inequality $\xi \leq 1$ is violated (i.e. when $\Delta(\phi) < \phi$), the cells fire sequentially, so their firing order does not alternate, while the violation of the condition $\Phi(\phi) \leq 1$ (i.e. if $\Delta(\xi) > \xi$) indicates that the postsynaptic cell will emit more than two consecutive spikes. The latter is true for instance for $n{:}n$ bursting states with $n > 2$ (see Figure 1(d)), in which case one can derive an extended map analogous to Eq. 2.6: $\Phi(\phi) \equiv 1 - \xi_{n-1} + \Delta(\xi_{n-1})$, $\xi_n = 1 + \xi_{n-1} - \Delta(\xi_{n-1})$. An additional alternating-order constraint $\Phi(\phi) > 0$ requires that $\Delta(\xi) > -(1 - \xi)$. This condition is automatically satisfied if the resetting is sign-definite (pure delay resetting).

Stability of the 2:2 periodic spiking depends on the value of the derivative of the phase map given by Eq. 2.6 at equilibrium:

$$\Phi'(\phi) = [\Delta'(\xi) - 1][1 - \Delta'(\phi)] \tag{2.12}$$

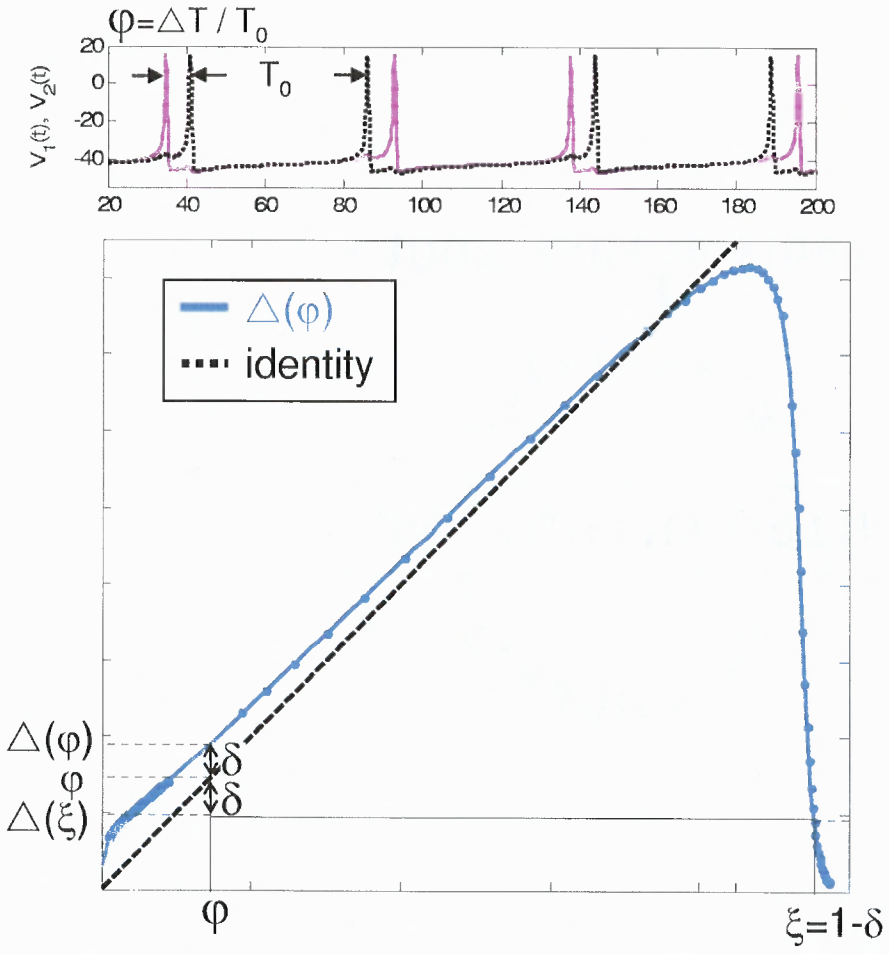

Figure 2.9 Phase-map analysis of alternating-order spiking. Top panel shows the cell potential time course of the two coupled ML oscillators as red and black traces, for $\bar{g}_{syn} = 0.2$. Equilibrium inter-spike phase difference ($\phi = 0.144$) in the alternating-order state satisfies Eq. 2.8. Note that $\delta = \Delta(\phi) - \phi = \phi - \Delta(\xi)$, where ξ is the phase of the postsynaptic cell at the time of arrival of the second spike, $\xi = 1 - \delta$. In this simulation, $\delta = 0.0468$, and $\Delta(1 - \delta) = 0.095$. The stability condition given by Eq. 2.12 is satisfied.

The fixed point will be stable if $|\Phi'(\phi)| < 1$. Therefore, the periodic alternating-order firing is stable when the slope of the STRC at the time of arrival of either of the two synaptic inputs (corresponding to phases ϕ and $\xi = 1 + \phi - \Delta(\phi)$) is sufficiently close to 1. This is equivalent to the stability condition derived by Maran and Canavier [53]. The stability of synchronous firing is determined by an analogous map slope expression, with $\phi = 0^+$ and $\xi = 1^-$ (Eq. 12 in [27]). Since $\Delta'(1) \approx 0$ in the Morris-Lecar model (see Figure 2.10), the bifurcation from synchronous to leap-frog firing occurs when the slope $\Delta'(\phi)$ at $\phi = 0$ becomes greater than 2, forcing ϕ to increase (and thus ξ to decrease) until the stability condition is satisfied. Thus, the characteristic sharp initial rise of $\Delta(\phi)$ followed by a less steep increase at larger ϕ, seen both in Figures 2.8(a) and 2.9 of this work, and in Figure 2(b) of Maran and Canavier [53], is essential for the transition from synchronous to leap-frog spiking. This feature corresponds to the characteristic dip to negative values in the phase transition return map noted by Maran and Canavier [53].

Finally, let's briefly consider the case where the intervals ϕ_1 and ϕ_2 between the spikes of the pre- and the post-synaptic cells alternate between two distinct values, as in Figure 2.1(c). We call this state the period-2 alternating-order 2:2 firing, since it results from the period-doubling of the equal-phase alternating-order state (Figure 2.2). Both ϕ_1 and ϕ_2 are period-2 fixed points of the map given by Eq. 2.8, i.e. $\Phi(\Phi(\phi_{1,2})) = \Phi(\phi_{2,1}) = \phi_{1,2}$, therefore

$$\begin{aligned} \Phi(\phi_1) &= 1 + \Delta(\xi_1) - \xi_1 = \phi_2 \\ \Phi(\phi_2) &= 1 + \Delta(\xi_2) - \xi_2 = \phi_1 \end{aligned} \tag{2.13}$$

where $\xi_i = 1 + \phi_i - \Delta(\phi_i)$, $i = 1, 2$.

We note that our choice of the "period-2" designation is somewhat arbitrary, since it can also be applied to the equal-phase leap-frog spiking: both of these states are characterized by a period-2 trajectory of each cell in its phase space, composed of

two unequal loops comprising one period of the oscillation (see Figure 2.5). Note also that the cell permutation symmetry does not hold in this case, and therefore this map is closer to the more general leap-frog spiking map derived by Maran and Canavier [53]. The stability of period-2 leap-frog spiking depends on the derivative of the map $F(\phi) = \Phi(\Phi(\phi))$ at equilibrium values ϕ_1 and ϕ_2: $\Phi'(\phi_2)\Phi'(\phi_1) = [\Delta'(\xi_1) - 1][1 - \Delta'(\phi_1)][\Delta'(\xi_2) - 1][1 - \Delta'(\phi_2)]$. We note that this stability conditions is equivalent to the stability condition for a sequential phase-locked mode obtained by Oprisan and Canavier [61] (see also [63]).

An important feature of higher-period 2:2 modes is the large value of the equilibrium inter-spike interval relative to the unperturbed period. In the ML network we consider, this interval can constitute as much as 70% of the uncoupled oscillation period (Figures 2.1(c) and 2.2), and is an order of magnitude larger than the time scale of synaptic interaction that underlie this dynamic state.

2.3.5 Second-Order STRC

Figure 2.10 shows that the second-order phase resetting $\Delta_2(\phi)$ is non-zero only for phase values close to 1, since the synaptic time constant is short ($\tau_{syn} = 1-2$ ms). For the two characteristic phases in Figure 2.9, the second-order phase resetting values equal $\Delta_2(0.144) \approx 0$ and $\Delta_2(0.9532) \approx 1.4 \cdot 10^{-4}$. Therefore, second-order resetting provides only negligible contribution to the alternating-order periodic firing shown in top panel of Figure 2.9. This is to be contrasted with the network of Wang-BuzsáKB model cells studied by Maran and Canavier [53], who showed that 2-nd order phase resetting provides a more significant, albeit not necessary, contribution to leap-frog spiking in that network.

Although the second-order phase resetting is not critical to achieving stable alternating-order activity, it will influence the critical value of $\bar{g}_{syn}$ at the bifurcation from synchrony to leap-frog spiking, since it affects the stability of both states. Noting

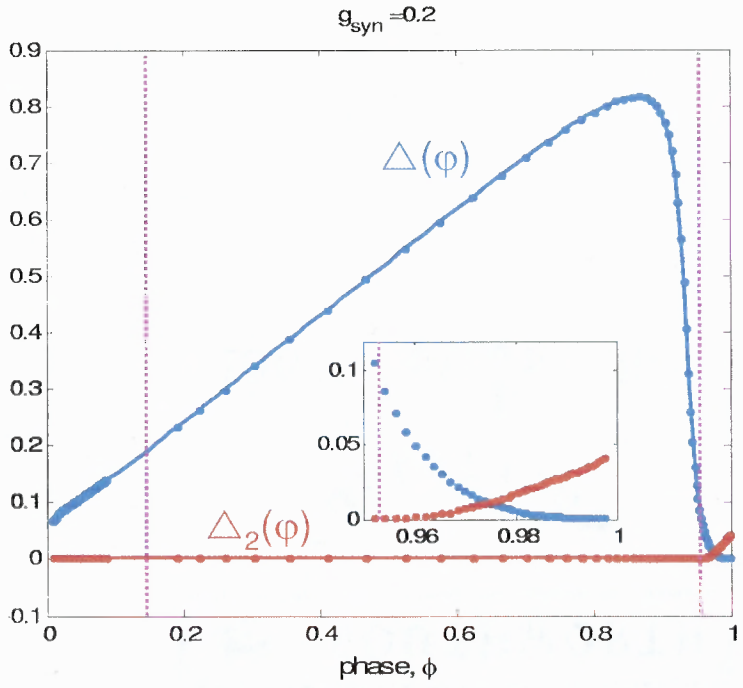

Figure 2.10 Comparison between the first- and the second-order spike-time response curves of the Morris-Lecar oscillator. The first-order STRC is shown in blue ($\Delta(\phi)$), while the second-order STRC is shown in red ($\Delta_2(\phi)$), for synaptic conductance of $\bar{g}_{syn} = 0.2$. The inset zooms in on the part of the phase domain where $\Delta_2(\phi)$ is non-negligible. The two functions satisfy the consistency condition $\Delta(0^+) = \Delta_2(1^-)$. Vertical dashed lines mark the two phase intervals characterizing the leap-frog state, ϕ and ξ in Figure 2.9. Note that $\Delta_2(\phi) = 0$, $\Delta_2(\xi) \simeq 1.4 \cdot 10^{-4}$, therefore second-order phase resetting does not contribute to the alternating-order dynamics for this value of coupling strength.

once again that the second-order phase-resetting is negligible for small values of the phase, we find that the map slope previously given by Eq. 2.12 is modified according to (see Appendix A for derivation):

$$\Phi'(\phi) = [\Delta'(\xi) - 1][1 - \Delta'(\phi)] + \Delta_2'(\xi) \tag{2.14}$$

In particular, synchronous firing is stable if

$$|[\Delta'(1^-) - 1][1 - \Delta'(0^+)] + \Delta_2'(1^-)| < 1 \tag{2.15}$$

Further, taking into account the small slope of the first-order STRC at $\phi = 1$ (see Figure 2.10), we obtain an approximate condition

$$|\Delta'(0^+) + \Delta_2'(1^-) - 1| < 1$$

Since both derivatives are positive, synchrony is stable if

$$\Delta'(0^+) + \Delta_2'(1^-) < 2 \tag{2.16}$$

Therefore, the bifurcation from synchronous to leap-frog spiking occurs when $\Delta'(0^+) + \Delta_2'(1^-) = 2$. The stability condition (Eq. 2.14) suggests that second-order phase resetting has a generally destabilizing effect on both synchronous and alternating-order activity. This agrees with our finding that stable alternating-order spiking cannot be achieved when τ_{syn} is comparable to the length of the uncoupled oscillation period (see Subsection 2.3.8).

2.3.6 Effect of Variation in Coupling Strength

Given the knowledge of the STRC, one can readily determine the stable network activity modes for the corresponding value of the coupling strength. However, the full range of activity states demonstrated in the bifurcation diagram of Figure 2.2 requires one to know the STRC at each value of the synaptic conductance. In the

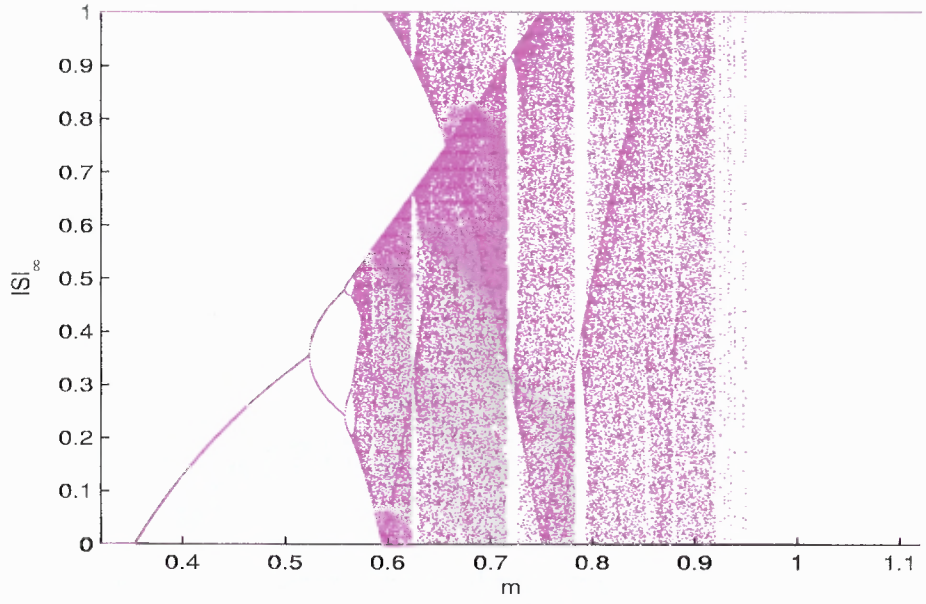

Figure 2.11 Emulated bifurcation diagram for the inter-spike (inter-event) interval differences as a function of the amplitude of a quadratic STRC, $\Delta(\phi) = 4m\phi(1-\phi)$. Asymptotic inter-spike interval differences ISI_∞ are plotted as a function of the STRC peak amplitude, m. Bifurcation from synchronous to alternating-order event sequence occurs at $m_{crit} = 2^{-3/2}$, while the oscillator death requires $m \geq 1$. Note that bursting dynamics similar to Figure 1(e) is also obtained, for instance for $m = 0.785$.

case of weak coupling, the STRC is assumed to scale linearly with the strength of the coupling, a condition which is violated in the case of non-weak interactions that we consider, as shown in Figure 2.8(a). In particular, the right-ward shift in the peak of the STRC curve evident in Figure 2.8(a) is a well-known feature of the Morris-Lecar model [18]. The question then arises whether this change in the shape of the STRC has a qualitative effect on the bifurcation structure of the network dynamics shown in Figure 2.2, or whether this bifurcation structure describes a stereotypical period doubling cascade, representing universal behavior expected for a large class of STRC functions with respect to a simple scaling of their amplitudes.

To verify the generality of the observed leap-frog spiking and the associated bifurcation structure, we considered the case of a quadratic STRC defined as $\Delta(\phi) =$

$4m\phi(1-\phi)$. Note that the STRC of this shape agrees with the existence conditions for leap-frog spiking, illustrated in Figure 2.9, as does any continuous function with a sharp initial rise and downward concavity at small phases, and decaying to zero as the phase approaches 1^-. We employed the "emulator" algorithm introduced by Canavier et al. [9] to artificially generate the "inter-spike" phase sequence,

$$\phi_{n+1} = \Delta(\phi_n) + \Delta(1 + \phi_n - \Delta(\phi_n)) - \phi_n$$

for the quadratic STRC, and explored the effect of increasing the STRC amplitude, m. We verified that the entire bifurcation structure of the ML network dynamics is reproduced by the quadratic STRC emulator, and is presented in Figure 2.11 (cf. Figure 2.2). Note that the map amplitude corresponding to the bifurcation from synchronous to alternating-order firing can be obtained analytically for the case of quadratic PRC, using Equation 2.12: $\Phi'(0) > 1$ for $m > m_{crit} = 2^{-3/2}$ (see Figure 2.11). The bifurcation to the oscillator death is also easily analyzed, and occurs at $m = 1$. Finally, the bursting states such as the one shown in Figure 1(e) are also obtained using the quadratic STRC. Although it is well-known that the iteration of a quadratic map leads to a period-doubling cascade and chaos, these results are of value in proving that the alternating-order firing is a general phenomenon for models characterized by STRC of a given shape, and that the observed bifurcation structure is explained by the change in STRC amplitude only, and does not require a change in the shape of the STRC characteristic of the Morris-Lecar oscillator.

2.3.7 Alternating-Order Spiking in a Pulse-Coupled Network

As discussed in Subsection 2.3.3, leap-frog spiking can be achieved in a purely pulse-coupled network if the coupled cells do not represent phase oscillators, but include an additional subthreshold branch, implemented for instance by augmenting the standard S^1 phase domain with a negative phase value interval, leading to the dynamics

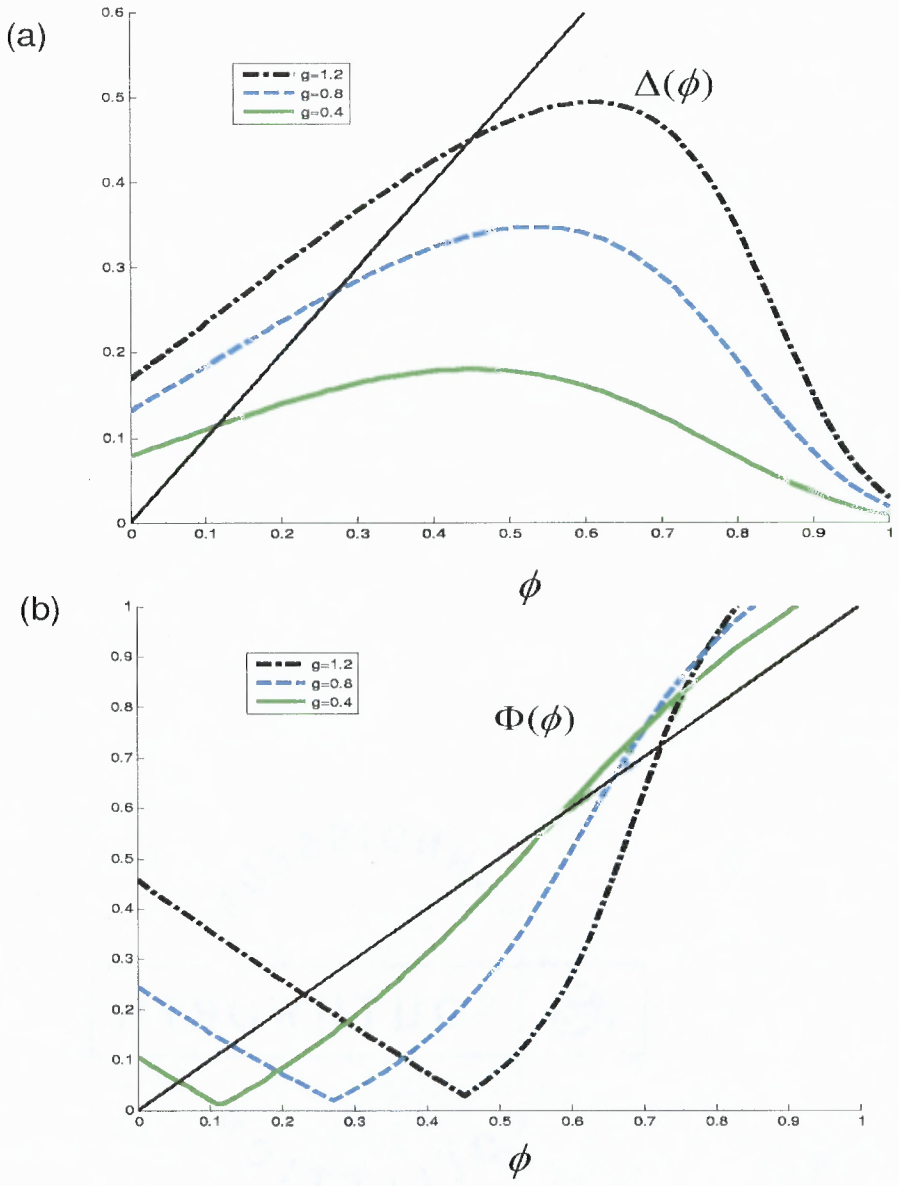

Figure 2.12 Phase-resetting analysis of a pulse-coupled network of two quadratic integrate-and-fire cells, $dv_i/dt = v_i^2 + 1 - g\ \delta(t - t_j)$, with asymmetric threshold and reset values, $v_t = 5$ and $v_r = -1$ (a) STRCs for pulse amplitude values of g=0.4, 0.8, and 1.2 are given by $\Delta(\phi) = \phi + [\arctan v_r - \arctan(\tan(T\phi + \arctan v_r) - g)]/T$, where $T = \arctan v_t - \arctan v_r$ is the oscillation period. (b) Phase return maps corresponding to each of the STRCs shown in (a). As in Figure 2.8, each of the three curves switches from order-alternating to order-preserving map at point $\phi = \Delta(\phi) = [\pi/4 + \arctan(g - 1)]/T$. For each value of g, there is one stable leap-frog spiking fixed point, and one unstable fixed point corresponding to phase-locked order-preserving dynamics. The equal-phase (period-1) leap-frog spiking is stable for $g < 4/3$.

in Figure 2.6(b). This negative-phase branch represents the tail of the "tadpole"-shaped trajectory shown in Figure 2.5(b). The topology of such an extended phase model is in fact equivalent to the topology of an integrate-and-fire class of models, as noted by Golubitsky et al. [32]. If a given IF model includes a finite reset potential, then the interval between such reset value and the threshold potential can be identified with an S^1 phase domain. However, an inhibitory perturbation of sufficient strength can lower the voltage of a cell below the reset value, which can be viewed as a negative phase.

Since the standard integrate-and-fire model is characterized by a monotonically increasing STRC with downward concavity [56], it does not satisfy leap-frog firing existence conditions, Eqs. 2.9-2.11. However, the *quadratic* integrate-and-fire model (QIF) is a more promising candidate, due to its close association with the canonical model of type-I SNIC excitability bifurcation ([16, 18, 38]). In order to satisfy the leap-frog existence conditions, we modify the standard non-dimensionalized QIF model, $dv/dt = v^2 + 1$, by assuming finite threshold and reset values, which we set asymmetrically to $v_t = 5$ and $v_r = -1$, respectively, in order to obtain an STRC shown in Figure 2.12(a). This STRC shares the characteristic shape of the STRC of the Morris-Lecar model shown in Figs. 2.8 and 2.9, and therefore it too satisfies the leap-frog spiking conditions, Eqs. 2.9-2.11. Figure 2.12(b) shows the corresponding phase return map for the three different values of pulse amplitude, illustrating both the order alternating and the order preserving maps. For each of the three chosen values of the coupling strength, the order-alternating state is stable. Although a finite threshold value is not necessary for achieving alternating-order firing, note that a finite reset value is crucial for creating a multi-branched phase domain.

2.3.8 Effect of Increasing Synaptic Decay Time

The dynamics of the two-cell network that we study undergoes a qualitative change as the synaptic decay time is increased beyond short durations of 1-4 ms. Namely, we observe emergence of bistability between synchronous spiking and alternating-order dynamics, and a narrower domain of stability of the alternating-order state, which disappears completely when the synaptic decay time becomes longer than about 1/6 of the unperturbed oscillations period in our ML model. Note that bistability between synchrony and leap-frog spiking was also observed by Maran and Canavier [53] in the Wang-BuzsáKB model network. This change in dynamics can be understood in terms of the measured changes in the first- and second-order STRC, shown in Figure 2.13. The two panels (a) and (b) of this Figure also present the phase return map, $\Phi(\phi)$, for synaptic decay times of 6 and 7 ms, respectively. Note that the second-order STRC becomes more pronounced at larger τ_{syn}, which is associated also with an increase in non-zero value of the 1-st order STRC at zero phase. Therefore, the second-order STRC cannot be ignored, leading to the modified stability conditions, Eq. 2.14, derived in the Appendix (Eq. A.6) and approximated as $\Delta'(\phi) + \Delta_2'(\xi) < 2$ (Eq. A.7). Note that the increase in $\Delta(0^+)$ is associated with a decrease in the initial slope of the STRC at longer synaptic decay time, as is evident in Figure 2.13 (cf. Figure 2.8). This leads to stable synchronous firing, achieved when $0 < \Delta'(0^+) + \Delta_2'(1^-) < 2$ (Eq. 2.16), and results in the bistability between synchronous and leap-frog spiking, captured by the alternating-order phase return maps shown in Figure 2.13.

Finally, we note that the STRC analysis is not applicable if the synaptic decay time is large enough to be comparable in duration to the interval between incoming spikes.

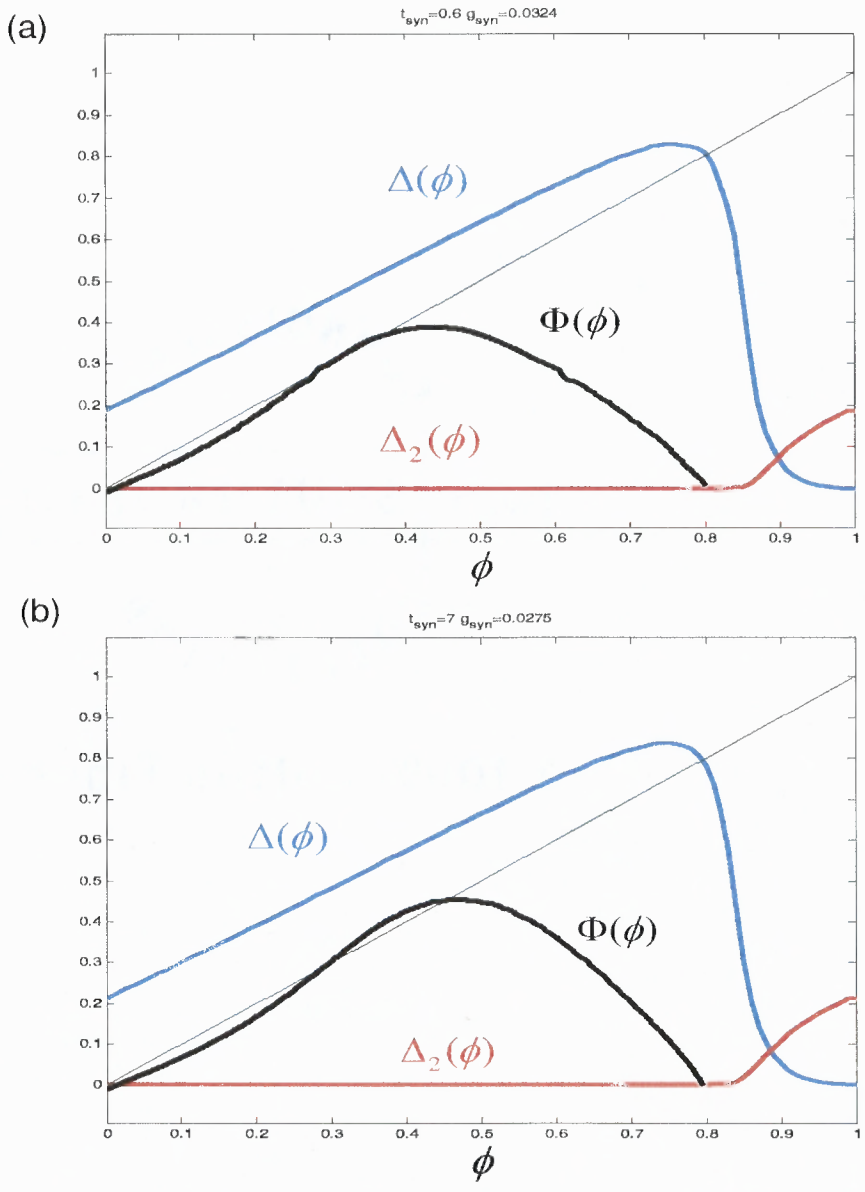

Figure 2.13 Longer synaptic decay leads to bistability between synchronous and leap-frog dynamics. Each of the two panels shows the first-order STRC ($\Delta(\phi)$, blue), second-order STRC ($\Delta_2(\phi)$, red) and the phase-return map (black) for $\tau_{syn} = 6$ ms in (a) and $\tau_{syn} = 7$ ms in (b). Note the two stable and one unstable fixed points for each τ_{syn}, with one stable equilibrium at the origin, corresponding to synchronous firing, and another stable fixed point corresponding to leap-frog spiking.

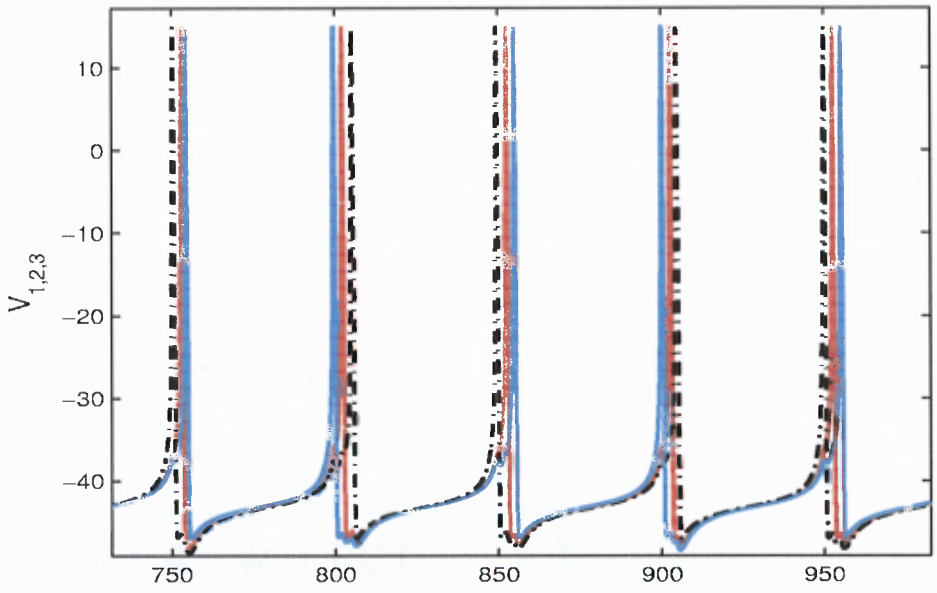

Figure 2.14 Network of three all-to-all coupled ML oscillators exhibits splay states in a certain range of synaptic coupling strength ($\bar{g}_{syn} = 0.14$). The potentials of the three cells are shown as black, red, and blue traces. Note the change in spiking order: 1,2,3 → 3,2,1 → 1,2,3 → ...

2.4 Three-Cell Network

In order to explore the effects of non-weak inhibitory coupling in a larger network, we simulated the dynamics of three identical neuron with all-to-all coupling, and observed a diversity of network behaviors that are analogous to the activity states exhibited by a two-cell network. As the coupling strength ($\bar{g}_{syn}$) is increased, the synchronized state becomes unstable, giving way to the alternating order state shown in Figure 2.14, which is followed by a period-doubling cascade to chaotic activity, and at sufficiently strong value of the coupling we observe the transition to the oscillator death mode. Note that in the three-neuron network, the alternating order state represents a splay state (Figure 2.14). Our results are in agreement with the results of Maran and Canavier [53] for the heterogeneous network of Wang-BuzsáKB model neurons. Larger networks of up to ten neurons were examined by Maran and Canavier

[53], who described similar activity states, with an additional property of clustering, whereby distinct synchronized subgroups of neurons fire in a splay-state temporal order (see Figure 12 therein).

2.5 Classification of STRC Shapes Leading to Alternating-Order Firing

We found that the alternating-order dynamics exhibited by the Morris-Lecar model network can be explained by the particular shape of the STRC characterizing each of the two cells. The question then arises about the generality of such order-alternating dynamics. Here we examine the general conditions on the shape of STRC of coupled oscillators that leads to leader switching based on phase return map.

For the existence for alternating-order firing, $\Phi(\phi) = \phi$ should have at least one solution in $(0, 1)$ where $\Phi(\cdot)$ is a phase return map defined in Subsection 2.3.4. Let

$$F(\phi) \equiv \Phi(\phi) - \phi = \Delta(\phi) + \Delta(1 + \phi - \Delta(\phi)) - 2\phi = 0 \tag{2.17}$$

where $\Delta(\cdot)$ is a STRC.

We assume that STRC is continuous in $[0, 1]$. Then we use the Intermediate-value theorem to find the condition on STRC that the function F in Eq. 2.17 has at least one root, satisfying the existence conditions, Eq. 2.9-2.11. We classify the condition without requiring the existence of the second derivative of STRC, $\Delta''(\cdot)$, in several cases:

2.5.1 Case of One Root of $\Delta(\phi) = \phi$

Let ϕ_c be the single solution of $\Delta(\phi) - \phi = 0$ in $(0, 1)$, i.e. $\Delta(\phi_c) = \phi_c$, and suppose that STRC satisfies the condition $\Delta(\phi) > \phi$ for $0 < \phi < \phi_c$ (see Figure 2.15), which means the root of function F should be in $(0, \phi_c)$ if the alternating-order firing exists. Let ψ be the root of F when it exits, and use the expression of $\xi_\psi = 1 + \psi - \Delta(\psi)$ for the phase of post-synaptic cell at the time arrival of the second synaptic input as

in Subsection 2.3.4. Then we need $\Delta(\xi_\psi) < \xi_\psi$ from the condition Eq. 2.11 which is equivalent to

$$\phi_c < 1 + \psi - \Delta(\psi)$$

Since $\psi < \phi_c$, this inequality leads to the following condition, satisfied for all cases we consider below:

$$\Delta(\psi) < 1 \tag{2.18}$$

for $\psi \in (0, \phi_c)$.

Case 1 $\Delta(1) < \phi_c$

For $\phi = \phi_c$, we have

$$F(\phi_c) = \Delta(1) - \phi_c < 0$$

If $F(0) = \Delta(0) + \Delta(1 - \Delta(0)) > 0$ then there exists at least one non-zero root of F in $(0, \phi_c)$. Taking into account the constraint on the phase domains, $0 \leq 1 - \Delta(0) \leq 1$, it is equivalent to $0 \leq \Delta(0) \leq 1$. We consider three subcases depending on STRC value at two end points of phase domain, 0 and 1.

1. $\Delta(0) = \Delta(1) = 0$.

   Since $F(0) = 0$, we need another condition with $F'(0) > 0$ to show that F has at least one non-zero root in $(0, \phi_c)$. This is equivalent to

$$(\Delta'(0) - 1)(1 - \Delta'(1)) > 1 \tag{2.19}$$

If we consider a symmetric STRC, we can find the more specific condition since $\Delta'(1) = -\Delta'(0)$:

$$\begin{aligned} F'(0) &= \Delta'(0) + \Delta'(1)(1 - \Delta'(0)) - 2 \\ &= \Delta'(0) - \Delta'(0)(1 - \Delta'(0)) - 2 \\ &= \Delta'(0)^2 - 2 > 0 \end{aligned} \tag{2.20}$$

So if $\Delta'(0) > \sqrt{2}$ then F has at least one non-zero root in $(0, \phi_c)$. In other words, the symmetric STRC satisfying Eq. 2.20 can generate alternating-order firing in $(0, \phi_c)$. In particular, a simple quadratic function represented by $\Delta(\phi) = 4m\phi(1 - \phi)$ has alternating-order spiking if $m > \frac{\sqrt{2}}{4} \approx 0.3536$ which is same as the $m_{crit} = 2^{-3/2}$ bifurcation from synchronous to alternating-order event sequence shown in Subsection 2.3.6 and Figure 2.11

2. $\Delta(0) = 0$ and $\Delta(1) \neq 0$.

   We have $F(0) = \Delta(0) + \Delta(1 - \Delta(0)) = \Delta(1)$, which should be greater than 0 to generate alternating-order firing. So we need following condition:

$$\Delta(1) > 0 \tag{2.21}$$

3. $\Delta(0) \neq 0$.

   From $F(0) = \Delta(0) + \Delta(1 - \Delta(0))$, a STRC needs the lower bound at $1 - \Delta(0)$ to generate alternating-order firing:

$$\Delta(1 - \Delta(0)) > -\Delta(0) \tag{2.22}$$

Case 2 $\Delta(1) > \phi_c$.

For $\phi = \phi_c$, we have

$$F(\phi_c) = \Delta(1) - \phi_c > 0$$

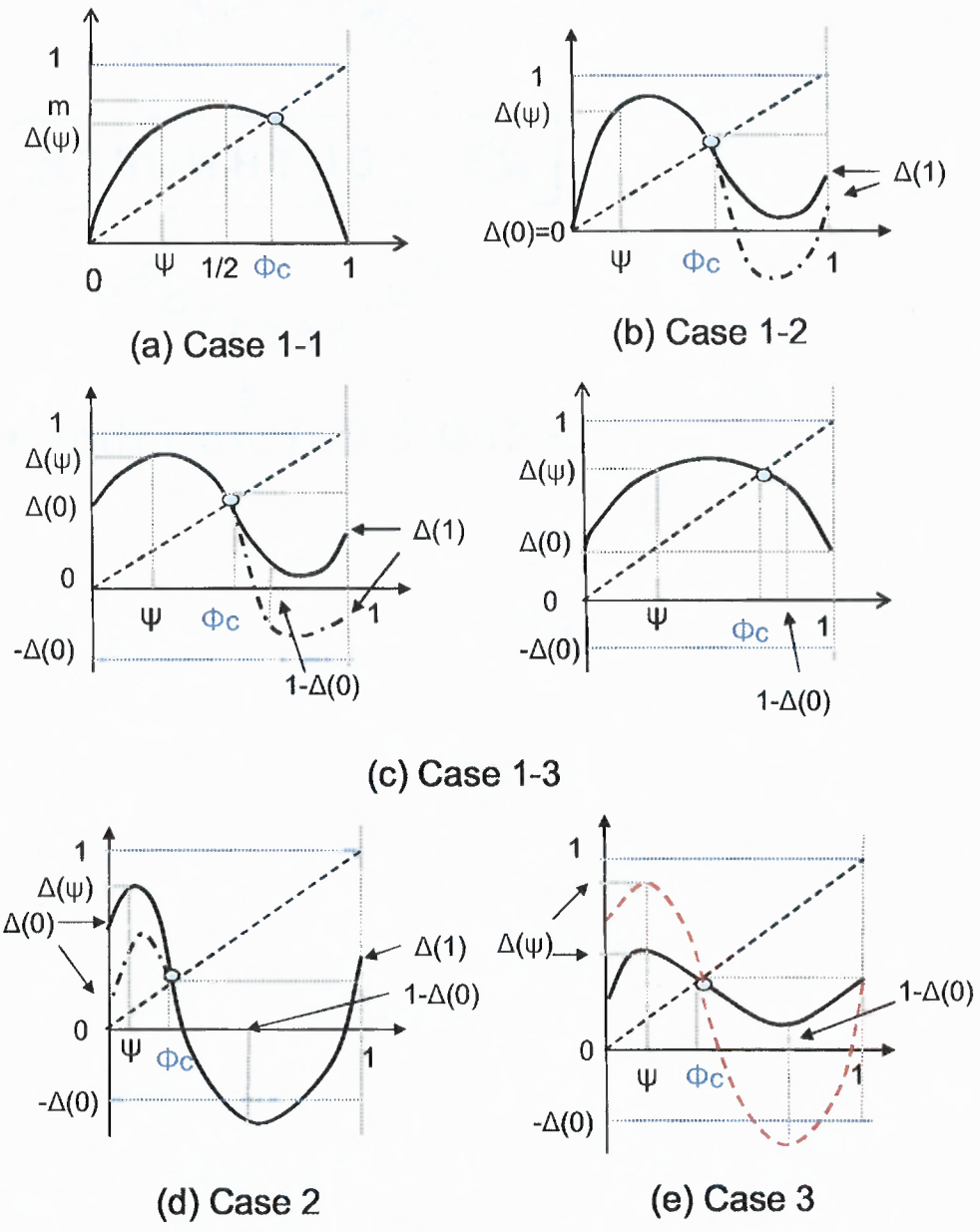

Figure 2.15 Classification of STRC shapes leading to alternating-order firing in the case of a single root of $\Delta(\phi_c) = \phi_c$ and assuming $\Delta(\phi) > \phi$ for all $\phi \in (0, \phi_c)$. The root of F, ψ, should satisfy $\Delta(\psi) < 1$ from the condition Eq. 2.11 in all cases. (a) case 1-1 ($\Delta(1) < \phi_c$ and $\Delta(0) = \Delta(1) = 0$): a symmetric quadratic case represented by $\Delta(\phi) = 4m\phi(\phi - 1)$ and amplitude m should be greater than $\frac{\sqrt{2}}{4}$ (b) case 1-2 ($\Delta(1) < \phi_c$ and $\Delta(0) = 0$ & $\Delta(1) \neq 0$): the required condition is $\Delta(1) > 0$ (c) case 1-3 ($\Delta(1) < \phi_c$ and $\Delta(0) \neq 0$): the required condition is $\Delta(1 - \Delta(0)) > -\Delta(0)$ (d) case 2 ($\Delta(1) > \phi_c$): the required condition is $\Delta(1 - \Delta(0)) < -\Delta(0)$ and $0 < \Delta(0) < 1$ (e) case 3 ($\Delta(1) = \phi_c$): the required condition is $\Delta(1 - \Delta(0)) > -\Delta(0)$ and $(\Delta'(\phi_c) - 1)(1 - \Delta'(1)) < 1$ for the black curve, and $\Delta(1 - \Delta(0)) < -\Delta(0)$ and $(\Delta'(\phi_c) - 1)(1 - \Delta'(1)) > 1$ for the red dashed curve. The black dot-dashed curve represents possible variation of the STRC in each case

If $F(0) = \Delta(0) + \Delta(1 - \Delta(0)) < 0$ then there exists at least one root of F in $(0, \phi_c)$. So a STRC needs the upper bound at $1 - \Delta(0)$ to generate alternating-order firing:

$$\Delta(1 - \Delta(0)) < -\Delta(0) \tag{2.23}$$

This condition is violated both for $\Delta(0) = 0$ and for $\Delta(0) = 1$. Thus we need to restrict $\Delta(0)$ as $0 < \Delta(0) < 1$.

Case 3 $\Delta(1) = \phi_c$

For $\phi = \phi_c$, we have

$$F(\phi_c) = \Delta(1) - \phi_c = 0.$$

We consider two subcases depending on the sign of $F(0)$.

1. ($F(0) > 0$ i.e. $\Delta(1 - \Delta(0)) > -\Delta(0)$)

   If $F'(\phi_c) < 0$ then there exists at least one root of F in $(0, \phi_c)$. This is equivalent to

   $$(\Delta'(\phi_c) - 1)(1 - \Delta'(1)) < 1 \tag{2.24}$$

2. ($F(0) < 0$ i.e. $\Delta(1 - \Delta(0)) < -\Delta(0)$)

   If $F'(\phi_c) > 0$ then there exists at least one root of F in $(0, \phi_c)$. This is equivalent to

   $$(\Delta'(\phi_c) - 1)(1 - \Delta'(1)) > 1 \tag{2.25}$$

2.5.2 Case of Two Roots of $\Delta(\phi) = \phi$

Now let ϕ_{1c} and ϕ_{2c} be two solutions of $\Delta(\phi) - \phi = 0$ in $(0, 1)$, i.e. $\Delta(\phi_{1c}) = \phi_{1c}$ and $\Delta(\phi_{2c}) = \phi_{2c}$ for $0 < \phi_{1c} < \phi_{2c} < 1$ and let STRC satisfy the condition $\Delta(\phi) > \phi$

only for $\phi_{1c} < \phi < \phi_{2c}$ (see Figure 2.16), which means the root of function F should be in (ϕ_{1c}, ϕ_{2c}) if the alternating-order firing exists. For the root, ψ, of F and $\xi_\psi = 1 + \psi - \Delta(\psi)$ for the phase of post-synaptic cell at the time arrival of the second synaptic input, we need $\Delta(\xi_\psi) < \xi_\psi$ from the condition Eq. 2.11 which is equivalent to (i) $0 < 1 + \psi - \Delta(\psi) < \phi_{1c}$ or (ii) $\phi_{2c} < 1 + \psi - \Delta(\psi) < 1$. We obtain

$$1 + d_{1c} < \Delta(\psi) < 1 + \psi = 1 + d_{1c} + \phi_{1c} \tag{2.26}$$

where $d_{1c} = \psi - \phi_{1c} > 0$ from the inequality in (i) or

$$\Delta(\psi) < 1 - d_{2c} \tag{2.27}$$

where $d_{2c} = \phi_{2c} - \psi > 0$ from the inequality in (ii).

Case 4 $\phi_{1c} < \Delta(1) < \phi_{2c}$

For $\phi = \phi_{1c}$ and $\phi = \phi_{2c}$, we have

$$\begin{aligned} F(\phi_{1c}) &= \Delta(1) - \phi_{1c} > 0 \\ F(\phi_{2c}) &= \Delta(1) - \phi_{2c} < 0 \end{aligned}$$

The function F always has at least one root in (ϕ_{1c}, ϕ_{2c}) then the root, ψ, of F should satisfy the condition Eq. 2.26 or Eq. 2.27 depending on the position of $\xi_\psi = 1 + \psi - \Delta(\psi)$. These two conditions correspond respectively to the dashed and the solid STRC curves in Figure 2.16 (a) and (d).

Case 5 $\Delta(1) < \phi_{1c}$

For $\phi = \phi_{1c}$ and $\phi = \phi_{2c}$, we have

$$\begin{aligned} F(\phi_{1c}) &= \Delta(1) - \phi_{1c} < 0 \\ F(\phi_{2c}) &= \Delta(1) - \phi_{2c} < 0 \end{aligned}$$

If $F(\phi_c) = \Delta(\phi_c) + \Delta(1 + \phi_c - \Delta(\phi_c)) - 2\phi_c > 0$ for some $\phi_c \in (\phi_{1c}, \phi_{2c})$ then there exists at least two roots of F in (ϕ_{1c}, ϕ_{2c}). Since the phase of the post-synaptic cell at the time of arrival of the second synaptic input is expressed by $\xi_c = 1 + \phi_c - \Delta(\phi_c)$ as in Subsection 2.3.4, this condition can be written as

$$\Delta(1 + \phi_c - \Delta(\phi_c)) = \Delta(\xi_c) > 2\phi_c - \Delta(\phi_c) \tag{2.28}$$

Taking into account the constraint on the phase domains, $0 \leq 1+\phi_c-\Delta(\phi_c) \leq 1$, it is equivalent to

$$\phi_c < \Delta(\phi_c) \leq 1 + \phi_c \tag{2.29}$$

Let ψ_1 and ψ_2 be the two roots of F in (ϕ_{1c}, ϕ_c) and (ϕ_c, ϕ_{2c}), respectively. Then both of ψ_1 and ψ_2 should satisfy the condition Eq. 2.26 or Eq. 2.27 depending on the position of $\xi_{\psi_1} = 1 + \psi_1 - \Delta(\psi_1)$ and $\xi_{\psi_2} = 1 + \psi_2 - \Delta(\psi_2)$. In other words, we have the following conditions for each ψ_1 and ψ_2:

$$\begin{aligned} 1 + d_{1c} &< \Delta(\psi_1) < 1 + \psi_1 = 1 + d_{1c} + \phi_{1c} \\ 1 + d'_{1c} &< \Delta(\psi_2) < 1 + \psi_2 = 1 + d'_{1c} + \phi_{1c} \end{aligned} \tag{2.30}$$

or

$$\begin{aligned} \Delta(\psi_1) &< 1 - d_{2c} \\ \Delta(\psi_2) &< 1 - d'_{2c} \end{aligned} \tag{2.31}$$

where $d_{1c} = \psi_1 - \phi_{1c}$, $d'_{1c} = \psi_2 - \phi_{1c}$, $d_{2c} = \phi_{2c} - \psi_1$, and $d'_{2c} = \phi_{2c} - \psi_2$.

Case 6 $\phi_{2c} < \Delta(1) \leq 1$

For $\phi = \phi_{1c}$ and $\phi = \phi_{2c}$, we have

$$\begin{aligned} F(\phi_{1c}) &= \Delta(1) - \phi_{1c} > 0 \\ F(\phi_{2c}) &= \Delta(1) - \phi_{2c} > 0 \end{aligned}$$

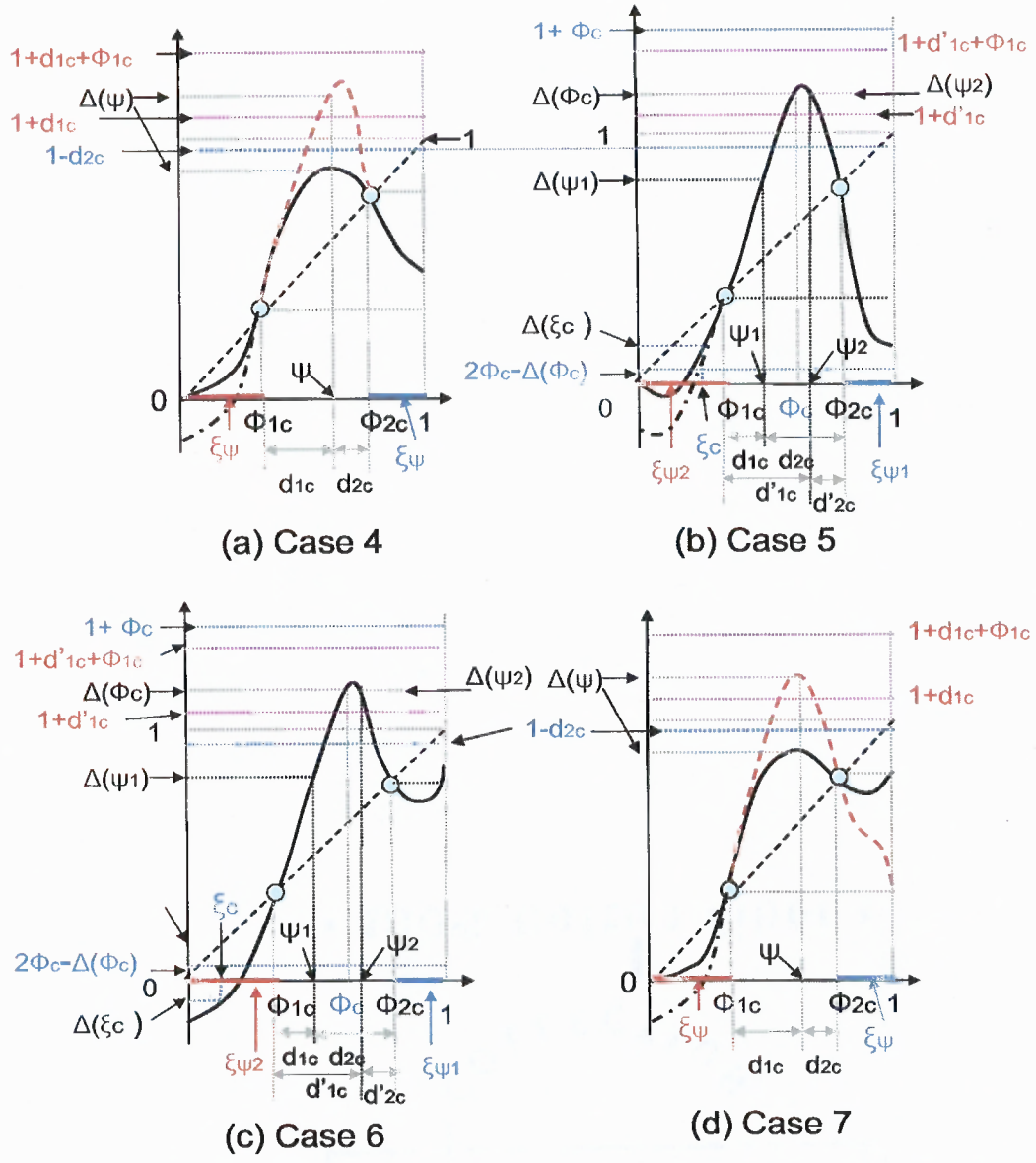

Figure 2.16 Classification of STRC shapes leading to alternating-order firing in the case of two roots of $\Delta(\phi_c) = \phi_c$ and assuming $\Delta(\phi) > \phi$ for all $\phi \in (\phi_{1c}, \phi_{2c})$. The root, ψ, of F should satisfy $1+d_{1c} < \Delta(\psi) < 1+\psi = 1+d_{1c}+\phi_{1c}$ (i.e. $0 < \xi_\psi < \phi_{1c}$ which corresponds to the red bar on x-axis of each figure) or $\Delta(\psi) < 1-d_{2c}$ (i.e. $\phi_{2c} < \xi_\psi < 1$ which corresponds to the blue bar on x-axis of each figure) where $d_{1c} = \psi - \phi_{1c}$ and $d_{2c} = \phi_{2c} - \psi > 0$ (a) case 4 ($\phi_{1c} < \Delta(1) < \phi_{2c}$): F always has at least one root in (ϕ_{1c}, ϕ_{2c}) (b) case 5 ($\Delta(1) < \phi_{1c}$): the required condition is $\Delta(\xi_c) > 2\phi_c - \Delta(\phi_c)$ and $\Delta(\phi_c) < 1 + \phi_c$ where $\xi_c = 1+\phi_c-\Delta(\phi_c)$ (c) case 6 ($\phi_{2c} < \Delta(1) \leq 1$): the required condition is $\Delta(\xi_c) < 2\phi_c-\Delta(\phi_c)$ and $\Delta(\phi_c) < 1 + \phi_c$ (d) case 7 ((i) $\Delta(1) = \phi_{1c}$ or (ii)$\Delta(1) = \phi_{2c}$): the required condition is (i)$(\Delta'(\phi_{1c}) - 1)(1 - \Delta'(1)) > 1$ for the red dashed curve or (ii)$(\Delta'(\phi_{2c}) - 1)(1 - \Delta'(1)) < 1$ for the black curve. The black dot-dashed curve represents possible variation of the STRC in each case.

If $F(\phi_c) = \Delta(\phi_c) + \Delta(1 + \phi_c - \Delta(\phi_c)) - 2\phi_c < 0$ for some $\phi_c \in (\phi_{1c}, \phi_{2c})$ then there exist at least two roots of F in (ϕ_{1c}, ϕ_{2c}). This condition can be written as

$$\Delta(1 + \phi_c - \Delta(\phi_c)) = \Delta(\xi_c) < 2\phi_c - \Delta(\phi_c) \tag{2.32}$$

Further, the two roots ψ_1 and ψ_2 of F, and $\Delta(\phi_c)$ have to also satisfy the conditions, Eqs. 2.29 - 2.31 as in Case 5.

Case 7 (i) $\Delta(1) = \phi_{1c}$ or (ii) $\Delta(1) = \phi_{2c}$

For $\phi = \phi_{1c}$ and $\phi = \phi_{2c}$, we have

$$\begin{aligned} F(\phi_{1c}) &= \Delta(1) - \phi_{1c} = 0 \\ F(\phi_{2c}) &= \Delta(1) - \phi_{2c} < 0 \end{aligned}$$

in case of (i) $\Delta(1) = \phi_{1c}$ or

$$\begin{aligned} F(\phi_{1c}) &= \Delta(1) - \phi_{1c} > 0 \\ F(\phi_{2c}) &= \Delta(1) - \phi_{2c} = 0 \end{aligned}$$

in case of (ii) $\Delta(1) = \phi_{2c}$.

If $F'(\phi_{1c}) > 0$ in case of (i) or $F'(\phi_{2c}) < 0$ in case of (ii) there exists at least one root of F in (ϕ_{1c}, ϕ_{2c}). This is equivalent to

$$(\Delta'(\phi_{1c}) - 1)(1 - \Delta'(1)) > 1 \tag{2.33}$$

in case of (i) $\Delta(1) = \phi_{1c}$ or

$$(\Delta'(\phi_{2c}) - 1)(1 - \Delta'(1)) < 1 \tag{2.34}$$

in case of (ii) $\Delta(1) = \phi_{2c}$. Note that the root of F, ψ, has to also satisfy one of the conditions given by Eqs. 2.26 and 2.27.

2.6 Conclusion

We have shown that phase-locked firing of two coupled type-I oscillators becomes destabilized if the inhibition from one cell is sufficient to transiently bring the post-synaptic cell below the excitation threshold. In this case, the two cell network will exhibit leap-frog (alternating-order) spiking, which was also demonstrated recently by Maran and Canavier [53] in the case of a heterogeneous network of type-I oscillators. Thus, the range of applicability of the weak coupling results may be quite narrow in inhibitory networks of type-I oscillators that are close to their excitation thresholds [38]. As the coupling strength is increased, the leap-frog spiking state gives way to a period-doubling cascade, leading to more complex $m{:}n$ bursting states, as well as chaotic activity. Finally, at sufficiently strong values of the coupling strength oscillator death occurs, whereby only one of the cells continues spiking, suppressing the activity of the post-synaptic cell. The entire bifurcation structure of the network activity as a function of the synaptic coupling can be explained by the first-order spike-time response curve.

Here we proved that the leap-frog dynamics cannot be achieved by a standard phase reduction of the coupled system, and that more than two degrees of freedom are required to obtain leap-frog spiking in a model with continuous coupling function. However, we also demonstrated that the alternating-order spiking in the network of two pulse-coupled ML model neurons can be described entirely in terms of the augmented phase model with the phase domain extended to negative values, which represents the suppression of each cell below the excitation threshold in each cycle of the oscillation. We note that the topology of the augmented phase model is similar to the topology of an integrate-and-fire model. Therefore, it is possible to achieve alternating-order spiking in a network of appropriately modified integrate-and-fire model neurons, as shown in Figure 2.12

Our results for the Morris-Lecar network hold in a certain range of synaptic decay times that are significantly shorter than the uncoupled period of each cell. In the particular parameter regime we consider, second-order phase resetting effects become significant and can no longer be ignored when the synaptic decay time becomes larger than about 1/8 of the unperturbed oscillation period. In this case we see significant bistability between the synchronous and alternating-order states (Figure 2.13), which is consistent with the observed change in the shape of the STRC with increasing τ_{syn}. As the synaptic decay time is increased, the region of attraction of the leap-frog state shrinks, and at sufficiently large τ_{syn}, the homogeneous network is no longer capable of sustaining leap-frog activity. In this case significant heterogeneity may be required to destabilize phase-locking; this conjecture is in agreement with the results of Maran and Canavier [53].

Finally, we showed that the network dynamics we report is not specific to the details of the model and the coupling, since the same activity states and the transitions between them can be obtained in an emulated network of phase oscillators with a simplified quadratic phase-resetting curve. In fact, the alternating-order dynamics can be explained by the particular shape of the STRC characterizing each of the two cells. Here we provided a complete classification of STRC shapes that lead to periodic order-alternating dynamics studied in Chapter 2. This would allow one to extend our analysis and results beyond networks of Morris-Lecar type. Note in particular that most STRC shapes considered here may have negative values on part of the phase domain. Therefore the results obtained here are applicable to networks of excitable cells not belonging to type-I excitability class. Note that the stability condition given by Eq. 2.12 is straightforwardly extended to all STRC shapes considered here, since they only involve the value of the derivative of STRC at fixed point of the return map i.e. root of $F = \Phi(\phi) - \phi$.

CHAPTER 3

NEGATIVE PHASE AND STRC

3.1 Negative Phase and Extended STRC

In Chapter 2 we have shown that a one-dimensional phase reduction of a non-weakly perturbed limit cycle oscillator may require the extension of the phase variable defining the state of the oscillator to a multi-branched phase domain. Such multi-branched domain is easiest to implement by extending the $[0, 1]$ phase interval to negative values. The simplest illustration of such negative phase is provided by a model of the integrate-and-fire type, when it is hyperpolarized below its reset potential. As we have shown, this notion of negative phase enables us to extend the phase return map analysis based on the STRC characteristic to describe novel dynamical states of non-weakly coupled oscillators, in particular the alternating-order spiking state.

Note however that until now we have restricted the STRC to the usual $[0, 1]$ interval (see Figures 2.8, 2.9, and 2.10), and we did not examine the case whereby the perturbation arrives while the phase of the cell is negative. This is because we were primarily concerned with the dynamics of a two-cell network, with only one synaptic input per period. In this situation the phase of the postsynaptic cell is positive when the perturbation arrives from the presynaptic cell. However, in the case of sufficiently strong synaptic input, the phase of the postsynaptic cell may not have time to return to positive values at the time of arrival of the second synaptic input. Although for a two-cell network such a scenario is only possible in the spike-suppressed (oscillator death) state, this situation is more common in the case of three or more coupled cells (Figure 2.14), since in a larger network there will be in general several spikes arriving from several different cells within a single oscillation cycle. This strong coupling,

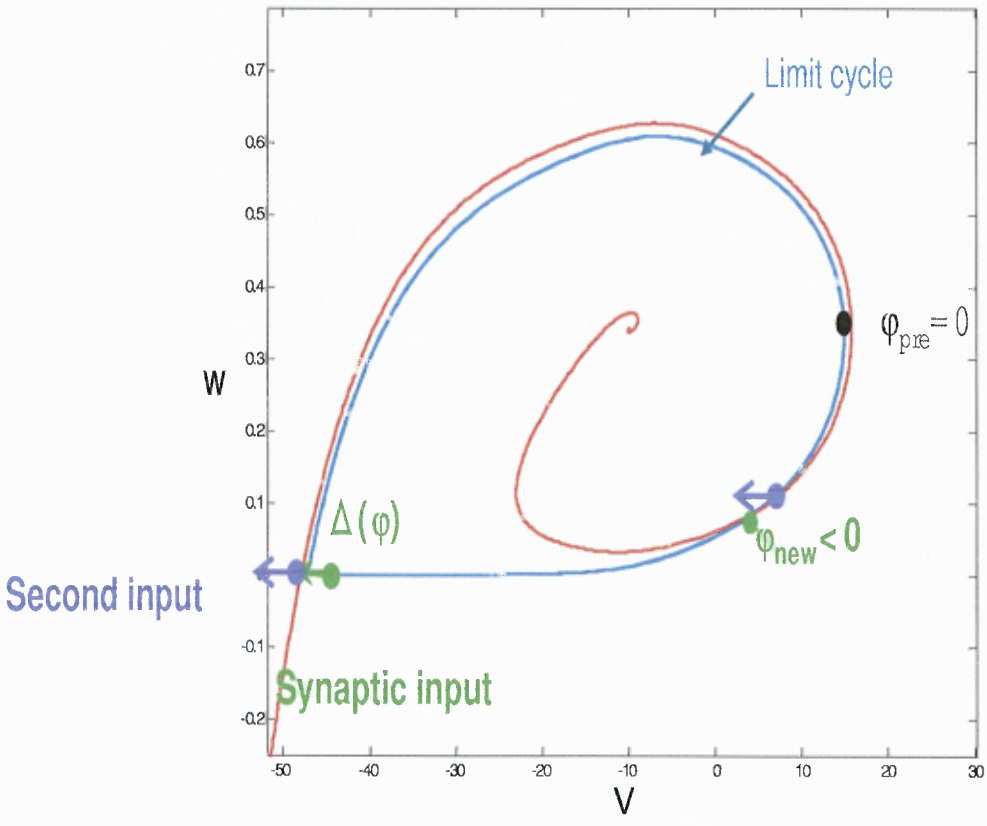

Figure 3.1 Effect of two consecutive synaptic perturbations. When one of the cells reaches phase 0, corresponding to the peak of its potential ($\phi_{pre} = 0$), a synaptic current hyperpolarizes the postsynaptic cell, which has phase ϕ. If this first synaptic input (green arrow) is sufficiently strong, the resulting phase delay is greater than the phase difference between the two cells (i.e. $\Delta(\phi) > \phi$), and the new phase will be negative, $\phi_{new} = \phi - \Delta(\phi) < 0$. This negative phase corresponds to an isochron that intersects the limit cycle at a position retrograde to the peak of the action potential (red curve). If the next synaptic input arrives from some other cell immediately after the first one (purple arrow), the phase of the postsynaptic cell will still be negative, and the resulting phase delay will require the knowledge of the STRC at this hyperpolarized branch of the trajectory.

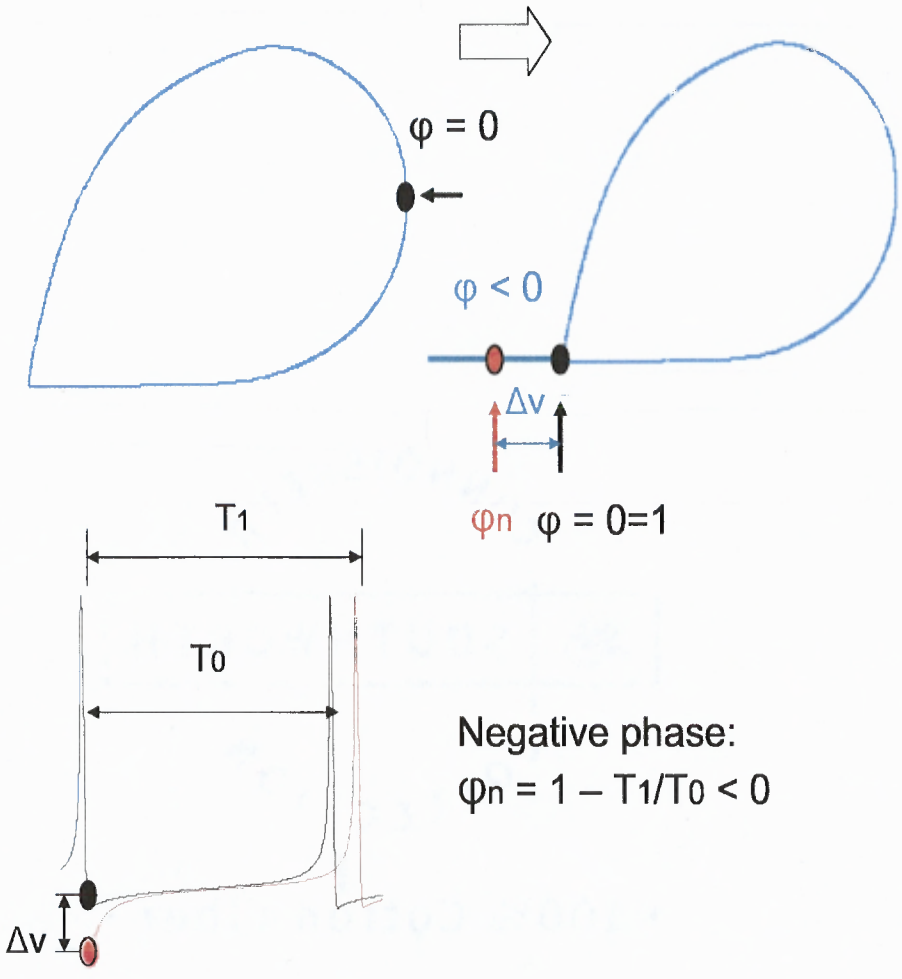

Figure 3.2 Defining the negative phase on the subthreshold branch. Zero phase is redefined as the minimum value of voltage (top panel). All points on the subthreshold branch of the hyperpolarized trajectory are defined as negative phase $\phi_n = 1 - \frac{T_1}{T_0} < 0$, where T_0 is the intrinsic period of the cell, and T_1 is the time it takes for the cell to spike and its potential to reach its minimum (zero phase).

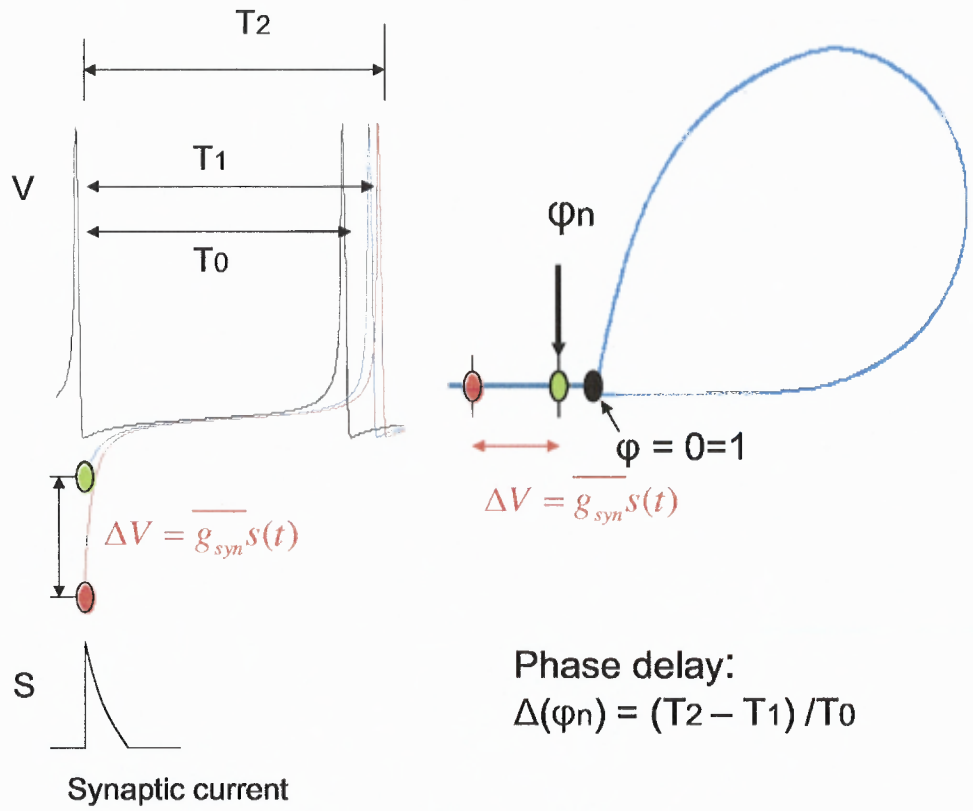

Figure 3.3 Constructing the STRC on the negative phase domain. For any point corresponding to a negative phase ϕ_n, phase resetting is defined as $\Delta(\phi_n) = \frac{T_2 - T_1}{T_0}$ where T_2 is the perturbed period of cell (red curve) after receiving synaptic current at $\phi_n (< 0)$, T_1 is the corresponding first-passage time in the absence of perturbation, and T_0 is the intrinsic period of the cell

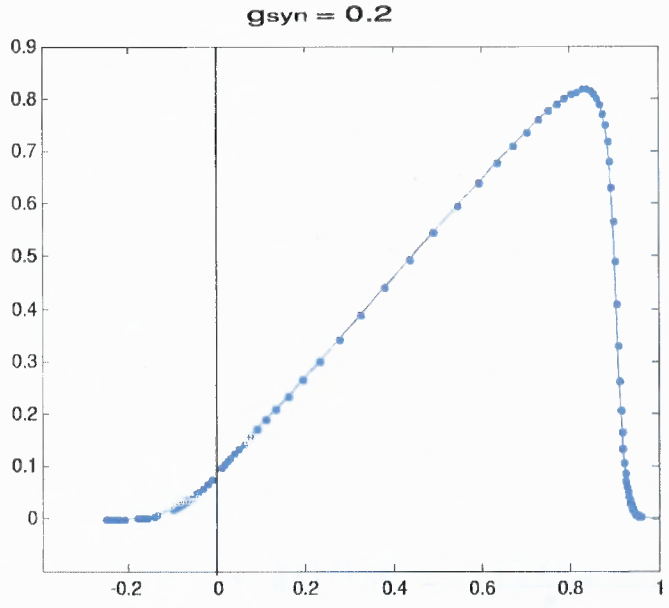

Figure 3.4 Numerically generated STRC of the Morris-Lecar oscillator with type-I excitability, extended to the negative phase domain. This STRC corresponds to a synaptic current perturbation generated by a single presynaptic spike, with the synaptic conductance value of $\bar{g}_{syn} = 0.2$

negative phase scenario is described on the limit cycle plot in Figure 3.1. In order to describe the network dynamics in this case, the information provided by the STRC values on the $[0, 1]$ domain (Figures 2.8, 2.9, and 2.10) are not sufficient, and we also have to know the values of the STRC along the negative branch of the phase domain.

Since negative phase corresponds to the hyperpolarized values of the membrane potential, it is convenient to re-define the zero phase as the boundary of this hyperpolarized branch, which is the minimum of V along the unperturbed limit cycle, and not its maximum according to our previous definition of the zero phase (Figure 3.2). All points on the limit cycle always correspond to positive phase values between 0 to 1, as in the S^1 phase model, whereas negative phase values correspond to the hyperpolarized potentials which are below the minimum of voltage along the unperturbed limit cycle. Let ϕ_n correspond to any point on this hyperpolarized

potentials. Then the negative phase value ϕ_n is defined as

$$\phi_n = 1 - \frac{T_1}{T_0} < 0$$

where T_0 is the intrinsic period of the cell, and T_1 is the time it takes for the cell to spike and its potential to reach its minimum (zero phase).

We are now ready to extend STRC to the negative phase domain, as shown in Figure 3.3. For any point corresponding to the negative phase ϕ_n, the phase resetting is defined as

$$\Delta(\phi_n) = \frac{T_2 - T_1}{T_0} \tag{3.1}$$

where T_2 is the time it takes for the cell to spike and its potential to reach its minimum following a synaptic perturbation, and T_1 is the corresponding first-passage time in the absence of perturbation.

Figure 3.4 shows the resulting numerically generated STRC. Note that the STRC is not periodic on $[0, 1]$, i.e $\Delta(0) \neq \Delta(1)$, indicating the presence of second-order phase resetting (shown in Figure 2.10 for a different phase domain definition). The STRC is continuous across phase 0, and decreases to zero as the absolute value of negative phase increases, as one moves along the subthreshold branch in the negative V direction. This decrease in the value of $\Delta(\phi)$ indicates the weakening effect of an inhibitory perturbation of a given amplitude administered at strongly hyperpolarized potentials, since for large hyperpolarizations the rate of repolarization is faster. This increase in membrane potential recovery speed can be easily understood geometrically since large negative V values correspond to phase plane regions far from the V-nullcline, where the dynamics of the V variable become exponentially fast. In this case a slight change in membrane potential achieved by synaptic perturbation does not significantly influence the first passage time of the postsynaptic cell ($T_2 \approx T_1$). We observe that the phase delay becomes approximately zero at the negative

phase values less than -0.2, for a wide range of perturbation amplitudes, $\bar{g}_{syn}$, and for different values of synaptic decay time, τ_{syn}. Figure 3.4 shows the STRC extended to the negative phase domain when the synaptic coupling is $\bar{g}_{syn} = 0.2$.

3.2 Phase Prediction for Two Close Inputs: Using STRC Extended to Negative Phase Domain

As discussed above, if the synaptic current is sufficiently strong and the time interval between two inputs is sufficiently small, the phase of the postsynaptic cell at the time of arrival of the second perturbation is negative. We predict that in this case the knowledge of the STRC on the negative phase domain is indispensable in order to accurately describe the dynamics of the postsynaptic cell. Here we analyze this case by examining the dynamics of a single model neuron in response to two close synaptic inputs (open-loop configuration), and test the accuracy of the spike time prediction based on the STRC extended to negative phase values, as shown in Figure 3.5.

For our Morris-Lecar model, when the time interval between two synaptic inputs is fixed at $ts = 4$ms, the phase ϕ_2 at the time of arrival of the second synaptic input becomes negative if maximum conductance of synaptic current, $\bar{g}_{syn}$, is made greater than 0.28. Note that the time interval between two synaptic currents should be greater than the synaptic decay time, τ_{syn}, in order for the STRC approach to be applicable. The first synaptic input is applied at fixed time of 0.3ms following the spike repolarization, corresponding to the phase of $\phi_1 = 0.0067$. The second synaptic input is applied at a phase ϕ_2 which is obtained from

$$\phi_2 = \phi_1 - \Delta(\phi_1) + \frac{ts}{T_0}$$

where T_0 is the intrinsic period, $\Delta(\phi_1)$ is the phase delay at ϕ_1, and ts is the time interval between two synaptic currents. For our example in Figure 3.5, $\phi_2 = -0.063$ when $\bar{g}_{syn} = 1.5$.

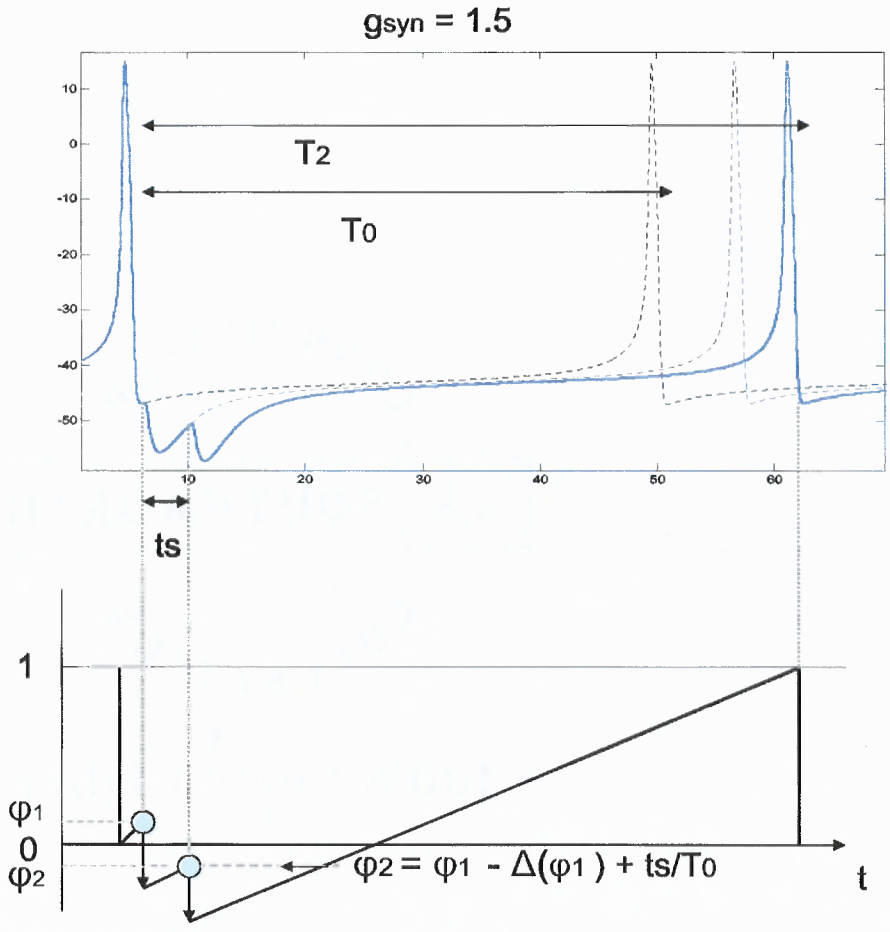

Figure 3.5 Effect of two close synaptic inputs for strong value of the coupling, $\bar{g}_{syn} = 1.5$. The first synaptic input is applied at a fixed interval of $0.3ms$ (i.e $\phi_1 = 0.0067$) following the time of repolarization of the cell (time when the voltage is minimal, $\phi = 0$). The second synaptic input is applied at phase $\phi_2 = -0.063$, $ts = 4$ms after the first input. The second phase is obtained from $\phi_2 = \phi_1 - \Delta(\phi_1) + \frac{ts}{T_0}$. The actual total phase delay due to both inputs is measured as $\Delta(\phi_1, \phi_2) = \frac{T_2 - T_0}{T_0}$ where T_2 is the period perturbed by the combined application of both inputs in one cycle of the oscillation (solid blue curve), and T_0 is the intrinsic period.

The actual total phase delay produced by the two synaptic inputs received at phases ϕ_1 and ϕ_2 is measured as

$$\Delta(\phi_1, \phi_2) = \frac{T_2 - T_0}{T_0} \tag{3.2}$$

where T_2 is the period perturbed by both synaptic inputs arriving in one cycle (solid blue curve in Figure 3.5), and T_0 is the intrinsic period of the cell. The phase delay at each phase is predicted using the numerically computed extended STRC as $\Delta(\phi_1)$ and $\Delta(\phi_2)$. Thus, we get the prediction

$$\frac{T_2 - T_0}{T_0} = \Delta(\phi_1, \phi_2) \approx \Delta(\phi_1) + \Delta(\phi_2) \tag{3.3}$$

In Figure 3.6 we compare this prediction to the actual value of the perturbed period, and show that the extended STRC gives a good approximation to the total phase delay even if $\phi_2 < 0$. We vary the coupling strength $\bar{g}_{syn}$ from 0.5 to 1.5, the strong coupling parameter range corresponding to the spike-suppress (oscillator death) state in the two-cell network in Figure 2.1, and compare the actual value of the total delay obtained by numerically integrating the model equations using MATLAB with the predicted value obtained using three distinct STRC-based methods: (1) using the STRC computed on the negative phase domain (red dashed curve, Eq. 3.3); (2) using the STRC defined only in $[0, 1]$, as in Chapter 2, and assuming that the phase of the cell is "frozen" by the first inhibitory input for the duration equal to $\Delta(\phi_1)$, in which case $\Delta(\phi_2) = \Delta(\phi_1)$ when $\phi_2 < 0$ (blue dot-dashed curve); and finally (3) again using the STRC defined only in $[0, 1]$ as in (2), but with STRC extended to negative values by the condition of periodicity, $\Delta(\phi) = \Delta(\phi + 1)$, for $\phi \in [-1, 0]$ (green dotted curve). Note that the absolute magnitude of the negative phase at the time of arrival of the second synaptic input is increasing as the coupling strength $\bar{g}_{syn}$ increases (Figure 3.6, bottom panel). These results show that computing the STRC on the negative phase domain gives the best approximation among these three

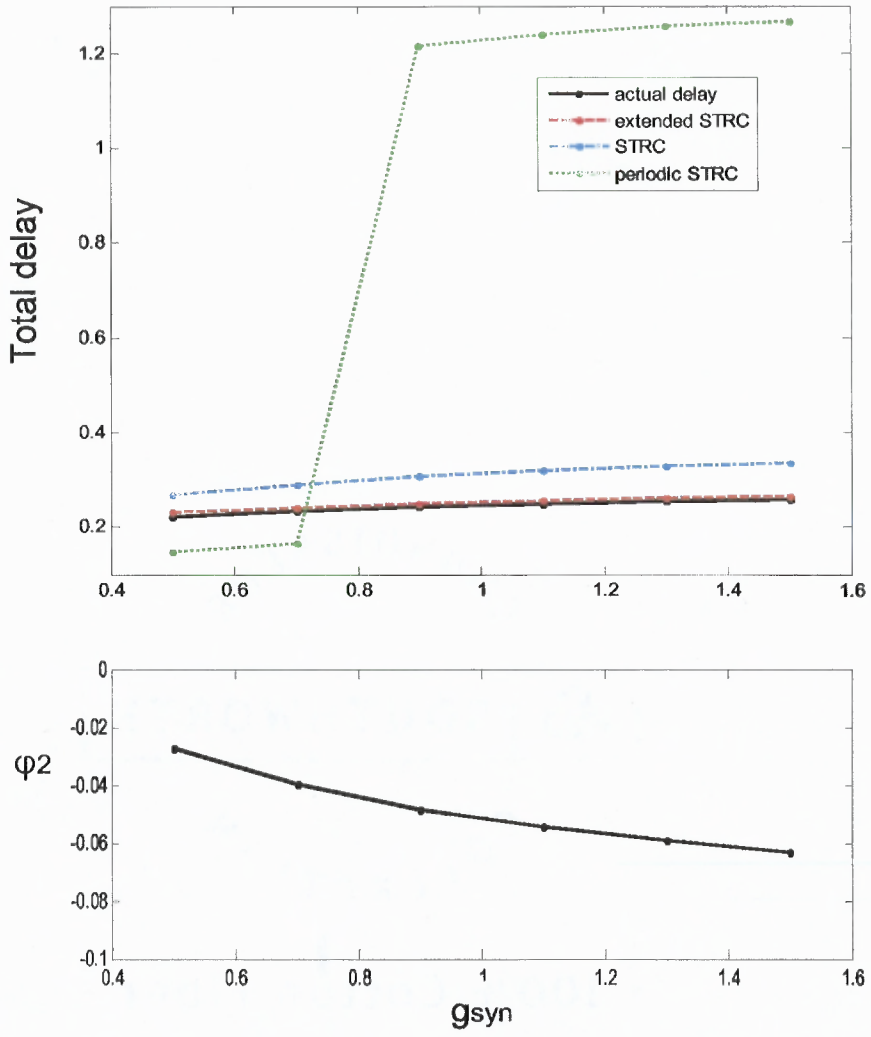

Figure 3.6 Comparing the actual and the predicted combined phase delay produced by a pair of close synaptic inputs. Black solid curve labels the actual total inhibition measured by Eq. 3.2, red dashed curve presents the predicted total phase delay using STRC extended to the negative phase domain (Eq. 3.3), blue dot-dashed curve shows the total delay according to the "frozen" phase assumption, using the STRC only defined in [0,1], and the green dotted curve shows the total phase delay obtained using the periodic extension of the STRC to negative phase values, $\Delta(\phi) = \Delta(\phi + 1)$ if $-1 < \phi < 0$. The coupling strength $\bar{g}_{syn}$ varies form 0.5 to 1.5. The lower panel shows the value of phase at the time of arrival of the 2nd synaptic input, for each value of $\bar{g}_{syn}$

.

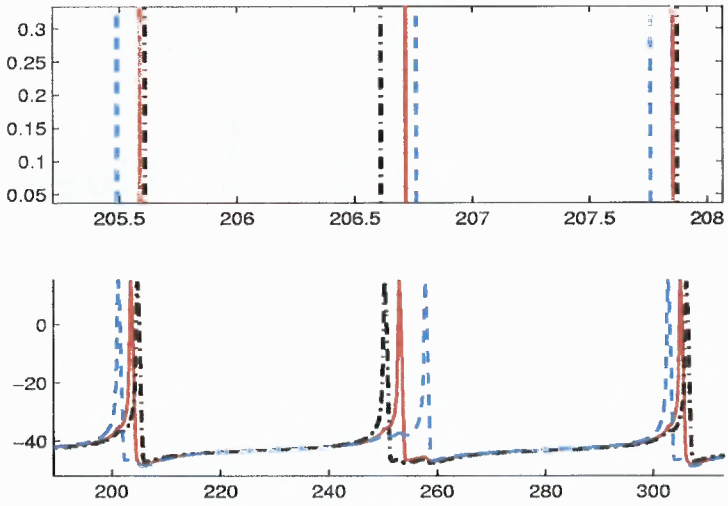

Figure 3.7 Reconstructing three-cell network dynamics using phase description based on the STRC extended to the negative phase domain, for $\bar{g}_{syn} = 0.15$. Voltage versus time trace by the emulator (top panel) and by the real model (bottom panel).

methods, even in the case of strong coupling strength. The absolute error between the actual total inhibition and the predicted phase delay using the extended STRC approach (case 1) remains within 1% over the entire range of $\bar{g}_{syn}$ that we used. Note that the "frozen" phase model (case 2) is the second-best method, whereas the third prediction method based on the simple periodic extension of the STRC is the least accurate, since such a periodic extension is completely arbitrary and is not justified by the dynamical properties of the underlying spiking model.

Three-cell network gives a concrete example of the usefulness of extending the STRC to the negative phase domain. For the splay state shown in Figure 3.7 (bottom panel), there are two consecutive synaptic inputs arriving to each cell in every cycle, and the phase of the postsynaptic cell may remain negative at the time of arrival of the second input. Using the phase description based on the STRC on the extended phase domain, numerically calculated for a particular $\bar{g}_{syn}$ value, we were able to accurately reproduce the splay state activity, as shown in Figure 3.7 (top panel). Since the second

input is usually applied before the first synaptic input has decayed, synaptic currents of two inputs overlap by $1 - 2ms$. So there is a measurable quantitative discrepancy between the actual total phase delay and the one predicted using the STRC, but the error is relatively small and the qualitative features of network activity are accurately predicted.

3.3 Extending the Spike Emulator to Negative Phase Values

Note that the utility of the negative phase extension of the STRC is more crucial for strong values of $\bar{g}_{syn}$. In particular, in Subsection 2.3.6 we presented the bifurcation diagram of a spike emulator model based on a simple quadratic STRC. This predicted the spike-suppress state when the STRC amplitude satisfied $m > 1$, and more complicated dynamics for yet higher values of m, approximately 1.5. In the latter case the phase of the suppressed cell drops below zero as m increases, and this phase does not recover to a positive value when the next input arrives. Therefore we assumed that the phase of the cell is "frozen" upon receiving inhibition for the duration equal to $\Delta(\phi)$, instead of reducing the phase by $\Delta(\phi)$. These two approaches are equivalent if the period between two synaptic inputs is greater than $\Delta(\phi)$. However, during the spike-suppress state this leads to a monotonic reduction of the phase value with each synaptic input, so the phase diverges with time. In contrast, we would expect the phase of a biophysically realistic model to reach a negative but stationary value when receiving a constant-frequency inhibitory input. Therefore, extending the phase domain to negative values is crucial in order for the spike emulator approach to be more realistic.

Introducing the negative phase domain requires changing the shape of the STRC. The STRC now has non-zero value at phase $\phi = 0$. The question arises whether this change in the shape of the STRC has a qualitative effect on the bifurcation structure of the spike emulator dynamics shown in Figure 2.2. To verify this, we have

(a) α-function (b) bifurcation

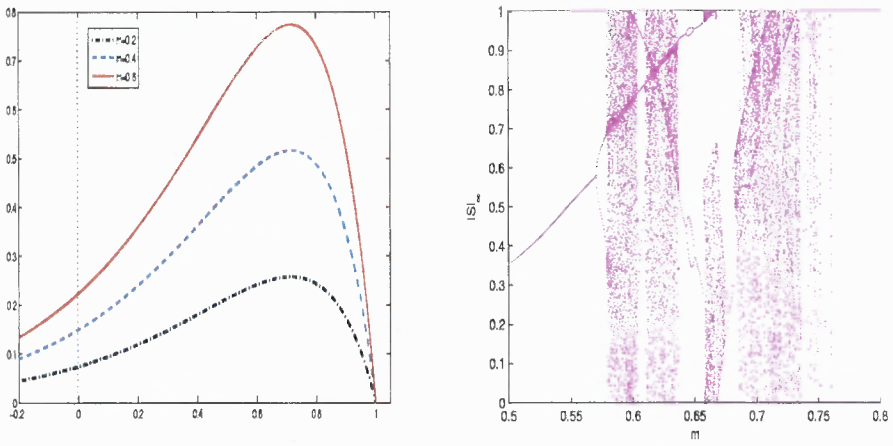

Figure 3.8 (a) Spike emulator STRC is chosen as an α-function defined as $\Delta(\phi) = -ma^2(\phi-1)exp(a(\phi-1))$ where $a = 3.5$ and $\phi \in [-0.2, 1]$, for three different values of amplitude $m = 0.2$ (dot-dashed black curve), $m = 0.4$ (dashed blue curve), and $m = 0.6$ (solid red curve) (b) Emulated inter-spike interval bifurcation diagram as a function of the amplitude of the α-function STRC. We obtain the alternating-order firing and bursting dynamics similar to Figure 2.1 (b),(c), and (e). Note that stable synchrony is not obtained.

chosen an α-function as our model STRC, defined as $\Delta(\phi) = -ma^2(\phi-1)exp(a(\phi-1))$ where $a = 3.5$ and $\phi \in [-0.2, 1]$. Note the $a = 3.5$ is chosen so that the STRC agrees with the existence conditions for leap-frog spiking illustrated in Figure 2.9, and this STRC is continuously extended to the negative phase domain. We employed the emulator algorithm to generate the corresponding inter-spike phase sequence, and explored the effect of increasing the STRC amplitude, m. We verified that the entire bifurcation structure of the ML network dynamics is qualitatively reproduced by the α-function STRC, as shown in Figure 3.8, except for the synchronous state (cf. Figures 2.2 and 2.11). Reducing the amplitude of the STRC doesn't rescue the stable synchrony state since the slopes of STRC at phase 0 and 1 are not close to 1, and therefore the stability condition of synchronous firing determined by map slope expression (Eq. 12 in Goel and Ermentrout [27]) are not satisfied. But the iteration of α-function as STRC does lead to period-1 and 2 leap-frog firing, chaotic

and spike-suppress states similar to those illustrated in Figures 2.2 and 2.11 for the quadratic STRC. A more complicated functional form of STRC would clearly allow us to obtain stable synchrony as well, and to match more closely the bifurcation structure of the Morris-Lecar network.

3.4 Conclusion

The extension of phase domain to negative values naturally arise when deriving phase return maps in the case of non-weak inhibition, as previously shown by Canavier and coworkers [10, 53]. However, the geometric meaning of such negative phase domain has not been previously analyzed. Further, in previous studies the domain of the STRC was always restricted to positive values.

For the first time, we have shown that the phase return map approach based on the STRC can be extended to models with multi-branched phase domain supplanted with a negative value branch, which arises in the analysis of strongly coupled networks of cells that are characterized by fast closing of K^+ channels. We showed that the utility of negative phase extension of the STRC is more crucial for strong values of coupling strength $\bar{g}_{syn}$ and accurately describes the dynamics of the postsynaptic cell in a larger network by allowing to predict the effect of multiple consecutive synaptic inputs. Although the value of STRC on the negative phase domain is relatively small in our Morris-Lecar neuron model (see Figure 3.4), the extension of STRC approach to the multi-branched domain may be useful in analyzing the dynamics of networks of other cells with more significant phase delays at hyperpolarized potentials.

Note that the redefinition of phase zero as the minimum of potential rather than its peak allowed us to maintain the continuity of the STRC, $\Delta(\phi)$ across $\phi = 0$, the boundary between the two branches of the extended phase domain. However, the advantage of the standard definition of zero phase as the peak of potential that we adapted in Chapter 2 is that the negative phase necessarily leads to order alternation,

whereas in the new phase definition there is a small range of negative phase values for which the spiking order is preserved. In our model, this range is $-0.03 < \phi < 0$. Note also that the phase map (Eq. 2.6) derived in Chapter 2 relied on the standard definition of phase, and would be somewhat modified with the new definition of zero phase.

CHAPTER 4

HETEROGENEOUS NETWORK

4.1 Introduction

Modeling studies showed that it is possible to obtain synchronous output from purely inhibitory networks [89] over a decade ago. Since then, several modeling and theoretical studies of inhibitory networks have been performed [76, 86]. The prediction that slow inhibition leads to synchrony under assumptions of homogeneity [20, 24, 86], must be modified in the presence of mild heterogeneity. Heterogeneity of inputs to inhibitory networks strongly affect their ability to synchronize [30, 84, 88, 91]. In addition, the effects of inhibition are more complex in mildly heterogenous networks that in homogenous ones. Synchrony is never perfect in mild heterogeneous networks, i.e. near synchronous modes were explored in several studies [77, 78, 91, 53].

In two recent studies Skinner and coworkers [77, 78] explored how the amount of input heterogeneity of two-cell inhibitory network affects their dynamics and found that the ability of heterogeneous inhibitory networks to synchronize depends non-monotonically on each of the synaptic time constant, synaptic conductance and external drive parameters. Further, recent work by Maran and Canavier's [53] showed how nearly synchronous modes including both 1:1 and 2:2 phase-locked modes arise in heterogenous networks of type-I Wang-Buzsáki neurons. They used the phase resetting curve to derive the existence and stability criteria for 2:2 phase-locked modes in reciprocally coupled two-neuron circuits, without the assumption of weak coupling (see also [64]).

Here we extend the approach of Maran and Canavier to analyze how the amount of input current heterogeneity affects the dynamics of the network of two Morris-Lecar oscillators that we studied in Chapter 2. Our goal here is to describe the changes

in network dynamics caused by increase in heterogeneity in terms of the differences between the STRCs of the two cells. We extend the phase return maps derived in Subsection 2.3.4 to the heterogeneous network case, for both the alternating-order firing and the order-preserving non-zero phase locked state.

4.2 Model

We consider a pair of two model neurons with type-I excitability, each modeled as a Morris-Lecar oscillator, same as in Chapter 2. I_{app} represents the applied or external drive to the cell, and we use this parameter to introduce heterogeneity into the system. We consider two-cell networks that are reciprocally coupled. The external drive to cells 1 and 2 is:

$$\begin{aligned} I_{app,1} &= I_{app}, \\ I_{app,2} &= I_{app} - \delta \end{aligned}$$

respectively, where $I_{app} = -14\mu A/cm^2$. We define the heterogeneity, ϵ, as

$$\epsilon = \frac{T_1 - T_2}{T_2} \tag{4.1}$$

where T_1 and T_2 are the intrinsic periods of the isolated cells 1 and 2, respectively. Note that the intrinsic frequency is increasing as I_{app} increases.

4.3 Activity of a Heterogeneous Two-Cell Network

Figure 4.1 shows the diversity of behaviors exhibited by the two-cell Morris-Lecar network for different values of the maximal synaptic conductance, $\bar{g}_{syn}$, and heterogeneity, $\epsilon(\%)$. When mild heterogeneity is introduced into the two-cell inhibitory network, the network exhibits the alternating-order firing, chaotic, and oscillation death states that are also observed in a two-cell homogeneous network. However, for small values

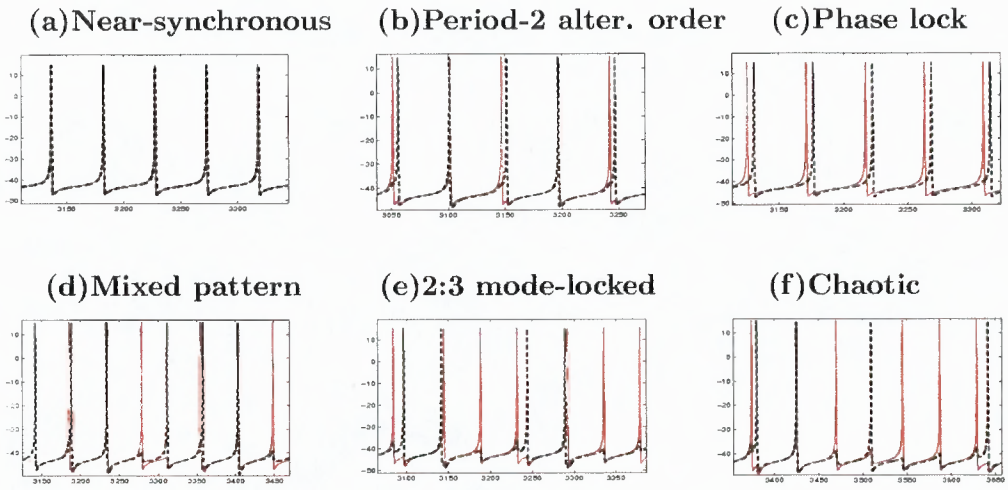

Figure 4.1 Network activity states in heterogeneous two-cell networks. The potentials of the two cells are shown as red and black traces, respectively. (a) Near-synchronous phase-locked firing when $\bar{g}_{syn} = 0.05, I_{app,2} = 14.005\mu A/cm^2(\epsilon = 1.68\%)$. The spiking order is preserved. (b) Period-2 alternating-order (leap-frog) spiking , when $\bar{g}_{syn} = 0.1, I_{app,2} = 14.005\mu A/cm^2(\epsilon = 1.68\%)$ (c) Phase locked firing when $\bar{g}_{syn} = 0.03, I_{app,2} = 14.01\mu A/cm^2(\epsilon = 3.3\%)$. The spiking order is preserved (d) Mixed pattern with alternating-order and order preserving phase-locked firing when $\bar{g}_{syn} = 0.2, I_{app,2} = 14.01\mu A/cm^2(\epsilon = 3.3\%)$. Note the change in spiking order:$1 \rightarrow 2 \rightarrow 1 \rightarrow 1 \rightarrow 2 \rightarrow 2 \rightarrow 1 \rightarrow 2 \rightarrow \cdots$ (e) $2:3$ mode-locked alternating-order spiking when $\bar{g}_{syn} = 0.28, I_{app,2} = 14.01\mu A/cm^2(\epsilon = 3.3\%)$ (f) Chaotic state, irregular inter-spike intervals when $\bar{g}_{syn} = 0.26, I_{app,2} = 14.02\mu A/cm^2(\epsilon = 6.3\%)$

of the coupling, we observe a near-synchronous state instead of exact synchrony, with a small but non-zero interval between the neighboring spikes of the two cells.

Bifurcation diagram presented in Figure 4.2 explores the transitions between these different behaviors, showing the coupling-strength dependence of the asymptotic intervals between two consecutive spikes for two different values of heterogeneity, $\epsilon = 3.3\%$ and $\epsilon = 6.3\%$. In case of mild heterogeneity, $\epsilon = 3.3\%$, network activity shows more varied behaviors: as the coupling strength is increased, the activity changes from the order-preserving near synchronous firing, becoming the non-zero phase-locked state, which bifurcates to alternating-order firing, mixed activity with order alternation and non-zero phase locking (Figure 4.1 (d)), then to chaotic, $2:3$ mode-locked alternating-order firing (Figure 4.1 (e)), then chaotic and spike-suppress

(a) $\epsilon = 3.3\%$ (b) $\epsilon = 6.3\%$

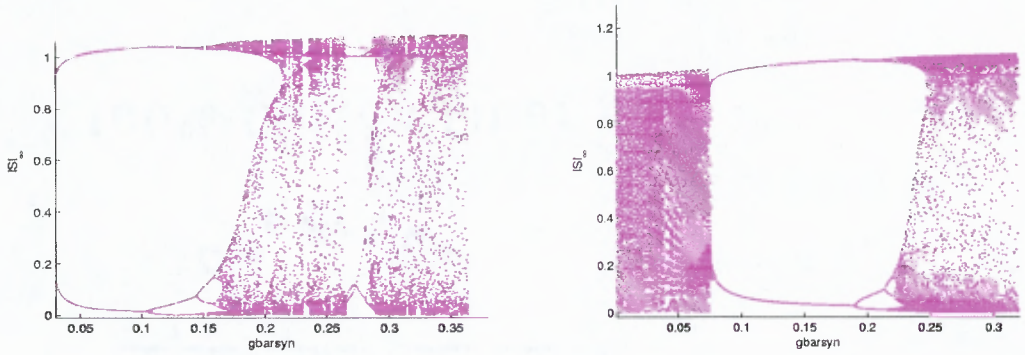

Figure 4.2 Bifurcation diagram of the heterogeneous two-cell Morris-Lecar model network. ISI_∞, the asymptotic values of the intervals between consecutive spikes (not necessarily spikes of the same cell) are plotted as a function of the coupling strength, $\bar{g}_{syn}$, for two values of heterogeneity: (a) $\epsilon = 3.3\%$ and (b) $\epsilon = 6.3\%$.

state (in that order). In contrast, Figure 4.2(b) shows that the diversity of network states becomes smaller for larger heterogeneity ($\epsilon > 4.8\%$). In this case there is asynchronous firing at small synaptic coupling strength, followed by the order-preserving phase-locked firing, and followed again by the asynchronous or chaotic firing, and the spike-suppress state at large coupling values.

Figure 4.3 presents the dependence of network activity on the degree of heterogeneity, as a two-parameter bifurcation diagram. The non-zero phase locked state (including near-synchrony state) is observed for mild to moderate heterogeneity, $\epsilon < 11\%$. Note that spiking order is preserved in near-synchrony and non-zero phase locked state. For a network with mild heterogeneity (Figure 4.2(a)), this non-zero phase locked state appears for small coupling strength. The minimum value of coupling strength required for this pattern increases as the heterogeneity increases. The period of the non-zero phase locked solution and the phase difference between the spikes of two cells vary depending on both on the coupling strength ($\bar{g}_{syn}$) and heterogeneity (ϵ). For example, when $\bar{g}_{syn} = 0.17$ and $\epsilon = 4.81\%$, the period-2 phase locked solution is observed with phase difference between the spikes of two cells of 0.4% to 7% of

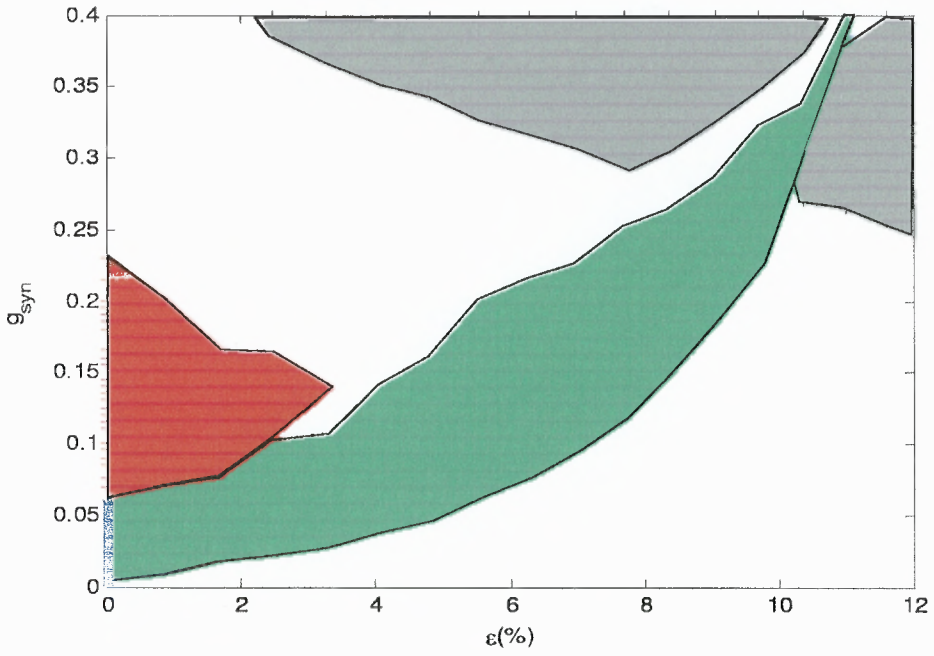

Figure 4.3 Dynamic states of the network on the coupling strength - heterogeneity ($\bar{g}_{syn} - \epsilon$) parameter plane. Stable synchrony appears for $\bar{g}_{syn} = 0$ to 0.06 when only $\epsilon = 0\%$ (blue thick bar on $\bar{g}_{syn}$ axis). The red region represents stable alternating-order firing. The green region represents stable non-zero phase-locked firing including near-synchrony state (order-preserving). The gray region represents the spike-suppress state. White area includes all other patterns - chaotic, mixed patterns, and bursting.

the unperturbed period, whereas for $\bar{g}_{syn} = 0.05$ and $\epsilon = 6.3\%$ the phase difference of period-16 non-zero phase locked solution constitutes from 0.3% to 67% of the unperturbed period (data is not shown).

The alternating-order firing state is exhibited when coupling strength is varied in the range $0.08 < \bar{g}_{syn} < 0.21$ in a mildly heterogeneous network ($\epsilon < 4.8\%$), but the interval between the neighboring spikes of the two cells is small, whereas it can reach 70% of the unperturbed period in homogeneous network case. Also, Figure 4.3 shows that the coupling strength parameter region supporting alternating-order firing becomes narrower as heterogeneity is increased. If heterogeneity (ϵ) is greater than 4.8%, the alternating-order firing can not be observed for any value of coupling strength, $\bar{g}_{syn}$.

Mixed pattern appears for a narrow region of coupling strength parameter ($0.16 < \bar{g}_{syn} < 0.22$) in the transition from alternating-order firing to chaotic state in mild heterogeneity ($\epsilon < 4.8\%$). The possible coupling strength parameter region showing mixed pattern shrinks as heterogeneity increases, and no $\bar{g}_{syn}$ value generates this pattern when heterogeneity, ϵ, is greater than 4.8%. Finally, $2:3$ mode-locked alternating-order spiking is observed for a very narrow region of coupling strength parameter ($0.27 < \bar{g}_{syn} < 0.29$) in the transition between two chaotic states when the heterogeneity is small ($\epsilon < 4\%$), as shown in Figure 4.2 (a) when $\epsilon = 3.3\%$.

4.4 STRC in the Heterogeneous Case

Since heterogeneity is implemented by increasing the applied current of one of the cells, this induces a change of the intrinsic period of the corresponding cell, resulting in a change of its STRC as a function of heterogeneity level. In Figure B(a) we numerically constructed STRC for different values of heterogeneity from 0% to 16% to show how the amount of input current heterogeneity affects the difference between STRCs of the two cells. The peak amplitude of STRC decreases and the peak of STRC is shifted slightly to the left as heterogeneity is increased (i.e. intrinsic frequency is increased) for fixed stimulus amplitude. Note that the corresponding changes in STRC are relatively small, and mostly occur at its peak (cf. Figure 2.8). We fit a 2nd order polynomial with $m = -0.15\epsilon^2 - 0.21\epsilon + 0.75$ to describe the change in the peak amplitude of the STRC, m, versus heterogeneity ϵ, neglecting the shift of the peak of STRC, as illustrated in Figure B (b).

In a mildly heterogeneous two-cell network let $\Delta^1(\cdot)$ and $\Delta^2(\cdot)$ be the STRCs of cells 1 and 2, respectively. Then the STRC of one cell can be approximated by one of the other cell:

$$\Delta^2(\phi) \approx \Delta^1(\phi) + \delta(\phi, \epsilon) \tag{4.2}$$

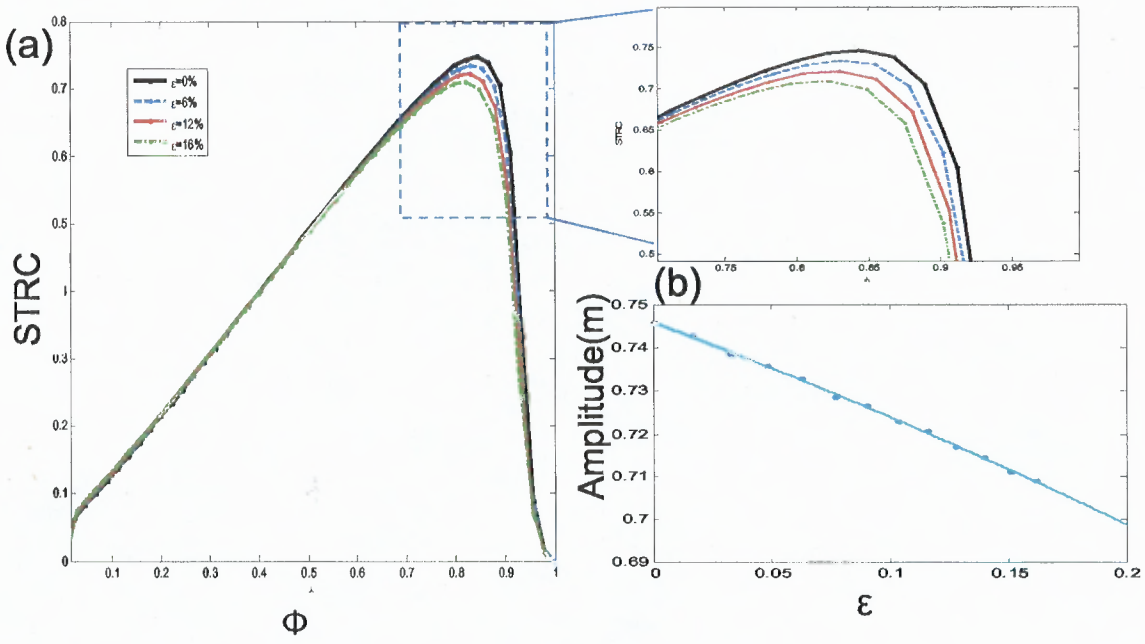

Figure 4.4 (a) Numerically constructed STRC for different values of heterogeneity from 0% to 16%. Four curves correspond to $\epsilon = 0\%$ (black curve), $\epsilon = 6\%$ (blue dashed curve), $\epsilon = 12\%$ (red curve), and $\epsilon = 16\%$ (green dash-dotted curve). The amplitude of STRC decreases and is slightly shifted to the left as heterogeneity increases. (b) The amplitude (m) of numerically constructed STRC in (a) versus heterogeneity (ϵ). The change of amplitude is interpolated in terms of ϵ by 2nd-order polynomial with $m = -0.15\epsilon^2 - 0.21\epsilon + 0.75$.

where $\epsilon << 1$ and $\delta(\phi, \epsilon)$ represents the discrepancy between two STRCs, which is a quantity of order ϵ. Note that obviously $\delta(0, \epsilon) = \delta(1, \epsilon) = 0$ for any value of ϵ

4.5 Analysis Based on Phase Return Map

In Subsection 2.3.4 we derived the phase return map in homogenous network to analyze the dynamics of coupled network on a quantitative level. Now we extend it to the heterogenous network case, with only first-order phase resetting, as in the homogenous network, and with Eq. 4.2 relating the two STRCs. In the heterogeneous network case, the phase return map should consider the phase dynamics of both coupled cells, since they have different intrinsic frequencies, whereas it was sufficient to analyze the phase dynamics of only one of the two cells in the homogeneous network

case. We will derive the phase return maps for each of the two firing patterns, the alternating-order firing and the order-preserving non-zero phase locked state.

First, we consider firing pattern for the order-preserving non-zero phase-locked state given in Figure 4.5(a), and define the phase return map for the phase intervals ϕ_{11} and ϕ_{12} in cell 1. We consider one period of phase-locked firing for each cell, while the cell receives one spike from the partner cell (represented as the bold part of each trace in Figure 4.5 (a)). The inter-stimulus time intervals t_j and s_j represent the time elapsed between the firing of cell 1 and the reception of the j-th input from cell 2, and between the firing of cell 2 and the reception of the j-th input from cell 1, respectively. Let ϕ_{1j} in cell 1 (red spike and red trace in Figure 4.5 (a)) and ξ_{2j} in cell 2 (blue spike and blue trace in Figure 4.5 (a)) denote the phase of each cell at the arrival time of the j-th synaptic current pulse due to the spike of the pre-synaptic cell, and ξ_{1j} in cell 1 and ϕ_{2j} in cell 2 be the phase of each cell at the next spike time, after receiving the j-th input from the other cell. Then the time intervals t_j and s_j can be expressed in terms of the phase variables ϕ_{ij} and ξ_{ij}, as follows:

$$t_j = \phi_{1j}T_1 = \phi_{2j}T_2, \quad s_j = \xi_{1j}T_1 = \xi_{2j}T_2 \tag{4.3}$$

where T_i $(i = 1, 2)$ are the unperturbed oscillation periods of cells 1 and 2. Since the amount of phase delay of cell 1 induced by the synaptic input at phase ϕ_{11} equals $\Delta^1(\phi_{11})$, where $\Delta^1(\cdot)$ is the STRC of cell 1, the phase ξ_{11} is given by $\xi_{11} - \Delta^1(\phi_{11}) + \phi_{11} = 1$, which follows from the first-passage time condition in cell 1. Similarly, we get $\xi_{21} - \Delta^2(\xi_{21}) + \phi_{22} = 1$ where $\Delta^2(\cdot)$ is the STRC of cell 2, from considering one period of cell 2 (represented in bold in Figure 4.5 (a)). Combining it with the relation $\xi_{21} = \frac{T_1}{T_2}\xi_{11}$ and $\phi_{22} = \frac{T_1}{T_2}\phi_{12}$ from Eq. 4.3, we obtain

$$\phi_{12} = \frac{T_2}{T_1} - \xi_{11} + \frac{T_2}{T_1}\Delta^2\left(\frac{T_1}{T_2}\xi_{11}\right) \tag{4.4}$$

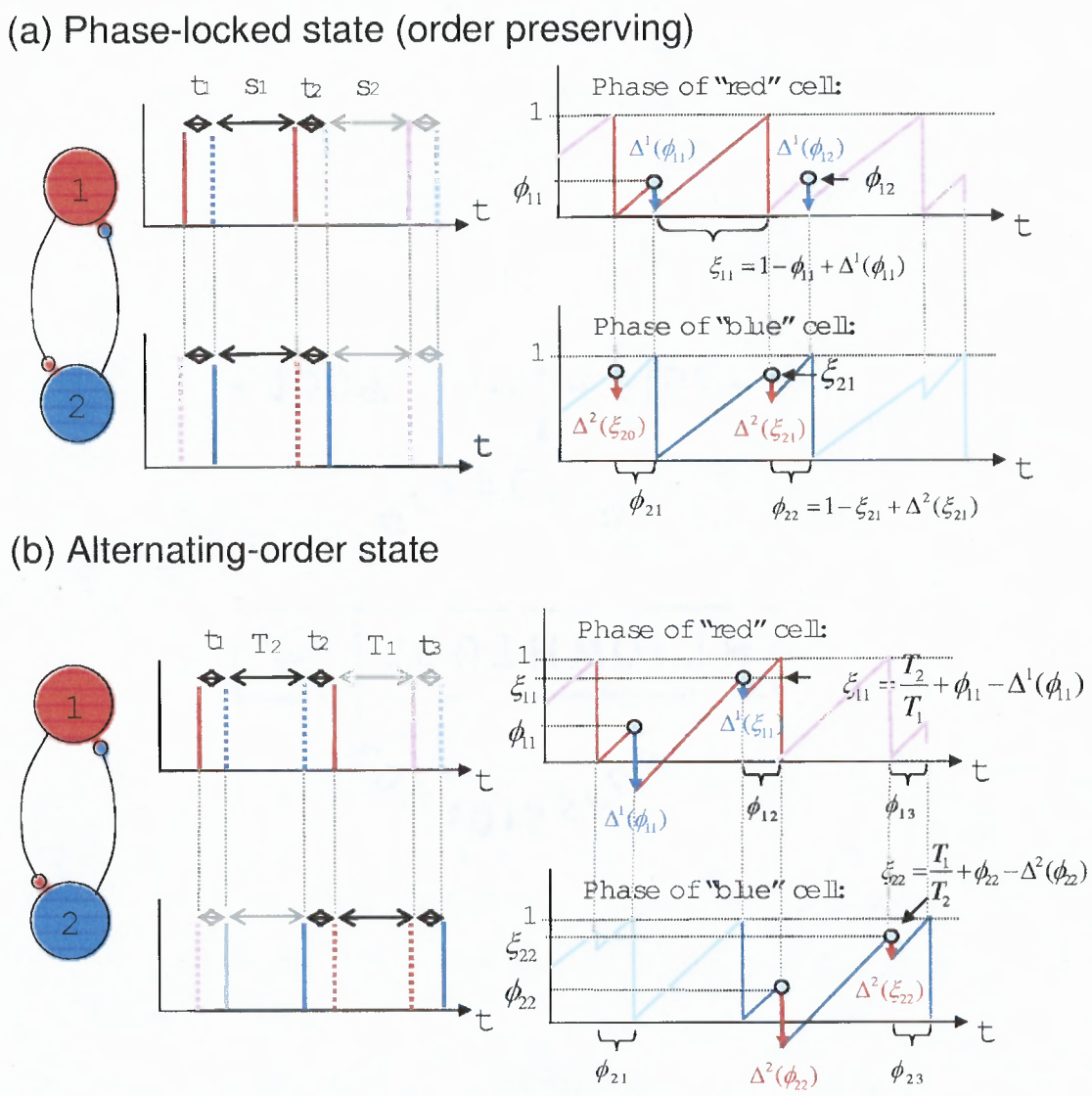

Figure 4.5 Constructing the inter-spike phase return map. Right panel shows the phase time-course of each cell emitting the spikes in left panel. (a) Phase-locked spiking: the phase intervals ϕ_{ij}, ξ_{ij} $(i = 1, 2)$ are inter-spike intervals normalized by the unperturbed period of each oscillator, T_1 and T_2. The phase delays due to one spike from partner cell equal $\Delta^1(\phi_{11})$ in cell 1 and $\Delta^2(\xi_{21})$ in cell 2. The next inter-spike intervals are $\xi_{11} = 1 - \phi_{11} + \Delta^1(\phi_{11})$ in cell 1 and $\phi_{22} = 1 - \xi_{21} + \Delta^2(\xi_{21})$ in cell 2. Note that $\xi_{21} = \frac{T_1}{T_2}\xi_{11}$ and $\phi_{22} = \frac{T_1}{T_2}\phi_{12}$. The inter-spike interval ϕ_{12} in cell 1 is found by combining two equations for inter-spike interval ξ_{11} and ϕ_{22} in each cell, yielding the phase return map, Eq. 4.4 (b) Alternating-order spiking: the phase intervals ϕ_{ij} $(i = 1, 2)$ are inter-spike intervals normalized by the unperturbed period of each oscillator, T_1 and T_2. The phase delays due to each of the two spikes equal $\Delta^1(\phi_{11})$ & $\Delta^1(\xi_{11})$ in cell 1, and $\Delta^2(\phi_{22})$ & $\Delta^2(\xi_{22})$ in cell 2, where ξ_{11}, ξ_{22} are the cell phases at the time of arrival of the second input in cell 1 and cell 2, respectively, $\xi_{11} = \frac{T_2}{T_1} + \phi_{11} - \Delta^1(\phi_{11})$ and $\xi_{22} = \frac{T_1}{T_2} + \phi_{22} - \Delta^2(\phi_{22})$. The second inter-spike interval ϕ_{12} in cell 1 and ϕ_{23} in cell 2 is found by the first-passage time condition $\xi_{11} - \Delta^1(\xi_{11}) + \phi_{12} = 1$ and $\xi_{22} - \Delta^2(\xi_{22}) + \phi_{23} = 1$, respectively, yielding the map in each cell, Eq. 4.11 and 4.13. The phase return map is obtained by the composition of two maps in each cell.

Therefore, the return map for the phase intervals ϕ_{1j} in cell 1 is given by

$$\phi_{12} \equiv \Phi(\phi_{11}) = \frac{T_2}{T_1} - 1 + \phi_{11} - \Delta^1(\phi_{11}) + \frac{T_2}{T_1}\Delta^2\left(\frac{T_1}{T_2}(1 - \phi_{11} + \Delta^1(\phi_{11}))\right) \quad (4.5)$$

substituting $\xi_{11} = 1 - \phi_{11} + \Delta^1(\phi_{11})$ into Eq. 4.4. Or it can be expressed in terms of the heterogeneity defined as $\epsilon = \frac{T_1}{T_2} - 1$:

$$\phi_{12} \equiv \Phi(\phi_{11}) \approx -\epsilon + \phi_{11} - \Delta^1(\phi_{11}) + (1-\epsilon)\Delta^2[(1+\epsilon)(1 - \phi_{11} + \Delta^1(\phi_{11}))] \quad (4.6)$$

where $\frac{T_2}{T_1} \approx 1 - \epsilon$ if terms of higher order in ϵ are ignored in the asymptotic series.

To simplify the phase return map in mildly heterogeneous network we expand the last term in Eq. 4.6 in a Taylor series with respect to ϵ, and use $\Delta^2(\phi) = \Delta^1(\phi) + \delta(\phi, \epsilon)$ from Eq. 4.2 to represent the two different STRCs. Then we obtain for the last term:

$$\begin{aligned}
\Delta^2((1+\epsilon)\xi_{11}) &\approx \Delta^2(\xi_{11}) + \epsilon\xi_{11}\frac{\partial\Delta^2(\xi_{11})}{\partial\xi} + O(\epsilon^2) \\
&\approx \Delta^1(\xi_{11}) + \delta(\xi_{11},\epsilon) + \epsilon\xi_{11}\left(\frac{\partial\Delta^1(\xi_{11})}{\partial\xi} + \frac{\partial\delta(\xi_{11},\epsilon)}{\partial\xi}\right) + O(\epsilon^2) \\
&\approx \Delta^1(\xi_{11}) + \epsilon\xi_{11}\frac{\partial\Delta^1(\xi_{11})}{\partial\xi} + \delta(\xi_{11},\epsilon) + \epsilon\xi_{11}\frac{\partial\delta(\xi_{11},\epsilon)}{\partial\xi} + O(\epsilon^2)
\end{aligned}$$

where $\xi_{11} = 1 - \phi_{11} + \Delta^1(\phi_{11})$ and $\epsilon << 1$. Therefore the phase return map is approximated as

$$\begin{aligned}
\phi_{12} &= \Phi(\phi_{11}) \\
&\approx -\epsilon + \phi_{11} - \Delta^1(\phi_{11}) + (1-\epsilon)\Delta^1(\xi_{11}) + \epsilon\xi_{11}\frac{\partial\Delta^1(\xi_{11})}{\partial\xi} + \delta(\xi_{11},\epsilon) \quad (4.7)
\end{aligned}$$

if second- and higher-order terms in ϵ are neglected.

If we consider the condition for synchronous firing, $\phi_{11} = 0$ and $\xi_{11} = 1$, we obtain

$$\begin{aligned}
\Phi(0) &= -\epsilon - \Delta^1(0) + (1-\epsilon)\Delta^1(1) + \epsilon\frac{\partial\Delta^1(1)}{\partial\xi} + \delta(1,\epsilon) \\
&= -\epsilon - \Delta^1(0) \neq 0 \quad (4.8)
\end{aligned}$$

since $\Delta^1(1) = 0$, $\delta(1, \epsilon) = 0$ and $\frac{\partial \Delta^1(1)}{\partial \xi} = 0$. Therefore, even for the case $\Delta^1(0) = 0$, synchrony state doesn't exist for non-zero heterogeneity ϵ.

To derive the condition for non-zero phase-locked firing, ϕ, we have to find the roots of

$$F(\phi) = \Phi(\phi) - \phi = -\epsilon - \Delta^1(\phi) + (1 - \epsilon)\Delta^1(\xi) + \epsilon\xi \frac{\partial \Delta^1(\xi)}{\partial \xi} + \delta(\xi, \epsilon) \tag{4.9}$$

For $\phi = \phi_c$ denoting ϕ_c the root of $\phi_c = \Delta(\phi_c)$, we get

$$F(\phi_c) \;=\; -\epsilon - \Delta^1(\phi_c) < 0$$

Note that $F(\phi)$ has to be a decreasing function of ϕ at the stable fixed point, ϕ_{eq}, $(-2 < F'(\phi_{eq}) < 0)$. Given that $F(\phi_c) < 0$, this means that $F(\phi)$ has to change sign to positive values on the interval $[\phi_c, 1)$, followed by a change in sign back to negative values at the stable fixed point of $\Phi(\phi)$. Therefore, a necessary but not sufficient condition for the existence of a stable phase locked spiking is $F(1) \leq 0$. To first order in ϵ we have

$$F(1) \;=\; \Delta^1(0) - \epsilon(1 + \Delta^1(0)) \leq 0$$

Thus, we obtain the following lower bound on the heterogeneity parameter ϵ: $\epsilon \geq \frac{\Delta^1(0)}{1+\Delta^1(0)}$. Note that in the case $\Delta^1(0) = 0$ stable order-preserved firing is achieved even for zero heterogeneity value, in which case synchronous firing is obtained. For sufficiently high values of ϵ the map $\Phi(\phi)$ has no stable fixed points, since $F(\phi) < 0$ on the entire phase domain $[0, 1]$. Note that the condition we obtained does not depend on the discrepancy, $\delta(\xi, \epsilon)$, of STRCs.

In the case of the alternating-order firing, phase return map is similar but more complex than in homogenous network case. Since the intrinsic periods of cell 1 and cell 2 (red and blue traces in Figure 4.5) are not same, the map relating phases ϕ_{11} and ϕ_{12} is not identical to the map relating phases ϕ_{12} and ϕ_{13} in Figure 4.5 (b).

Therefore, the corresponding phase return map should combine the dynamics of both cells, describing the evolution of their phases while each cell receives two spikes from its partner cell. So we take two consecutive cycles of alternating-order firing from each cell (represented as bold part of each trace in Figure 4.5(b)) and define the maps for the phase intervals ϕ_{11} and ϕ_{12} in cell 1, and ϕ_{22} and ϕ_{23} in cell 2.

Let t_j be the inter-stimulus time interval between the firing of the two cells, and let ϕ_{ij} $(i = 1, 2)$ denote the inter-spike intervals normalized by the unperturbed period of the ith oscillator, T_i. Then $t_j = \phi_{1j}T_1 = \phi_{2j}T_2$. If synaptic inhibition is sufficiently strong at ϕ_{11}, i.e. $\Delta^1(\phi_{11}) > \phi_{11}$, then pre-synaptic cell 2 has a chance to spike again, and the time interval between the two consecutive spikes of cell 2 is equal to its intrinsic period T_2, which corresponds to the phase interval of $\frac{T_2}{T_1}$ in cell 1. This second synaptic current from cell 2 arrives when the phase of cell 1 equals $\xi_{11} \equiv \frac{T_2}{T_1} + \phi_{11} - \Delta^1(\phi_{11})$ and the resulting phase delay is equal to $\Delta^1(\frac{T_2}{T_1} + \phi_{11} - \Delta^1(\phi_{11}))$. Therefore, the total phase delay due to both inputs is equal to

$$\phi_{11} + \phi_{12} = 1 - \frac{T_2}{T_1} + \Delta^1(\phi_{11}) + \Delta^1\left(\frac{T_2}{T_1} + \phi_{11} - \Delta^1(\phi_{11})\right) \tag{4.10}$$

Thus, the return map for the phases ϕ_{11} and ϕ_{12} in cell 1 is given by

$$\phi_{12} \equiv \Phi_1(\phi_{11}) = 1 - \frac{T_2}{T_1} + \Delta^1(\phi_{11}) + \Delta^1\left(\frac{T_2}{T_1} + \phi_{11} - \Delta^1(\phi_{11})\right) - \phi_{11} \tag{4.11}$$

or, expressed in terms of the phase of the post-synaptic cell at the time of arrival of the second spike, $\xi_{11} = \frac{T_2}{T_1} + \phi_{11} - \Delta^1(\phi_{11})$:

$$\phi_{12} \equiv \Phi_1(\phi_{11}) = 1 + \Delta^1(\xi_{11}) - \xi_{11} \tag{4.12}$$

Similarly, the return map for the phases ϕ_{22} and ϕ_{23} in cell 2 is given by

$$\phi_{23} \equiv \Phi_2(\phi_{22}) = 1 - \frac{T_1}{T_2} + \Delta^2(\phi_{22}) + \Delta^2\left(\frac{T_1}{T_2} + \phi_{22} - \Delta^2(\phi_{22})\right) - \phi_{22} \tag{4.13}$$

also, expressed in terms of the phase of the post-synaptic cell at the time of arrival of the second spike, $\xi_{22} = \frac{T_1}{T_2} + \phi_{22} - \Delta^2(\phi_{22})$:

$$\phi_{23} \equiv \Phi_2(\phi_{22}) = 1 + \Delta^2(\xi_{22}) - \xi_{22} \tag{4.14}$$

Finally, combining Eq. 4.11 (or 4.12) and Eq. 4.13 (or 4.14), and applying $\phi_{1j} = \frac{T_2}{T_1}\phi_{2j}$, the return map in cell 1 is given by

$$\phi_{13} \equiv \Phi(\phi_{11}) = \frac{T_2}{T_1}\Phi_2\left(\frac{T_1}{T_2}\Phi_1(\phi_{11})\right) = (1-\epsilon)\Phi_2((1+\epsilon)\Phi_1(\phi_{11})) \tag{4.15}$$

where $\frac{T_2}{T_1} \approx 1-\epsilon$ if higher order terms are ignored in asymptotic series of heterogeneity parameter ϵ.

Eq. 4.15 can be used to examine both the existence and stability of alternating-order firing in terms of the heterogeneity parameter, ϵ.

4.6 Conclusion

For homogeneous network, it has been known that slowly decaying inhibition generally has a synchronizing influence [24, 83, 86]. However, for mildly heterogenous networks, the relationship between the frequency and the synaptic decay time must also be considered in affecting network dynamics [91, 77, 78]. In our studies, synaptic decay time is fixed as $t_{syn} = 1ms$, which is very fast ($t_{syn}/T << 1$) and the amount of heterogeneity (ϵ) due to the change of applied current is used as a parameter in two-cell network studies, emphasizing the role of heterogeneity in affecting network dynamics.

Our results show that the network oscillations depends on the applied current and the synaptic conductance. With mild heterogeneity, we have shown that stable alternating-order firing and order-preserving non-zero phase locked state occur. The alternating-order state is lost as the heterogeneity is increased, which happens much earlier than the breaking of non-zero phase lock state including near-synchrony. When

these two states break, states of asynchrony, mixed pattern firing, bursting or spike-suppression may arise in certain range of coupling strength, $\bar{g}_{syn}$ and heterogeneity, ϵ.

We have shown that the phase return map approach based on the STRC can be extended in heterogeneous network case, and it is expressed in terms of the difference between the STRCs of the two cells and the difference between their periods, expressed in terms of heterogeneity parameter, ϵ. The heterogeneity induces the small discrepancy between STRCs of the two cells, which is of order ϵ. Interestingly, our predictions of phase dynamics based on the phase return map depend mostly on the heterogeneity in the periods of the two oscillators, and are much less sensitive to the difference between the STRCs of the two cells, $\delta(\phi, \epsilon)$. In fact, for small heterogeneity the existence criteria for a particular pattern derived here hold regardless of the form of $\delta(\phi, \epsilon)$, as long as $\delta(0, \epsilon) = \delta(1, \epsilon) = 0$.

Note that our results (Eqs. 4.6 - 4.9) can also be used to analyze the case where heterogeneity is primarily due to the differences in individual synaptic conductances rather than the differences in intrinsic periods of the cells. Contrary to the case examined above, in this case the main heterogeneity parameter would be $\delta(\phi)$, the difference in STRCs of the two cells.

CHAPTER 5

DISCUSSION

We have shown that the non order-preserving activity recently observed by Maran and Canavier [53] in an inhibitory network of Wang-Buzsáki oscillators can also be obtained in a network of lower-dimensional Morris-Lecar model neurons, and therefore is a general property of a wider class of type-I excitable cells. Namely, we found that such "leap-frog" dynamics results when the inhibition from one cell is sufficient to transiently bring the post-synaptic cell below the excitability threshold, producing a phase delay that is greater than the time elapsed since the preceding spike. As the coupling strength is increased, the leap-frog spiking state gives way to a period-doubling cascade, leading to more complex m:n periodic bursting states, as well as chaotic activity. Finally, at sufficiently strong values of the coupling strength oscillator death occurs, whereby only one of the cells continues spiking, suppressing the activity of the postsynaptic cell. Analogous activity states can also be obtained in larger inhibitory networks of type-I oscillators, including heterogeneous networks [53].

Interestingly, in a narrow range of synaptic conductance values, one obtains $m : m$ mode-locked states whereby each cell emits several consecutive spikes in each cycle, followed by several spikes of the partner cell (see Figure 2.1(e)). Note that this represent a novel mechanism of bursting, which is much simpler than the more widely known mechanisms [41], since it does not rely on any intrinsic cell currents. This bursting mechanism is an emergent property of the synaptic interaction between the two oscillators, and there is no intrinsic time scale setting the length of the burst. We will explore the possible implications of this bursting mechanism in our future work.

One of our goals was to reveal the conditions required for periodic alternating-order dynamics, and we showed that it can be achieved under two different sets of conditions. First, it can be exhibited by a network of phase oscillators, in the presence of independent synaptic degrees of freedom with non-zero synaptic decay time. Second, leap-frog spiking is also possible in networks of oscillators whose dynamics cannot be reduced to a single phase variable. In the latter case order alternation can be achieved even in a purely pulse-coupled network. This is true in particular for a network of appropriately modified quadratic integrate-and-fire model cells (Figure 2.12). We found that the ML network we examined also falls within the latter class of models, in that order alternation is achieved for very short synaptic decay time, and the periodic trajectory of each cell significantly deviates from the unperturbed limit cycle due to periodically received inhibition.

In both classes of models, periodic spike-order alternation requires the same conditions on the phase resetting characteristic of the coupled cells. To establish these conditions, we followed the approach of Maran and Canavier [53], but restricted ourselves to the case of a homogeneous network in Chapter 2, in order to determine the most basic requirements leading to spiking order alternation (Eqs. 2.9-2.11). In Chapter 4, we extended our analysis to the heterogenous network case, and analyzed both the order-alternating firing and the order-preserving non-zero phase locked state in this case. The principle condition for order alternation is that the phase delay produced by an input arriving shortly after the spike-time should be larger than the time elapsed since this last spike, $\Delta(\phi) > \phi$. Thus, the phase-transition map (Eq. 2.6) is complementary to the map of Goel and Ermentrout [27] derived under the assumption of phase map invertibility, $\Delta(\phi) < \phi$. In a pulse-coupled network, such strong resetting automatically breaks the phase structure of each oscillator, since it leads to a delay past the spike-time, requiring an additional negative-phase domain branch, or, alternatively, an additional condition that a cell does not emit a spike

unless its winding number is increased [5, 32]. In contrast, in a network of cells with a non-zero synaptic decay time this complication does not arise, since such strong phase delay resetting is spread out over a finite time interval, and the phase variable may remain positive. For the Morris-Lecar model in the type-I parameter regime we consider, this strong phase resetting property is directly related to the fast kinetics of the K^+ channels relative to the rate of change of the membrane potential, which clamps the trajectory to the w-nullcline during the quiescent subthreshold phase of the limit cycle. An inhibitory current pulse applied in this oscillation phase perturbs the dynamics along the w-nullcline, which plays the role of a slow manifold, allowing to achieve a phase delay greater than the time to the preceding spike.

For cells that can be reduced to such a dual-branched phase model, we showed that the extension of the STRC to negative phase values allows to accurately predict the response of the cell to several close non-weak perturbations. Such an extended STRC can then be used to analyze the dynamics of three or more non-weakly coupled cells, whereby more than one synaptic perturbation arrives per oscillation cycle into each cell. In the future work we will explore the implications of such an extended STRC approach for predicting the dynamics of networks with more than three cells.

Further, we also showed that the entire bifurcation structure of the network activity obtained by increasing the synaptic conductance parameter, and involving a period-doubling cascade to chaos and more complex $m : n$ mode-locked bursting patterns, can all be explained by a simple scaling of the peak amplitude of a simplified quadratic STRC function. Therefore, the observed dependence of network activity on the synaptic inhibition strength is very general, and does not require the non-trivial change in the shape of the STRC arising from the biophysics of a particular cell model.

These results further illustrate the qualitative features of periodic spike train patterns that can be produced by simple inhibitory networks of cells with type-I

excitability, beyond the simple phase-locked firing states that can be predicted using the weak-coupling theory (see also White et al. [91]). This may have implications for the study of central pattern generators, which are responsible for producing distinct firing sequences, for instance in enervating opposing muscle groups during motor activity, and which often contain subnetworks of several cells coupled by reciprocal inhibition. We note that the classification of possible network activity states, and its relationship to the underlying network architecture and the qualitative properties of cell dynamics, is a subject of significant recent interest [31, 32, 1].

Our results also demonstrate the fact that the range of applicability of the weak coupling results is quite narrow in inhibitory networks of type I cells that are close to their excitation thresholds [38]. Therefore, asynchronous dynamics may be quite prevalent in neuronal networks with strong inhibitory synaptic currents, possibly including some interneuron networks in the mammalian brain, even in cases where the weak coupling tends to synchronize the neurons. In our future work we will use computer simulations of networks consisting of a large number of coupled cells in order to investigate the interaction between synchronizing and desynchronizing effects of non-weak synaptic inhibition in large neural circuits.

It is important to explore whether the phenomenon we describe is even more general, and whether similar dynamical behavior is exhibited by non-weakly coupled cells of a different excitability class, satisfying the crucial condition of strong phase delay, $\Delta(\phi) > \phi$. To address this question, in Section 2.5 we fully examined the general conditions on the shape of STRC functions leading to order switching dynamics, using the conditions, Eqs. 2.9-2.11. This would allow one to extend our analysis and results to networks of excitable cells not belonging to type-I excitability class, whose phase-resetting characteristic can change the sign over part of its phase domain [18]. In this case an inhibitory synaptic input may produce a phase advance rather than a phase delay, and order alternation may in principle be achieved in an *excitatory*

network of such cells, given that the conditions Eqs. 2.9-2.11 on their phase resetting properties are satisfied. In the future we will search for specific biophysical excitable cell models that would yield some of the different STRC shapes examined in Section 2.5, with the aim to demonstrate the existence of periodic leader switching in excitatory networks. This would significantly increase the generality of our results.

Finally, we hope that future experimental studies will be able to validate some of our conclusions, through a detailed study of synaptically coupled simple-spiking (non-bursting) neurons. One promising experimental approach to verify our results about the behavior of non-weakly coupled networks is provided by the dynamic clamp protocol [67], which would allow one to artificially couple a small number of isolated cell in order to study in detail the effect of synaptic coupling parameters on the resulting network dynamics [58, 63].

APPENDIX A

DERIVATION OF THE ALTERNATING-ORDER PHASE MAP WITH SECOND-ORDER PHASE RESETTING

We will use the diagram in Figure 2.7(a) to derive the map in the case of non-negligible second-order phase resetting, $\Delta_2(\phi)$. Let $\{\phi_n, \xi_n\}$ denote the two phases of the postsynaptic cell at the time of arrival of each of the two spikes in n-th period of the oscillation. In the case of zero second-order resetting, Figure 2.7 illustrates the relationship between these phases, $\xi_n = 1 + \phi_n - \Delta(\phi_n)$. However, due to non-zero second-order phase resetting received by the presynaptic cell in the preceding cycle, $\Delta_2(\xi_{n-1})$ (where ξ_{n-1} is its phase at the time of arrival of the first black spike in Figure 7(a)), the interval between two spikes of the presynaptic cell in the current cycle, denoted γ_n, will not be equal to 1:

$$\gamma_n = 1 + \Delta_2(\xi_{n-1}) > 1 \tag{A.1}$$

Therefore, the modified relationship between ξ_n and ϕ_n reads

$$\xi_n = \gamma_n + \phi_n - \Delta(\phi_n) \tag{A.2}$$

Note that we neglect the much smaller second-order phase-resetting due to the first spike of the presynaptic cell in each period of the 2:2 mode: $\Delta_2(\phi_n) << \Delta_2(\xi_n)$. Finally, given the phase ξ_n of the postsynaptic cell right before receiving its second input, one can easily find its first passage time, ϕ_{n+1} (i.e. interval ϕ_2 in Figure 7(a)), using the first passage time condition

$$\xi_n - \Delta(\xi_n) + \phi_{n+1} = 1 \tag{A.3}$$

Solving this system of equations for ξ_n yields the map

$$\xi_{n+1} = 2 - \xi_n + \Delta(\xi_n) - \Delta(1 - \xi_n + \Delta(\xi_n)) + \Delta_2(\xi_n) \tag{A.4}$$

which can be re-written in a more compact form as

$$\xi_{n+1} = 1 + \phi_{n+1} - \Delta(\phi_{n+1}) + \Delta_2(\xi_n) \tag{A.5}$$

If we substitute the conditions for synchronous firing, $\xi_n = 1$, $\phi_n = 0$, we obtain $\Delta_2(1) = \Delta(0)$, which is the correct periodicity condition relating the first- and second-order STRC curves. Therefore, the synchronous solution is always a fixed point of Eq. A.4.

Differentiating Eq. A.5 yields the stability condition

$$|[1 - \Delta'(\phi)][\Delta'(\xi) - 1] + \Delta_2'(\xi)| < 1 \tag{A.6}$$

which agrees with Eq. 2.12 when $\Delta_2(\cdot)$=0. Close to the bifurcation from synchrony to leap-frog spiking, $\xi \approx 1$, $\Delta'(\xi) \approx 0$, and therefore

$$|\Delta'(\phi) + \Delta_2'(\xi) - 1| < 1$$

which yields

$$0 < \Delta'(\phi) + \Delta_2'(\xi) < 2 \tag{A.7}$$

Recall that $\phi = 1 - \xi + \Delta(\xi)$ (Eq. A.3). A more general stability condition for the case of non-negligible $\Delta_2(\phi_n)$ is given by Maran and Canavier [53].

APPENDIX B

STABLE LEAP-FROG DYNAMICS IN A PHASE OSCILLATOR NETWORK

The 2-cell network of phase oscillators producing stable alternating-order firing in Figure 2.6(a) is easy to implement. Here is the most straightforward implementation that is far from elegant, but serves the purpose:

$$\begin{cases} \frac{d\phi_1}{dt} &= 1 - g_{syn}P(\phi_1)S_2(t) \\ \frac{d\phi_2}{dt} &= 1 - g_{syn}P(\phi_2)S_1(t) \\ \frac{dS_1}{dt} &= k_{gr}(1 - S_1)\sigma(\phi_1) - k_{decay}S_1 \\ \frac{dS_2}{dt} &= k_{gr}(1 - S_2)\sigma(\phi_2) - k_{decay}S_2 \end{cases}$$

Where $k_{gr} = 3$ and $k_{decay} = 10$ are synaptic growth and decay rates, respectively, $g_{syn} = 200$ is the coupling constant, $\sigma(\phi)$ is a sigmoid spike thresholding function, and $P(\phi)$ is the STRC function defined by:

$$\begin{cases} \sigma(\phi) &= 1 + \tanh[40(\sin(2\pi\phi) - 0.999)] \\ P(\phi) &= \phi(1 - \phi)^2 \end{cases}$$

In the spike-time resetting term $P(\phi)$, the phase argument is assumed to be modulus 1. Note the asymmetric shape of the STRC.

The result of a run over 6 times units clearly shows the fast approach to stable leap-frog dynamics:

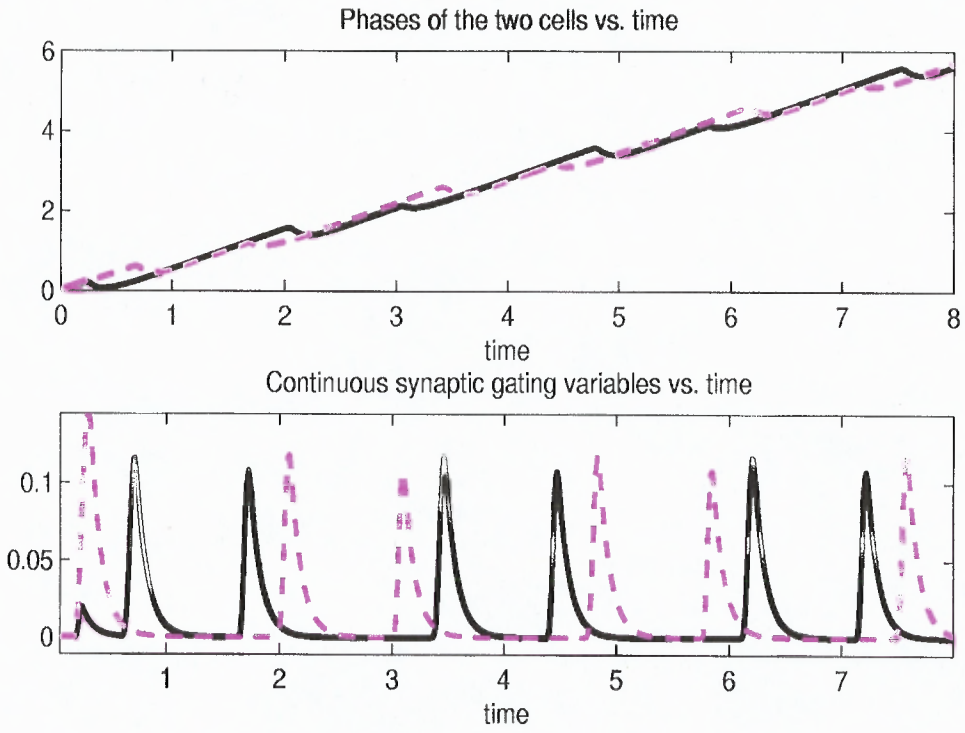
Phases of the two cells vs. time
6
4
2
0
0
1
2
3
4
5
6
7
8
time
Continuous synaptic gating variables vs. time
0.1
0.05
0
1
2
3
4
5
6
7
time

BIBLIOGRAPHY

[1] C.D. Acker, N. Kopell, and J.A. White, Synchronization of strongly coupled excitatory neurons: Relating network behavior to biophysics. *Journal of Compupational Neuroscience,* 15:71-90, 2003.

[2] A. Bose, N. Kopell, and D. Terman, Almost synchronous solutions for pairs of neurons coupled by excitation. *Physica D,* 140:69-94, 2000.

[3] P.C. Bressloff and S. Coombes, Desynchronization, mode locking, and bursting in strongly coupled integrate-and-fire oscillators. *Physical Review Letters,* 81:2168-2171, 1998.

[4] P.C. Bressloff and S. Coombes, Dynamics of strongly-coupled spiking neurons. *Neural Computation,* 12:91-129, 2000.

[5] E. Brown, J. Moehlis, and P. Holmes, On the phase reduction and response dynamics of neural oscillator populations. *Neural Computation,* 16:673-715, 2004.

[6] N. Brunel, Dynamics of saprsely conneted networks of exitatory and inhibitory spiking neurons. *Journal of Computational Neuronscience,* 8(3):183-208, 2000.

[7] J. Buck and E. Buck, Synchrnous fireflies. *Scientific American,* 234:74-85, 1976.

[8] J. Buck, Synchronous rhythmic flashing of fireflies. *II, Quart. Rev. Biology,* 63:265-289, 1988.

[9] C.C. Canavier, D.A. Baxter, J.W. Clark, and J.H. Byrne, Control of multistability in ring circuits of oscillators. *Biological Cybernetics,* 80:87-102, 1999.

[10] C.C. Canavier, R.J. Butera, R.O. Dror, D.A. Baxter, J.W. Clark, and J.H. Byrne, Phase response characteristics of model neurons determine which patterns are expressed in a ring circuit model of gait generation. *Biological Cybernetics,* 77:367-380, 1997.

[11] J.A. Connor, D. Walter, and R. McKown, Neural repetitive firing. Modifications of the Hodgkin Huxley axon suggested by experimental results from crustacean axons. *Biophysical Journal,* 18(1):81-102, 1977.

[12] D. Desmaison, J.D. Vincent, P.M. Lledo, Control of action potential timing by intrinsic subthreshold oscillations in olfactory bulb output neurons. *Journal of Neurosciences,* 19:10727-10737, 1999.

[13] R.O. Dror, C.C. Canavier, R.J. Butera, J.W. Clark, and J.H. Byrne, A mathematical critereon based on the phase response curves for stability in a ring of coupled oscillators. *Biological Cybernetics,* 80:11-23, 1999.

[14] J.T. Enright, Temporal precision in circadian systems: A reliable neuronal clock from unreliable components? *Science,* 209:1542-1545, 1980.

[15] G.B. Ermentrout and N. Kopell, Frequency plateaus in a chain of weakly coupled oscillators. *SIAM Journal of Mathematics Analysis,* 15: 215-237, 1984.

[16] G.B. Ermentrout and N. Kopell, Oscillator death in systems of coupled neural oscillators. *SIAM Journal of Applied Mathematics,* 50:125-146, 1990.

[17] G.B. Ermentrout and N. Kopell, Multiple pulse interactions and averaging in systems of coupled neural oscillators. *Journal of Mathematical Biology,* 29:195-217, 1991.

[18] G.B. Ermentrout, Type I membranes, phase resetting curves, and synchrony. *Neural Computation,* 8:979-1001, 1996.

[19] G.B. Ermentrout, Ermentrout-Kopell canonical model. *Scholarpedia,* 3:1398, 2008.

[20] U. Ernst, K. Pawelzik, and T. Geisel, Synchronization induced by temporal delays in pulse-coupled oscillators. *Physical Reveiw Letters,* 74:1570-1573, 1995.

[21] W.J. Freeman and W. Schneider, Changes in spatial patterns of rabbit olfactory EEG with conditioning to odors. *Psychophysiology,* 19:44-56, 1992.

[22] W.J. Freeman, Simulation of chaotic EEG patterns with a dynamic model of the olfactory system. *Biological Cybernetics,* 56:139-150, 1987.

[23] A. Frien, R. Eckhorn, R. Bauer, T. Woelbern, and H. Kehr, Stimulus-specific fast oscillations at zero phase between visual areas V1 and V2 of awake monkey. *Neuro. Report,* 5(17):2273-2277, 1994.

[24] W. Gerstner, JL. van Hemmen, and J. Cowen, What matters in neuronal locking? *Neural Computing,* 8:1653-1676, 1996.

[25] W. Gerstner and W.M. Kistler, Mathematical formulations of hebbian learning. *Biological Cybernetics,* 87:404-415, 2002.

[26] L. Glass, M.R. Guevara, J. Belair, and A. Shrier, Global bifurcations of a periodically forced biological oscillator. *Physical Review A,* 29:1348-1357, 1984.

[27] P. Goel and G.B. Ermentrout, Synchrony, stability, and firing patterns in pulse-coupled oscillators. *Physica D,* 163:191-216, 2002.

[28] D. Golomb and J. Rinzel, Clustering in globally coupled inhibitory neurons. *Physica D,* 71:259-282, 1994.

[29] D. Golomb and D. Hansel, The number of synaptic inputs and the synchrony of large, sparse neuronal networks. *Neural Computation,* 12(5):1095-1139, 2000.

[30] D. Golomb, D. Hansel, and G. Mato, Mechanisms of synchrony of neural activity in large networks. In:Handbook of biological Physics. *Elsevier Sciences B.V. Amsterdam,* 4:887-968, 2001.

[31] M. Golubitsky, I. Stewart, P.L. Buono, and J.J. Collins, Symmetry in locomotor central pattern generators and animal gaits. *Nature,* 401:693-695, 1999.

[32] M. Golubitsky, K. Josic and E. Shea-Brown, Winding numbers and average frequencies in phase oscillator networks. *Journal of Nonlinear Sciences,* 16:201-231, 2006.

[33] C.M. Gray, P. Konig, A.K. Engel, and W. Singer, Oscillatory responses in cat visual cortex exhibit intercolumnar synchronization which reflects global stimulus properties. *Nature,* 338:334-337, 1989

[34] C.M. Gray, Synchronous oscillations in neuronal systems:Mechanism and functions. *Journal of Computational Neuroscience,* 1:11-38, 1994

[35] D. Hansel, G. Mato and C. Meunier, Synchrony in excitatory neural networks. *Neural Computation,* 7:307-337, 1995.

[36] F.E. Hanson, Comparative studies of firefly pacemakers. *Federation Proceedings,* 2158-2164, 1978.

[37] J.J. Hopfield and C.D. Brody What is a moment? Trasient synchrony as a collective mechanism for spatiotemporal intergration. *Proceedings of the National Academy Sciences of USA,* 98(3):1282-1287, 2001.

[38] F.C. Hoppensteadt and E.M. Izhikevich, Weakly connected neural networks. *Springer-Verlag, New York,* 1997

[39] E.M. Izhikevich, Weakly pulse-coupled oscillators, FM interactions, synchronization, and oscillatory associative memory. *IEEE Transactions on neural networks,* 10(3):508-526, 1999

[40] EM. Izhikevich, Phase equations for relaxation oscillators. *SIAM Journal of Applied Mathematics,* 60:1789-1805, 2000.

[41] E.M. Izhikevich, Dynamics systems in neuroscience: The geometry of excitability and bursting. *MIT Press, Cambridge, Massachusetts,* 2006

[42] E.M. Izhikevich and Y. Kuramoto, Weakly coupled oscillators. In:Encyclopedia of Mathematical Physics. *Elsevier Academic Press, New York,* 5:448, 2006.

[43] S.R. Jones, D. Pinto, T. Kaper, and N. Kopell, Alpha-frequency rhythms desynchronize over long cortical distances: A modeling study. *Journal of Compututional Neuroscience,* 9:271-291, 2000.

[44] W.M. Kistler, J.L. van Hemmen, and C.I. De Zeeuw, Time window control: A model for cerebellar function based on synchronization, reverberation, and time slicing. In:Cerebellar Modules: Molecules, Morphology, and Function. *Progress in Brain Research, Elsevier, Amsterdam* 275-297, 2000.

[45] N. Kopell, Toward a theory of modeling central pattern generators. In:Neural Control of Rhythms. *Wiley, New York,* 1998.

[46] N. Kopell, Chains of coupled oscillators. In:Brain Theory and Neural Netowrks. *MIT Press, Cambrigde, Massachusetts,* 1995.

[47] N. Kopell, G.B. Ermentrout, M. Whittington, and R.D. Traub, Gamma rhythms and beta rhythms have different synchronization properties. *Proceedings of the National Academy Sciences of USA,* 97:1867-1872, 2000.

[48] N. Kopell, and G.B. Ermentrout, Mechanisms of phase-locking and frequency control in pairs of coupled neural oscillators. In:Handbook on Dynamical Systems: Toward applications. *Elsevier Academic Press, New York,* 2002.

[49] A.K. Kreiter, and W. Singer, Stimulus-dependent synchronization of neuronal reponses in the visual cortex of the awake macaque monkey. *Journal Neurosciences,* 16(7):2381-2396, 1996.

[50] Y. Kuramoto, Chemical oscillations, waves, and turbulence. *Springer-Verlag, Berlin* 1984.

[51] G. Laurent, Dynamical representation of odors by oscillating and evolving neural assemblies. *Trends Neuroscience,* 19:489-496, 1996.

[52] R. Llinás, The noncontinuous nature of movement execution. In:Motor Control: Concepts and Issues. *Wiley, New Yourk,* 223-242, 1991.

[53] S.K. Maran and C.C. Canavier, Using phase resetting to predict 1:1 and 2:2 locking in two neuron networks in which firing order is not always preserved. *Journal of Computational Neroscience,* 24:37-55, 2008.

[54] M.K. McClintock, Menstrual synchrony and suppression. *Nature,* 229:244-245, 1971.

[55] L. Mioche and W. Singer, Chronic recordings from single sites of kitten striate cortex during experience-dependent modifications of receptive-field properties. *Journal of Neurophysiology,* 62(1):185-197, 1989.

[56] R.E. Mirollo and S.H. Strogatz, Synchronization of pulse-coupled biological oscillators. *SIAM Journal of Applied Mathematics,* 50:1645-1662, 1990.

[57] C. Morris and H. Lecar, Voltage oscillations in the barnacle giant muscle fiber. *Biophysical Journal,* 35:193-213, 1981.

[58] T.I. Netoff, M.I. Banks, A.D. Dorval, C.D. Acker, J.S. Haas, N. Kopell, and J.A. White, Synchronization in hybrid neuronal networks of the hippocampal formation. *Journal of Neurophysiology,* 93:1197-1208, 2005.

[59] J. O'Keefe, Hippocampus, theta, and spatial memory. *Current Opinion in Neurobiology,* 3:917-924, 1993.

[60] A. Omurtag, B. Knight, and L. Sirovich On the simulation of large populations of neurons. *Journal of Computational Neuroscience,* 8:51-63, 2000.

[61] S.A. Oprisan, and C.C. Canavier, Stability analysis of rings of pulse-coupled oscillators: The effect of phase resetting in the second cycle after the pulse is important at synchrony and for long pulses. *Journal of Differential Equations and Dynamical Systems,* 9:243-258, 2001.

[62] S.A. Oprisan and C.C. Canavier, The influence of limit cycle topology on the phase resetting curve. *Neural Computation,* 14:1027-1057, 2002.

[63] S.A. Oprisan, A.A. Prinz, and C.C. Canavier, Phase resetting and phase locking in hybrid circuits of one model and one biological neuron. *Biophysical Journal,* 87:2283-2298, 2004.

[64] S.A. Oprisan and C.C. Canavier, Stability criterion for a two-neuron reciprocally coupled network based on the phase and burst resetting curves. *Neurocomputing,* 65-66:733-739, 2005.

[65] T. Pavlidis, Biological Oscillators: Their mathemaical analysis. *Academic Press, New York,* 1973.

[66] C.S. Peskin, Mathematical aspects of heart physiology. *New York University Courant Institute of Mathematical Sciences, New York,* 1975.

[67] A.A. Prinz, L.F. Abbott, and E. Marder, The dynamic clamp comes of age. *Trends Neuroscience,* 27: 218-224, 2004

[68] R.H. Rand, A.H. Cohen, and P.J. Holmes, Systems of coupled oscillators as models of central pattern generators. In:Neural Control of Rhythmic Movements in Vertebrates. *Wiley, New York,* 369-413, 1987

[69] J. Rinzel and G.B. Ermentrout, Analysis of neural excitability and oscillations. In:Methods in Neuronal Modeling: From Ions to Networks. 2nd edition, *MIT Press, Cambridge, Massachusetts,* 135-169, 1998

[70] J. Rubin and D. Terman, Geometric analysis of population rhythms in synaptically coupled neuronal networks. *Neural Computation,* 12:597-645, 2000.

[71] M.J. Russell, G.M. Switz, and K. Thompson, Olfactory influences on the human menstrual cycle. *Pharmacology Biochemistry and Behavior,* 13:737-738, 1980.

[72] Y.D. Sato and M. Shiino, Generalization of coupled spiking models and effects of the width of an action potential on synchronization phenomena. *Physical Review E,* 75:011909, 2007.

[73] J. Sherman, J. Rinzel, and J. Keizer, Emergence of organized bursting in clusters of pancreatic beta-cells by channel sharing. *Biophysical Journal,* 54:411-425, 1988.

[74] W. Singer and C.M. Gray, Visual feature integration and the temporal correlation hypothesis. *Annual Review Neuroscience,* 18:555-586, 1995

[75] W. Singer, Synchrony, oscillations, and relational codes. In:The Visual Neurosciences. *The MIT Press, Cambridge, Massachusetts, A Bradford Book,* 1665-1681,2004

[76] F.K. Skinner, N. Kopell, and E. Marder, Mechanisms for oscillation and frequency control in reciprocally inhibitory model neural networks. *Journal of Computational Neuroscience,* 1:69-87, 1994.

[77] F.K. Skinner, J.Y.J. Chung, I. Ncube, P.A. Murray, and S.A. Campbell, Using heterogeneity to predict inhibitory network model characteristics. *Journal of Neurophysiology,* 93:1898-1907, 2005.

[78] F.K. Skinner, H. Bazzazi, and S.A. Campbell, Two-cell to N-cell heterogeneous, inhibitory networks: Precise linking of multistable and coherent properties. *Journal of Computational Neuroscience,* 18:343-352, 2005.

[79] H.M. Smith, Synchronous flashing of fireflies. *Science,* 82:151, 1935.

[80] D. Somers and N. Kopell, Rapid synchronization through fast threshold modulation. *Biological Cybernetics,* 68:393-407, 1993.

[81] S.H. Strogatz, From Kuramoto to Crawford:Exploring the onset of synchronization in populations of coupled oscillators. *Physica D:Nonlinear Phenomena,* 143(1-4):1-20, 2000.

[82] D. Terman and D.L. Wang, Locally excitatory globally inhibitory oscillator networks. *IEEE Transactions on Nerual Netowrks,* 6(1):283-286, 1995.

[83] D. Terman, A. Bose, and N. Kopell, Functional reorganization in thalamocortical networks: Transition between spindling and delta sleep rhythms. *Proceedings of the National Academy Sciences of USA,* 93:15417-15422, 1996.

[84] P.H.E. Tiesinga and J.V. Jose, Robust gamma oscillations in networks of inhibitory hippocampal interneurons. *Network:Computational Neural Systems,* 11:1-23, 2000.

[85] R.D. Traub, R. Miles, and R.K.S. Wong, Model of the origin of rhythmic population oscillations in the hippocampal slice. *Science,* 243:1319-1325, 1989.

[86] C. Van Vreeswijk, L.F. Abbott, and G.B. Ermentrout, When inhibition not excitation synchronizes neural firing. *Journal of Computational Neurosciences,* 1:313-321, 1994.

[87] T.J. Walker, Acoustic synchrony: two mechanisms in the snowy tree cricket. *Science,* 166:891-894, 1969.

[88] X.J. Wang and Buzsáki, Gamma oscillation by synaptic inhibition in a hippocampal interneuronal network model. *Journal of Neuroscience,* 16:6402-6413, 1996.

[89] X.J. Wang and J. Rinzel, Alternating and synchronous rhythms in reciprocally inhibiory model neurons. *Neural Computing,* 4:84-97, 1992.

[90] J.P. Welsh, E.J. Lang, I. Sugihara, and R. Llinás. Dynamic organization of motor control within the olivocerebellar system. *Nature,* 374:453-457, 1995.

[91] J.A. White, C.C. Chow, J. Ritt, C. Soto-Trevino, and N. Kopell, Synchronization and oscillatory dynamics in heterogeneous, mutually inhibited neurons. *Journal of Computational Neuroscience,* 5:5-16, 1998.

[92] A.T. Winfree, Biological rhythms and the behavior of populations of coupled oscillators. *Journal of Theoretical Biology,* 16:15-42, 2967.

[93] A.T. Winfree, The timing of biological clocks. *Scientific American Press, New York,* 1987.

[94] A.T. Winfree, The Geometry of Biological Time. 2nd edition, *Springer-Verlag, New York,* 2001.